



MAX-PLANCK-GESELLSCHAFT



Effects of the glutamic acid decarboxylase (GAD) inhibitor semicarbazide and anti-GAD autoantibodies-containing immunoglobulin G on neuronal network activity within the motor cortex

Dissertation zur Erlangung des Doktorgrades der
Naturwissenschaften
Fakultät für Biologie der Ludwig-Maximilians-Universität
München

vorgelegt von
Christina Ingrid Holfelder

April 2010

1. Gutachter:	Prof. Mark Hübener
2. Gutachter:	Prof. Hans Straka
Tag der Einreichung:	29.04.2010
Tag der mündlichen Prüfung:	04.08.2010

Contents

Abbreviations	VII
1 Introduction	1
1.1 γ -Aminobutyric Acid (GABA)	1
1.2 Glutamic Acid Decarboxylase (GAD)	2
1.3 Semicarbazide (SMC)	4
1.4 Anti-GAD Autoantibodies (Anti-GAD AAbs)	6
1.5 Introduction to the Technique of Intrinsic Optical Signal (IOS) Recording	10
1.6 Goals of this PhD Thesis	12
2 Materials and Methods	15
2.1 Solutions and Drugs	15
2.2 Purification of SPS-IgG and Control IgG	17
2.2.1 Purification of IgG with Affinity Chromatography	17
2.2.2 Buffer Exchange	18
2.2.3 Quantification of IgG Concentration	18
2.3 Detection of Anti-GAD AAbs in Purified SPS-IgG	19
2.3.1 Purification of Mouse Brain Proteins	19
2.3.2 Western Blots	19
2.3.3 GAD-Dot	20
2.4 Preparation of Mouse Brain Slices	20
2.4.1 Animals	20
2.4.2 Preparation of Coronal Brain Slices	21
2.5 IOS Recordings	22
2.6 Analysis of IOSs	24
2.7 Patch-Clamp Recordings	25
2.8 Analysis of Patch-Clamp Experiments	26
2.9 Statistics	27
2.10 Index	27
3 Results	31
3.1 Analyzing IOSs and Long-term IOS Recording	31
3.1.1 Data Acquisition	31
3.1.2 Development of a Data Analysis Program for IOSs	32
3.1.2.1 Binning and Filtering	32
3.1.2.2 $\Delta F/F$ Calculation	34
3.1.2.3 Automatic Detection of a ROI and Calculation of Signal Traces	39

3.1.3	Long-term IOS Recording	48
3.1.3.1	Reproducibility of IOSs	49
3.1.3.2	Correlation of IOSs with Stimulation Strength	50
3.1.3.3	Long-term Measurements	51
3.1.4	Effects of BIM on IOSs	54
3.2	Effects of SMC on Motor Cortical Neuronal Network Activity	54
3.2.1	Effects of SMC on IOSs	54
3.2.1.1	Effects of Different SMC Concentrations on IOSs	54
3.2.1.2	Effects of SMC in Different Mouse Strains	56
3.2.2	Effects of SMC on Synaptic Transmission	58
3.2.2.1	Effects of SMC on GABA _A Minis	59
3.2.2.2	Effects of SMC on sEPSCs	59
3.3	Effects of SPS-IgG on Motor Cortical Neuronal Network Activity	61
3.3.1	Detection of Anti-GAD AAbs in Purified SPS-IgG	61
3.3.2	Effects of SPS-IgG on IOSs	63
3.3.3	Effects of SPS-IgG on Synaptic Transmission	65
3.3.3.1	Effects of SPS-IgG on GABA _A Minis	66
3.3.3.2	Effects of SPS-IgG on sEPSCs	67
4	Discussion	75
4.1	IOS Recordings	75
4.1.1	Physiological Interpretations of IOSs	75
4.1.2	Long-term IOS Recording	76
4.1.3	Effects of BIM on IOSs	78
4.2	Effects of SMC on Motor Cortical Neuronal Network Activity	79
4.2.1	Effects of SMC on IOSs	79
4.2.2	Effects of SMC on Synaptic Transmission	81
4.2.2.1	Effects of SMC on GABA _A Minis	81
4.2.2.2	Effects of SMC on sEPSCs	82
4.2.3	Possible Effects of SMC on Human Health	83
4.3	Effects of SPS-IgG on Motor Cortical Neuronal Network Activity	84
4.3.1	SPS - an Immunopathy?	84
4.3.2	Detection of Anti-GAD AAbs in Purified SPS-IgG	85
4.3.3	Effects of SPS-IgG on IOSs	86
4.3.4	Effects of SPS-IgG on Synaptic Transmission	87
4.3.5	Hypotheses Regarding the Induction of GAD Autoimmunity and Mechanism of Action	89
4.3.5.1	Induction of GAD Autoimmunity	89
4.3.5.2	Possible Mechanisms of Action of Anti-GAD AAbs in the CNS	91
	Summary	93
	List of Figures	97
	List of Tables	99

Bibliography	101
Publication	123
Danksagung	125
Curriculum Vitae	127
Erklärung	129

Abbreviations

AAb	Autoantibody
Ab	Antibody
ACSF	Artificial cerebrospinal fluid
ADC	Azodicarbonamide
AD/DA	Analog/digital digital/analog
ADP	Adenosine-5'-diphosphate
ALS	Amyotrophic lateral sclerosis
AMPA	α -amino-3-hydroxy-5-methyl-4-isoxazolepropionic acid
Anti-Amphiphysin AAb	Anti-Amphiphysin autoantibody
Anti-GAD AAb	Anti-GAD autoantibody
apo-GAD	Inactive GAD form
ATP	Adenosine-5'-triphosphate
Baf	Bafilomycin A1
BIM	(-)-Bicuculline methiodide
CCD	Charge-coupled device
CNS	Central nervous system
CSF	Cerebrospinal fluid
CSP	Cysteine string protein
D-AP5	D-(-)-2-amino-5-phosphonopentanoic acid
dSEVC	Discontinuous single electrode voltage-clamp
ECS	Extracellular space
ELISA	Enzyme-linked immunosorbent assay
EPSC	Excitatory postsynaptic current
EU	European Union
GABA	γ -aminobutyric acid
GABA _A Mini	GABA _A receptor-mediated miniature postsynaptic current
GABARAP	GABA _A receptor-associated protein
GAD	Glutamic acid decarboxylase
holo-GAD	Active GAD form
HSC70	Heat shock cognate 70
I.D.	Inner diameter
IDDM	Insulin dependent (type 1) diabetes mellitus
Ig	Immunoglobulin
IgG	Immunoglobulin G
IOS	Intrinsic optical signal
i.p.	Intraperitoneally
IR	Infrared
i.v.	Intravenously

Abbreviations

MHC	Major histocompatibility complex
MS	Multiple sclerosis
NBQX	1,2,3,4-tetrahydro-6-nitro-2,3-dioxo-benzo[f]quinoxaline-7-sulfonamide
NMDA	<i>N</i> -methyl <i>D</i> -aspartat
NOD	Non-obese diabetic
O.D.	Outer diameter
PDS	Paroxysmal depolarization shift
PLP	Pyridoxal-5'-phosphate
ppb	Parts per billion
PTSD	Post-traumatic stress disorder
RMP	Resting membrane potential
RMS	Root mean square
ROI	Region of interest
RT	Room temperature
SEM	Standard error of the mean
sEPSC	Spontaneous excitatory postsynaptic current
sIPSC	Spontaneous inhibitory postsynaptic current
SMC	Semicarbazide
SPS	Stiff-person syndrome
SPS-IgG	IgG fraction of SPS patient
TH	Threshold
TTX	Tetrodotoxin
VGAT	Vesicular GABA transporter
V-type ATPase	Vacuolar-type ATPase

1 Introduction

1.1 γ -Aminobutyric Acid (GABA)

The electrical activity of the brain is the result of a complex interaction between excitation and inhibition mediated by several types of neurotransmitters. In the middle of the last century, the amino acid GABA was discovered in the vertebrate brain and identified as its main inhibitory neurotransmitter (Awapara *et al.*, 1950; Roberts & Frankel, 1950; Bazemore *et al.*, 1956; Florey, 1991). Synaptic GABA release depends on Ca^{2+} influx into presynaptic terminals and GABA action is terminated by re-uptake into presynaptic terminals and/or surrounding glia. Two main classes of GABA receptors are known: GABA_A and GABA_B receptors. GABA_A receptors are ionotropic and their activation opens an ion channel permeable for Cl^- . GABA_B receptors are metabotropic receptors and coupled to G proteins, which cause an opening of K^+ conductances and, hence, a hyperpolarization of neurons. During embryogenesis and the first week of postnatal life, however, GABA acting via GABA_A receptors serves as an excitatory neurotransmitter due to an inverted Cl^- gradient in neurons (Ben-Ari *et al.*, 1997; Leinekugel *et al.*, 1999).

As the majority of neurons utilize either GABA or glutamate, the major excitatory neurotransmitter in the central nervous system (CNS), the interplay of these two neurotransmitters principally controls brain excitability. Therefore, imbalance between both neurotransmitter systems may cause severe pathophysiological conditions.

Alterations of GABA metabolism are suggested to play an important role in the development and spread of seizures. A reduced GABA concentration in the cerebrospinal fluid (CSF) (Wood *et al.*, 1979; Petroff *et al.*, 1996, 1999) and a decreased number of GABAergic neurons in the neocortex (Haglund *et al.*, 1992b; Marco *et al.*, 1996; Spreafico *et al.*, 1998; Ribak & Yan, 2000) have been reported in epileptic patients. Dysfunction in GABA neurotransmission has also been described in Huntington's chorea (Spokes *et al.*, 1980; Gourfinkel-An *et al.*, 2003), Parkinson's disease (de Jong *et al.*, 1984), and general anxiety disorder (Kosel *et al.*, 2004).

To increase GABAergic inhibition in the CNS, several pharmacological approaches are possible. GABA_A receptor modulators like benzodiazepines, e.g. diazepam, directly in-

crease the activity of GABA_A receptors (Krogsgaard-Larsen & Falch, 1981), whereas baclofen shows a similar effect on GABA_B receptors (Brooks *et al.*, 1992). GABA transporter blockers, e.g. tiagabine, inhibit GABA reuptake and, therefore, prolong GABA action in the synaptic cleft (Krogsgaard-Larsen, 1980; Clausen *et al.*, 2006). GABA synthesis and release can be stimulated by valproate or gabapentin (Pinder *et al.*, 1977; Löscher *et al.*, 1991), whereas vigabatrin slows GABA degradation (Gale & Iadarola, 1980).

1.2 Glutamic Acid Decarboxylase (GAD)

The enzyme GAD is the rate-limiting enzyme of GABA synthesis catalyzing the decarboxylation of glutamate to GABA and CO₂ (Roberts & Frankel, 1950, 1951a,b; Killam & Bain, 1957; Matsushima *et al.*, 1986). GAD-positive cells in the mouse motor cortex occur in all layers in the form of clusters with highest concentration in the cortical layer II and layer VI (Solberg *et al.*, 1988). In layer IV of the rat barrel cortex only 14% of neurons are GAD-positive. In this layer, however, the spatial distribution of GABAergic neurons corresponds to the organization of the barrel field with GABAergic neurons enclosing single barrels (Lin *et al.*, 1985). This organization suggests that inhibitory neurons shape the columns in the barrel cortex (Lübke & Feldmeyer, 2007). In other layers, however, the distribution of GAD-positive neurons is less organized.

GAD exists in two isoforms, GAD₆₅ and GAD₆₇, which are encoded by two distinct genes located on chromosomes 2 and 10 in humans (Erlander & Tobin, 1991; Bu *et al.*, 1992). GAD shows a high interspecies homology implying a high evolutionary pressure to maintain the primary sequence throughout the full length of the protein (Wyborski *et al.*, 1990; Erlander *et al.*, 1991). In rats, the amino acid sequence of GAD₆₅ and GAD₆₇ is 65% identical and 80% similar with the N-terminus being most divergent. GAD₆₇ is thought to produce GABA for general metabolic activity (Martin & Rimvall, 1993; Soghomonian & Martin, 1998) functioning among others as trophic factor for synaptogenesis during early development, protective factor after neuronal injury, source of energy via the GABA shunt, and regulator of redox potential during oxidative stress (Pinal & Tobin, 1998; Waagepetersen *et al.*, 1999; Lamigeon *et al.*, 2001). GAD₆₅ on the other hand provides GABA for synaptic transmission (Martin & Rimvall, 1993; Soghomonian & Martin, 1998).

In adult animals only about 30% of intracellular GABA levels derive from GAD₆₅, whereas the remaining 70% are produced by GAD₆₇ (Soghomonian & Martin, 1998; Martin, 2000a). During early postnatal development, however, GAD₆₅ contributes significantly to basal levels of GABA (Hensch *et al.*, 1998). In GAD₆₅ knock-out mice, GABA levels remain normal (Asada *et al.*, 1996; Kash *et al.*, 1997), whereas in GAD₆₇ knock-out

mice GABA content is reduced to 7% and GAD activity to less than 20% compared to wild-type mice (Asada *et al.*, 1997). This strong reduction in GABA levels leads to a high mortality due to a severe cleft palate. GAD₆₅ knock-out mice suffer from seizures, but apart from that appear inconspicuous (Asada *et al.*, 1996, 1997; Kash *et al.*, 1997).

The different function of both GAD isoforms is reflected by differences in their sub-cellular and cell type-specific distribution (Erlander *et al.*, 1991; Kaufman *et al.*, 1991; Feldblum *et al.*, 1993; Martin & Rimvall, 1993; Soghomonian & Martin, 1998). GAD₆₅ is predominantly found in nerve terminals and more concentrated in neurons, whose activation is highly dependent upon synaptic inputs. GAD₆₇ is located in the cell body and dendrites and more prominent in neurons that are known to fire tonically. This different intracellular distribution is presumably maintained by a different interaction of both isoforms with membranes of the Golgi apparatus and synaptic vesicles (McLaughlin *et al.*, 1975; Solimena *et al.*, 1993, 1994).

Apart from their different distribution patterns within neurons, the two GAD isoforms show different properties, which allow greater flexibility in regulating GABA synthesis. GAD₆₅ and GAD₆₇ appear to be regulated differently by phosphorylation with GAD₆₅ being activated while GAD₆₇ being inhibited upon phosphorylation (Wei *et al.*, 2004). Phosphorylation may change the affinity of the enzyme to its substrate or its cofactor pyridoxal-5'-phosphate (PLP), a derivative of vitamin B6 (Roberts & Frankel, 1951a). Furthermore, the structure of both isoforms differs (Fenalti *et al.*, 2007). The structure of GAD₆₇ shows a tethered loop, which covers the active site and, therefore, provides a catalytic environment that sustains GABA production. In GAD₆₅, this loop is inherently mobile. This mobility in the catalytic loop promotes a side reaction that results in cofactor release and GAD₆₅ inactivation.

The interaction of GAD with its cofactor PLP is the most important way to regulate GAD activity. GAD without a bound cofactor (apo-GAD) is inactive, whereas its active form (holo-GAD) is saturated with PLP. The inactive form is thought to serve as a reservoir that can be activated if additional GABA synthesis is required. GAD₆₇ binds PLP with a higher affinity compared to GAD₆₅ (Martin, 1987; Chen *et al.*, 2003). Almost the complete GAD₆₇ pool exists in its active PLP-bound holo-form, whereas about 50% of GAD₆₅ is present in its inactive apo-form (Kaufman *et al.*, 1991; Martin *et al.*, 1991; Martin & Rimvall, 1993; Lernmark, 1996). With only 50% of GAD₆₅ in its active form, GAD₆₅ does not operate at its maximal catalytic capacity. Adenosine-5'-triphosphate (ATP) (Martin & Martin, 1982), glutamate (Meeley & Martin, 1983), aspartate (Porter & Martin, 1987), and GABA (Porter & Martin, 1984) promote apo-GAD formation, while inorganic phosphate (Martin & Martin, 1979) and PLP (Martin & Martin, 1979) promote holo-GAD formation. Under physiological conditions, the apo-form is favored, but it

reacts sensitive to changes in energy state [inorganic phosphate, phosphocreatine, pH, magnesium, adenosine-5'-diphosphate (ADP), ATP] (Petroff, 2002). During depolarization of neurons, PLP associates with apo-GAD to form its active holo-form leading to an increased GABA synthesis by GAD₆₅ in nerve terminals (Gold & Roth, 1979; Miller & Walters, 1979).

GAD₆₅ is synthesized as a soluble cytosolic protein, but becomes post-translational modified and anchored to the cytosolic face of Golgi membranes, from where it is targeted to synaptic vesicle membranes (Solimena *et al.*, 1993, 1994). Even though palmitoylation of cysteines 30 and 45 is not necessary for binding GAD₆₅ to Golgi membranes (Shi *et al.*, 1994; Solimena *et al.*, 1994), palmitoylation is essential for post-Golgi trafficking to presynaptic clusters (Kanaani *et al.*, 2004). A cycle of depalmitoylation and repalmitoylation serves to cycle GAD₆₅ between Golgi and post-Golgi membranes and to regulate the level of enzyme directed to the synapse (Kanaani *et al.*, 2008). GAD₆₅ is bound to synaptic vesicles by forming a complex with the heat shock cognate 70 (HSC70), cysteine string protein (CSP), and vesicular GABA transporter (VGAT) (Hsu *et al.*, 2000; Jin *et al.*, 2003). A functional coupling between synaptic vesicle-associated GAD₆₅ and VGAT constitutes a machinery, which allows a more efficient packaging of newly synthesized GABA into synaptic vesicles (Jin *et al.*, 2003). VGAT preferentially transports newly synthesized GABA, which is generated by vesicle-associated GAD₆₅.

1.3 Semicarbazide (SMC)

The hydrazide SMC is a known GAD inhibitor (Roberts & Frankel, 1951a) reducing GAD activity and, hence, brain GABA levels (Killam & Bain, 1957; Maynert & Kaji, 1962; Abe & Matsuda, 1979; Yamashita & Hirata, 1979; Matsushima *et al.*, 1986). Administration of SMC induces clonic and tonic convulsions lasting four to five hours (Jenney & Pfeiffer, 1958; Yamashita, 1976) as well as running fits, which describe stereotyped running activity and disorderly escape behavior (Yamashita & Hirata, 1977, 1979). The convulsant dose in mice is 111.7 ± 4.7 mg/kg if injected intravenously (i.v.) and 116.4 ± 3.2 mg/kg if injected intraperitoneally (i.p.) (Jenney & Pfeiffer, 1958). Vitamin B6-deficient and fasted animals are more susceptible to SMC-induced effects (Jenney & Pfeiffer, 1958; Yamashita, 1976). Humans react more sensitive to SMC as the convulsant dose is only about one third of the convulsant dose in mice (≈ 40 mg/kg if injected i.v.) (Jenney & Pfeiffer, 1958). Audiogenic and photogenic stimulation reduce the convulsive dose to two thirds in mice and humans.

SMC shows a long latent period of one to several hours if it is systemically applied (Jenney & Pfeiffer, 1958; Yamashita, 1976; Yamashita & Hirata, 1977, 1979), possibly be-

cause hydrazides have a low oil/water partition coefficient and, therefore, are expected to penetrate only slowly into the brain (Schanker, 1961). However, if SMC is directly injected in the lateral ventricle or superior colliculus *in vivo*, the latent period is shortened to about 10 min and a lower dose is necessary to induce convulsions (Yamashita, 1976; Yamashita & Hirata, 1977).

SMC most likely interacts with the GAD cofactor PLP to form PLP-semicarbazone (Yamashita & Hirata, 1977; Sakurai *et al.*, 1981). This reduces GAD activity as the level of available PLP decreases and leads to diminished GABA synthesis. Moreover, PLP-semicarbazone itself seems to contribute to convulsions (Yamashita, 1976). The effect of SMC can be inhibited by application of the PLP-precursor pyridoxine (Yamashita, 1976; Yamashita & Hirata, 1977, 1979) and PLP itself (Killam & Bain, 1957).

In 2003 concern emerged, as traces of SMC were found in food packed in glass jars with metal lids sealed with the blowing agent azodicarbonamide (ADC) (Stadler *et al.*, 2004) as for some hydrazides carcinogenic properties have been described (Mori *et al.*, 1960; Parodi *et al.*, 1981). SMC is thought to be a thermal decomposition product of ADC, which migrates into the packed food (Stadler *et al.*, 2004). The SMC concentrations found in glass jar-packed food (e.g. jam, mustard, vegetables, sauces, baby food etc.) ranged up to 25 ppb (parts per billion \approx 1 μg per kg). Baby food contained the highest levels, because of a higher ratio of gasket area to food mass due to small pack sizes and because of the used heat treatment conditions. The daily intake of SMC by infants around the age of three to twelve months was estimated to about 0.6 μg /day (Nestmann *et al.*, 2005). Although the intake of SMC via contaminated food was believed to be of minor risk for health problems compared to the benefits (e.g. lack of microbial contamination due to the heating process) (Nestmann *et al.*, 2005), the use of ADC as blowing agent is now banned in the European Union (EU).

Relatively high concentrations of SMC (10 to 1200 ppb) are also found in bread as ADC is added to flour owing to its dough-improving properties (Noonan *et al.*, 2005, 2008), a procedure forbidden in the EU, but still used in the USA, Canada, and Brazil. In Brazil, ADC containing flour was regarded as source of SMC contamination in chicken coated with flour, salt, and spices (Pereira *et al.*, 2004). SMC was also detected in food treated with hypochloride for disinfection and bleaching (Hoenicke *et al.*, 2004). Furthermore, SMC is a protein-bound side-chain marker metabolite for nitrofurazone abuse, an antibiotic banned in the EU (Cooper *et al.*, 2005a,b). SMC may also form naturally, e.g. in wild crayfish (Saari & Peltonen, 2004), red seaweed, shrimps, and eggs (Hoenicke *et al.*, 2004), or derives from natural substances like arginine and creatine (Hoenicke *et al.*, 2004).

Most SMC in the body is present in protein-bound form, which is stable for several weeks (Cooper *et al.*, 2005a,b). The half-life of protein-bound SMC is about 15 days in

muscle and seven days in liver or kidney. Until now, no information about toxicokinetics or *in vivo* metabolism is available. *In vitro*, SMC is metabolized to formaldehyde and N₂ (Kroeger-Koepke *et al.*, 1981).

The impact of SMC on human health is still under debate. SMC exhibits a mild carcinogenic effect *in vitro* (Hayatsu *et al.*, 1966; Hayatsu & Ukita, 1966; Parodi *et al.*, 1981), but *in vivo* data are inconsistent (Toth *et al.*, 1975; Abramsson-Zetterberg & Svensson, 2005; Vlastos *et al.*, 2009). In animals, SMC impairs cross-linking of collagen and elastin inducing osteochondral and vascular lesions (Ramamurti & Taylor, 1959; Langford *et al.*, 1999; Dawson *et al.*, 2002; Mercier *et al.*, 2007; Takahashi *et al.*, 2009). Moreover, teratogenic effects such as induction of cleft palate and aortic aneurysms have been reported (Steffek *et al.*, 1972; de la Fuente & del Rey, 1986; Gong *et al.*, 2006). SMC application to rats causes an alteration of spontaneous motor and exploration behavior indicating an enhanced arousal and an ineffective modulation of response to novelty (Maranghi *et al.*, 2009). Furthermore, SMC acts as an endocrine disruptor altering the homeostasis of the endocrine system (Maranghi *et al.*, 2010).

1.4 Anti-GAD Autoantibodies (Anti-GAD AAbs)

Autoantibodies (AAbs) are antibodies (Abs) that are directed to one or more of the body's own proteins. AAbs directed against GAD are associated with several diseases. These include ataxia, a general term spanning different forms of movement disorders with limited control of target-oriented movements (Abele *et al.*, 1999; Honnorat *et al.*, 2001; Vianello *et al.*, 2003; Vulliemoz *et al.*, 2007) and polyendocrine autoimmune syndrome, a heterogeneous group of diseases characterized by autoimmune activity against endocrine organs (Tuomi *et al.*, 1996). Anti-GAD AAbs are also found in some epileptic patients (McKnight *et al.*, 2005; Vulliemoz *et al.*, 2007) and in patients suffering from Batten disease, in which a loss of GABAergic neurons is observed (Chattopadhyay *et al.*, 2002a,b; Ramirez-Montealegre *et al.*, 2005). Most investigations have been done on Anti-GAD AAbs found in patients with insulin-dependent (type 1) diabetes mellitus (IDDM) (Baekkeskov *et al.*, 1990; De Aizpurua *et al.*, 1992; Kaufman *et al.*, 1992; Seissler *et al.*, 1993; Velloso *et al.*, 1993; Solimena *et al.*, 1994) and stiff-person syndrome (SPS) (Solimena *et al.*, 1988, 1990, 1994; Walikonis & Lennon, 1998; Meinck *et al.*, 2001).

IDDM symptoms are caused by an autoimmune destruction of the insulin-producing β cells with onset in childhood (Dobersen & Chase, 1983; Gerich, 1986). The autoimmune response is thought to be mediated by autoreactive T cells and AAbs (Dobersen & Chase, 1983; Powers & Eisenbarth, 1985; Kukreja & Maclaren, 1999), among others also Anti-GAD AAbs (Baekkeskov *et al.*, 1990; De Aizpurua *et al.*, 1992). GAD is not

only expressed in the brain but also in β cells, kidneys, pituitary gland, thyroid, ovaries, testes, adrenals, and liver (Christie *et al.*, 1992). The specific role of GABA in β cells is still discussed, but GABA seems to be involved in paracrine signaling between β cells and their adjacent α and δ cells (Rorsman *et al.*, 1989; Reetz *et al.*, 1991; Franklin & Wollheim, 2004) as well as in energy metabolism of β cells (Sorenson *et al.*, 1991). As human islets of Langerhans only express GAD₆₅ (Kim *et al.*, 1993), in 70 to 83% of IDDM patients autoimmune response is directed against GAD₆₅, even though AAbs against GAD₆₇ were found in 9 to 26% of the patients (Kaufman *et al.*, 1992; Atkinson *et al.*, 1993; Hagopian *et al.*, 1993; Seissler *et al.*, 1993; Velloso *et al.*, 1993; Ujihara *et al.*, 1994). Anti-GAD AAbs in IDDM patients mainly recognize conformational epitopes (Daw & Powers, 1995). In some patients, however, Anti-GAD AAbs directed against linear epitopes were identified (Rharbaoui *et al.*, 1998). Sera with GAD inhibitory properties were only detected in few IDDM patients (2.7%) (Seissler *et al.*, 1993). During the first years after onset of disease, the amount of circulating Anti-GAD AAbs decreases. This is possibly linked to a parallel loss of GAD-expressing β cells, which may serve as antigenic stimulus (De Aizpurua *et al.*, 1992; Kaufman *et al.*, 1992; Seissler *et al.*, 1993). Moreover, a strong T cell response was observed, which is regarded as the major cause for the destruction of β cells in humans and non-obese diabetic (NOD)-mice, an animal model of IDDM (Kaufman *et al.*, 1993; Tisch *et al.*, 1993; Boyton *et al.*, 1998).

SPS was first described by Moersch and Woltman (1956), who collected data of 14 patients observed over 32 years. These authors observed their first case of SPS in 1924. The patient suffered from muscle weakness, awkward gait and sometimes fell like "a wooden man". Hence, the syndrome was termed "Stiff-man syndrome". However, as it became evident that women are affected more frequently (Lockman & Burns, 2007), the term was changed to "Stiff-person syndrome". The average age of onset is between the fourth and sixth decade (Dalakas *et al.*, 2000; Meinck & Thompson, 2002; Murinson, 2004). SPS is characterized by progressive, usually symmetric muscle stiffness, predominantly in axial and proximal limb muscles (Meinck *et al.*, 1994; Kissel & Elble, 1998; Dalakas *et al.*, 2000; Meinck & Thompson, 2002; Lockman & Burns, 2007). During the progress of disease, limb rigidity may cause full stretching of the legs, which hampers walking. Painful spasms are superimposed on rigidity and can be abrupt so that patients fall over. These spasms occur spontaneously or are triggered by external as well as internal stimuli (e.g. light and noise). The disease follows a slow progression over years until the condition stabilizes and thereafter remains stable for several years or even decades. Stiffness and spasms disappear during sleep or narcosis, which indicates an involvement of the CNS. Acute autonomic failure, a malfunction of the autonomic nervous system,

has been suggested as a possible cause of sudden death in few SPS patients (Mitsumoto *et al.*, 1991).

Apart from motor symptoms, SPS patients also exhibit non-motor features. About 44% of SPS patients develop task-specific phobia, which includes fear and avoidance of situations difficult to master because of motor symptoms (e.g. walking unaided in open space, crossing a street) (Henningsen & Meinck, 2003). In most cases, this phobia develops after the onset of motor symptoms. Two case reports further point to a possible correlation of SPS and mood disorders. The first describes a patient with post-traumatic stress disorder (PTSD) (Dinnerstein *et al.*, 2007) and the second a patient suffering from anxious depression (Culav-Sumić *et al.*, 2008). Both patients, however, developed SPS after the onset of psychiatric symptoms. A similar prevalence for task-specific phobia was observed among patients with or without a history of falls or fractures (Henningsen & Meinck, 2003). These findings suggest that at least in some patients psychiatric symptoms may develop independently of motor symptoms and are not just a psychological reaction to the motor symptoms.

However, it is important to mention that SPS is a rare neurological condition. Over a period of ten years, Meinck diagnosed SPS in 20 patients in the area of Heidelberg, Germany, and surroundings with a population of about two to three millions (Meinck & Thompson, 2002). Diagnosis of SPS is primarily based on clinical symptoms (Lorish *et al.*, 1989; Meinck *et al.*, 1994; Murinson, 2004). Due to its rare occurrence, however, SPS is quite often misdiagnosed, e.g. as hysterical paralysis (Fleischman *et al.*, 2009). Drugs enhancing the strength of GABAergic transmission, e.g. benzodiazepines, valproate, vigabatrin, tiagabine, baclofen, and gabapentin, reduce symptoms (Howard, 1963; Lorish *et al.*, 1989; Meinck, 2001; Vasconcelos & Dalakas, 2003; Dalakas, 2009). Plasmapheresis and intravenous immunoglobulin (Ig) infusions (Dalakas *et al.*, 2001; Vasconcelos & Dalakas, 2003; Dalakas, 2006, 2009; Rossi *et al.*, 2009), which are classical methods for the treatment of autoimmune diseases, provide an additional benefit.

Reduced GABA levels are found in the sensorimotor and posterior occipital cortex (Levy *et al.*, 2005) and in the CSF (Dalakas *et al.*, 2001) of SPS patients. Further studies showed a hyperexcitability of the motor cortex (Sandbrink *et al.*, 2000; Koerner *et al.*, 2004) and the brainstem (Molloy *et al.*, 2002). This possibly explains electromyographic findings, a technique for recording electrical activity produced by skeletal muscles. Electromyography shows that continuous background firing of motor units, which consist of single α -motor neurons and all of the corresponding muscle fibers they innervate, occurs despite the patient's attempt of muscle relaxation (Levy *et al.*, 1999). Furthermore, if patients attempt to contract a muscle in one direction, muscles that pull in the opposite direction are involuntarily activated. However, loss of GABAergic neurons in

the cerebellar cortex (Warich-Kirches *et al.*, 1997), degeneration of neurons in the spinal cord (Ishizawa *et al.*, 1999; Saiz *et al.*, 1999b; Warren *et al.*, 2002), and striatal lesions (Guardado Santervas *et al.*, 2007) were only described in few patients. An immunogenic background of SPS is suggested as the frequency of certain alleles, e.g. HLA-DR β 1 0301, encoding for subunits of major histocompatibility complex (MHC) class II molecules are elevated in SPS patients compared to the healthy population (Dalakas *et al.*, 2000).

An autoimmune origin of SPS is also suspected, since Solimena *et al.* (1988) detected AAbs directed against GAD. In other studies, Anti-GAD AAbs were found in about 60 to 98% of SPS patients (Solimena *et al.*, 1990; Walikonis & Lennon, 1998; Meinck *et al.*, 2001), mainly directed against GAD₆₅. Anti-GAD AAbs titers of SPS patients range from 7.0 to 125 μ g/ml in serum and from 92 to 2500 ng/ml in CSF. In IDDM patients, the titer is much lower (200 to 1760 ng/ml in serum) and Anti-GAD AAbs are absent in the CSF (Dalakas *et al.*, 2001). Anti-GAD AAbs levels in SPS patients correlate with motor cortex excitability (Koerner *et al.*, 2004), but no correlation was found with disease duration and severity (Murinson *et al.*, 2004) as well as CSF GABA concentration (Dalakas *et al.*, 2001). Serum and CSF of SPS patients strongly immunoreact with GAD₆₅ on Western Blots and with GABAergic neurons, while IDDM sera show no reactivity (Solimena & De Camilli, 1991; Tuomi *et al.*, 1994; Giometto *et al.*, 1996; Dalakas *et al.*, 2001; Vianello *et al.*, 2005, 2006). This immunoreaction persists, even if sera of SPS patients are diluted to match the Anti-GAD AAbs concentration of IDDM sera (Dalakas *et al.*, 2001). SPS patient sera and CSF as well as purified immunoglobulin G (IgG) fractions inhibit GAD activity *in vitro* (Dinkel *et al.*, 1998; Raju *et al.*, 2005), while Anti-GAD AAbs-positive sera of most IDDM patients do not (Seissler *et al.*, 1993; Björk *et al.*, 1994). This inhibition by SPS patient sera has been shown to be dose-dependent (Dinkel *et al.*, 1998) and could not be compensated by high concentrations of glutamate or the cofactor PLP, thus indicating a noncompetitive inhibitory mechanism (Raju *et al.*, 2005). Intracerebellar administration of IgG derived from SPS patients, but not IDDM-IgG, has been shown to induce SPS-like symptoms in rats (Manto *et al.*, 2007).

The different properties of Anti-GAD AAbs derived from either SPS or IDDM patients are partially explained by their difference in epitope recognition (Tuomi *et al.*, 1994; Raju *et al.*, 2005). Anti-GAD AAbs of SPS patients are mainly directed against a linear N-terminal epitope verified by Western Blots (Tuomi *et al.*, 1994), and against two conformation-dependent epitopes in the middle and close to the C-terminus (Butler *et al.*, 1993; Kim *et al.*, 1994; Daw *et al.*, 1996; Raju *et al.*, 2005; Burbelo *et al.*, 2008). In SPS patients, Anti-GAD AAbs directed against the C-terminus are supposed to be responsible for GAD inhibition (Ohta *et al.*, 1996; Raju *et al.*, 2005). Anti-GAD AAbs of IDDM patients mainly recognize conformational epitopes, which explains why Anti-GAD AAbs

of IDDM patients do not immunoreact with GAD under denaturing conditions prevailing during the Western Blotting procedure (Daw & Powers, 1995). This difference in epitope recognition possibly also explains why only about 30% of SPS patients develop IDDM despite of the presence of Anti-GAD AAbs in their blood (Solimena *et al.*, 1988; Walikonis & Lennon, 1998; Meinck & Thompson, 2002).

In the majority of SPS patients, an intrathecal Ab synthesis, a term describing Ab synthesis within the CSF and a prominent feature of neurological infections and inflammatory diseases, was observed (Solimena *et al.*, 1988; Levy *et al.*, 1999; Dalakas *et al.*, 2001; Meinck & Thompson, 2002; Skorstad *et al.*, 2008). Such an intrathecal Ab synthesis is mediated by a stable population of affinity-matured B cell clones within the CNS (Skorstad *et al.*, 2008). In contrast to the strong T cell response in IDDM (Kaufman *et al.*, 1993; Tisch *et al.*, 1993; Boyton *et al.*, 1998), T cell reactivity has only been reported in few SPS patients (Hummel *et al.*, 1998; Lohmann *et al.*, 2000, 2003; Holmøy *et al.*, 2009). Therefore, a significant effector role for T cells in SPS is denied (Ellis & Atkinson, 1996; Schloot *et al.*, 1999; Costa *et al.*, 2002; Raju & Hampe, 2008).

Although there is strong evidence for an autoimmune response in SPS patients, it is still a matter of debate whether Anti-GAD AAbs cause SPS or whether Anti-GAD AAbs are just a marker for the disease.

1.5 Introduction to the Technique of Intrinsic Optical Signal (IOS) Recording

IOSs originate from the interaction between light and brain tissue. Neuronal activity alters the optical properties of brain tissue compared to non-active states. Changes in optical properties of active nerves were first described by Hill and Keynes (1949). In the following decades, IOSs were also found in acute brain slices (Lipton, 1973; MacVicar & Hochman, 1991; Andrew & MacVicar, 1994; Holthoff *et al.*, 1994; Dodt *et al.*, 1996; Aitken *et al.*, 1999), in isolated whole brain preparations (Federico *et al.*, 1994), and *in vivo* in both animals (Grinvald *et al.*, 1986; Frostig *et al.*, 1990; Grinvald *et al.*, 1991) and humans (Haglund *et al.*, 1992a; Toga *et al.*, 1995; Pouratian *et al.*, 2003).

In vivo, the IOS bases on changes in light absorption caused by activity-dependent changes in blood volume and oxygenation levels (Jöbsis, 1977; Frostig *et al.*, 1990, 1995) as well as alterations in the amount of scattered light. The changes in light scattering are referred to cell swelling (MacVicar & Hochman, 1991; Andrew & MacVicar, 1994; Holthoff & Witte, 1996, 1998; Andrew *et al.*, 1999; Witte *et al.*, 2001; Fayuk *et al.*, 2002) and are thought to be the only cause for the IOS *in vitro*.

Light transmittance through brain tissue is affected by light reflection, refraction, absorption, and scattering (Jöbsis, 1977; MacVicar, 1984; Aitken *et al.*, 1999; Jarvis *et al.*, 1999). When brain slices become illuminated by light in the red and near infrared (IR) spectrum, light scattering represents the dominant light-tissue interaction and is inversely correlated to light transmittance. The amount of light transmittance is maximal in the red and near IR spectrum (650 to 800 nm) (Frostig *et al.*, 1990; MacVicar & Hochman, 1991; Frostig *et al.*, 1995), presumably because longer wavelengths penetrate brain tissue more easily than shorter ones (Svaasand & Ellingsen, 1983; MacVicar, 1984; Dodt & Zieglgänsberger, 1994, 1998). Hence, IOS recordings in brain slices require transmitted light microscopy with an IR filter.

A correlation between changes in cell volume and light transmittance was first described by Lipton (1973). The assumption that changes in cell volume cause the IOSs *in vitro* is further supported by a high spatial and temporal correlation between alterations in extracellular space (ECS) and the IOS (Holthoff & Witte, 1996, 1998; Witte *et al.*, 2001). Furthermore, a blockade in ECS volume changes (e.g. by means of a solution containing furosemide or low concentration of Cl^- ions) diminishes the IOS (MacVicar & Hochman, 1991; Holthoff & Witte, 1996). In addition, fast changes in osmolarity of the bath solution are also capable of triggering IOSs in brain slices (Andrew & MacVicar, 1994; Andrew *et al.*, 1999; Fayuk *et al.*, 2002). It is assumed that the uptake of electrolytes by cells and the concomitant water influx cause the dilution of macromolecules in the cytosol and, therefore, increase the distance between light scattering particles (Aitken *et al.*, 1999). As a consequence, more light is transmitted and brightness (light intensity) of the brain tissue increases.

As decrease in ECS volume is also induced by electrically evoked synaptic activity (Dietzel *et al.*, 1980, 1982), IOSs are capable of measuring neuronal activity via activity-dependent cell swelling. Additionally, IOSs have been shown to correlate with amplitude and spread of field potentials (Holthoff *et al.*, 1994; Dodt *et al.*, 1996; Holthoff & Witte, 1997; Cerne & Haglund, 2002) and to be reduced after blocking excitatory synaptic transmission (MacVicar & Hochman, 1991; Dodt *et al.*, 1996; Holthoff & Witte, 1996). As neurons are less susceptible to cell swelling compared to astrocytes (Hertz, 1981; Østby *et al.*, 2009), IOSs presumably predominately originate from swelling of these glial cells. A developmental study by Ransom *et al.* (1985) showed that an activity-dependent reduction of ECS volume occurred not before maturation of glial cells. The swelling of astrocytes is most likely caused by a net uptake of KCl mediated by a furosemide-sensitive $\text{Na}^+\text{-K}^+\text{-2Cl}^-$ cotransporter, which is followed by a passive water influx into astrocytes (Kimelberg & Frangakis, 1985; MacVicar & Hochman, 1991; Holthoff & Witte, 1996; Østby *et al.*, 2009).

Additionally, morphological changes associated with neurosecretion (Salzberg *et al.*, 1985; Bicknell *et al.*, 1989; Obaid *et al.*, 1989) and a rapid reorientation of membrane dipoles (Stepnoski *et al.*, 1991) may also contribute to IOSs. Advantages of IOS recordings are a good reproducibility and the absence of both pharmacological side effects and photodynamic damage (Grinvald *et al.*, 1986; Holthoff & Witte, 1996; Takashima *et al.*, 2001).

1.6 Goals of this PhD Thesis

As GAD is the rate-limiting enzyme for GABA synthesis, GAD inhibition will doubtlessly change neuronal network dynamics caused by impaired GABAergic inhibition. Due to the enormous complexity of neuronal networks, including disinhibition circuits, methods that display neuronal network activity are required to unveil the effects of GAD inhibitors at the network level. The two approaches used in this PhD study, IOS recordings and whole-cell patch-clamp measurements of GABA_A receptor-mediated miniature postsynaptic currents (GABA_A Minis) and spontaneous excitatory postsynaptic currents (sEPSCs) in acute brain slices, are able to do so. The cortical column, which represents the functional entity of the cortex, constitutes a suitable neuronal network model. As GAD inhibition is associated with movement abnormalities *in vivo*, primary motor cortical areas should be an appropriate brain region to study GAD inhibition.

IOSs can be used to investigate spread and strength of stimulus-evoked neuronal network activity, as these signals represent activity-dependent changes in the optical properties of brain tissue. IOS recording provides a direct approach to monitor changes in the activity of neuronal networks as it allows to survey whole cortical columns and their surrounding area. The patch-clamp technique serves to record miniature and spontaneous postsynaptic currents from neurons, which depend on transmitter release from the network of presynaptic neurons. Dependent on the kind of postsynaptic current modulation, drug action can be ascribed to pre- or postsynaptic mechanisms. Recording GABA_A Minis, which can be attributed to spontaneous action potential-independent presynaptic GABA release, shall help to investigate the effects of GAD inhibitors on GABAergic neurotransmission. Alterations in brain slice excitability due to reduced GABAergic inhibition may be displayed by changes in sEPSCs, which can be attributed to both spontaneous action potential-dependent and -independent excitatory presynaptic release of excitatory neurotransmitters.

To influence GABA synthesis itself, intracellular uptake of drugs inhibiting GAD activity has to be achieved. As this uptake and the depletion of the preexisting GABA pool is possibly slow, the effects of GAD inhibitors may take long to develop. In this

regard, the first project of this PhD thesis was to test the IOS technique for its capability of monitoring neuronal network activity over several hours. Additionally, a new software for the analysis of IOS data should be developed, which facilitates and significantly accelerates data analysis.

The present study next aimed to prove the ability of IOSs to sense changes in GABAergic inhibition. Therefore, experiments should be performed, in which the GABA_A receptor antagonist (–)bicuculline methiodide (BIM) was applied at a relatively low concentration to brain slices. Moreover, another series of experiments should examine whether the IOS technique is capable of displaying changes in neuronal network activity after impairing GAD activity with the well-known GAD inhibitor SMC. Comparing the effects of BIM and SMC should further reveal possible differences in changes in network activity after reducing postsynaptic receptor activity or inhibiting GABA synthesis.

In this work, SMC, due to the following reasons, should not only serve as a drug for method validation. SMC is found in several food products and causes several pathological symptoms in animals including alterations of the endocrine system and movement abnormalities. How SMC alters neuronal network dynamics is, however, nearly unknown. Therefore, a further goal was to assess concentration-dependent effects of SMC on neuronal network activity within the motor cortex. It was also planned to compare SMC effects in mice strains differing in their GAD activity. Complementary, recordings of GABA_A Minis and sEPSCs should elucidate putative changes in network activity detected by IOS recordings.

Beside exogenous GAD inhibitors, such as SMC, there exist also Anti-GAD AAbs that are endogenously produced under certain pathological conditions and, at least *in vitro*, can act as GAD inhibitors. A prominent neurological disorder with elevated Anti-GAD AAbs levels and alterations in motor behavior is SPS. Up to now, however, it is not assured, whether Anti-GAD AAbs contribute to the development and/or appearance of SPS symptoms or are merely a marker for disease. Therefore, the final aim of this study was to investigate potential effects of IgG derived from SPS patients on motor cortical neuronal network activity. This investigation was intended to be also conducted by a combination of IOS recordings and patch-clamp measurements in the motor cortex of brain slices.

2 Materials and Methods

2.1 Solutions and Drugs

Extracellular Artificial Cerebrospinal Fluid (ACSF) The ACSF, which provides the ingredients that allow neurons to survive for several hours *in vitro*, contained (in mM) 125 NaCl (VWR, Darmstadt, Germany), 2.5 KCl (Merck, Darmstadt, Germany), 1.25 NaH₂PO₄·H₂O (Merck), 25 D(+)glucose-monohydrate (Merck), 25 NaHCO₃ (Merck), 1 MgCl₂·6H₂O (Merck), and 2 CaCl₂·2H₂O (Merck) dissolved in dH₂O (Aqua ad iniectabilia; Braun, Melsungen, Germany). The osmolarity of the ACSF was 320 mOsm. The ACSF was bubbled with carbogen (5% CO₂/95% O₂) to adjust the pH to 7.4 and to saturate the ACSF with oxygen.

Intracellular Solutions for Patch-Clamp Recordings For the patch-clamp recordings, the pipettes were filled with an intracellular solution, which mimics the osmolarity of the cytoplasm. For the recording of GABA_A Minis, the solution contained (in mM) 100 CsCH₃SO₃ (Sigma-Aldrich, Munich, Germany), 60 CsCl (Merck), 5 lidocaine *N*-ethyl chloride (Sigma-Aldrich), 10 HEPES (Biomol, Hamburg, Germany), 0.2 EGTA (Sigma-Aldrich), 1 MgCl₂·6H₂O, 1 MgATP (Sigma-Aldrich), and 0.3 Na₃GTP (Sigma-Aldrich), dissolved in dH₂O (Wilson & Nicoll, 2001). The pH was adjusted to 7.3 with CsOH (Sigma-Aldrich).

For recording of sEPSCs, the solution contained (in mM) 130 CsCH₃SO₃, 5 CsCl, 0.5 EGTA, 2 MgATP, 10 HEPES, and 5 D(+)glucose-monohydrate dissolved in dH₂O. The pH was adjusted to 7.3 with CsOH.

Both intracellular solutions were stored at −20°C. Before usage, the intracellular solutions were filtered with a syringe filter (pore size 0.22 μm; Roth, Karlsruhe, Germany) and kept cool at 10 to 12°C.

Buffers for Affinity Chromatography For purification of the IgG with affinity chromatography, the buffers were either included in the MAbTrapTM Kit (GE Healthcare Bio-Sciences, Uppsala, Sweden) or self-made. The self-made binding buffer represented a phosphate buffer. The phosphate buffer was made by titration of 20 mM NaH₂PO₄ and 20 mM Na₂HPO₄ (Merck) to a pH of 7.0. The self-made elution buffer contained

0.1 M glycine (Sigma-Aldrich) [pH 2.7, adjusted with HCl (VWR)]. The self-made neutralization buffer contained Tris buffer (Sigma-Aldrich; pH 9.0, adjusted with HCl). The ACD-A solution contained 22 g/l sodium citrate, 24.5 g/l glucose-monohydrate, and 7.3 g/l citric acid. The ACD-A solution was obtained from the pharmacy of the Klinikum Schwabing (Munich, Germany).

RIPA Buffer and Extraction Buffer for Protein Extraction For protein extraction, a RIPA buffer was prepared including 50 mM Tris buffer (pH 7.4, adjusted with HCl), 150 mM NaCl, 1 mM EDTA (Sigma-Aldrich), 1% Triton[®]-X 100 (Sigma-Aldrich), and 0.1% SDS (Bio-Rad Laboratories Ltd., Hercules, CA, USA). The stock solution was frozen at -80°C . Before usage, proteinase inhibitors were added to the stock solution [970 μl RIPA buffer, 20 μl complete[™] (Roche Diagnostics, Indianapolis, IN, USA), 10 μl 100x PMSF (Sigma-Aldrich), and 1 μl Pepstatin A (1 mg/ml) (Sigma-Aldrich)]. RIPA buffer including proteinase inhibitors constituted the extraction buffer.

Buffers for Western Blots For Western Blots, a 10% acrylamid gel (≈ 20 ml) was prepared, including 6.65 ml 30% acrylamide/Bis (Bio-Rad Laboratories Ltd.), 5 ml Tris buffer (1.5 M, pH 8.8, adjusted with HCl), 200 μl 10% SDS, 10 μl TEMED (Serva, Heidelberg, Germany), 175 μl 10% APS (Serva), and 8.15 ml dH₂O. The running buffer contained (in mM) 25 Tris, 192 glycine (Sigma-Aldrich), and 3.47 SDS (Serva). The transfer buffer contained 25 mM Tris, 192 mM glycine, and 20% methanol (neoLab Migge Laborbedarf-Vertriebs GmbH, Heidelberg, Germany). TBS-T contained 100 mM Tris buffer (pH 7.5, adjusted with HCl), 154 mM NaCl, and 0.1% Tween[®] 20 (Sigma-Aldrich). For the blocking buffer, 5% skimmed milk powder (Roth) was added to TBS-T.

Drugs BIM (Sigma-Aldrich), a competitive antagonist of GABA_A receptors, was used at a concentration of 5 μM .

SMC hydrochloride, an inhibitor of the enzyme GAD, was used at a concentration of 0.5 or 2 mM and obtained from Sigma-Aldrich. Addition of SMC markedly lowered the pH level of ACSF if it was not saturated with carbogen. This effect, however, was buffered in carbogen-saturated ACSF so that the pH level remained stable at 7.4 during the course of experiments.

To isolate GABA_A Minis, the following drugs were used at the given final concentrations (in μM): 50 D-(-)-2-amino-5-phosphonopentanoic acid (D-AP5) [*N*-methyl-D-aspartat (NMDA) receptor antagonist], 5 1,2,3,4-tetrahydro-6-nitro-2,3-dioxo-benzo[*f*]-quinoxaline-7-sulfonamide (NBQX) disodium salt [α -amino-3-hydroxy-5-methyl-4-isoxazolepropionic acid (AMPA) receptor antagonist], and 1 tetrodotoxin (TTX) citrate (voltage-gated sodium channel antagonist). D-AP5, NBQX disodium salt and TTX were ob-

tained from Ascent Scientific (Avonmouth, Bristol, UK). The activity of these antagonists was tested for every new batch.

IgG Plasma filtrates of two SPS patients were a generous gift from Prof. Meinck (Heidelberg University Hospital, Heidelberg, Germany). Both patients were diagnosed according to their clinical symptoms following diagnostic guidelines (Lorish *et al.*, 1989) and showed high titers of Anti-GAD AAbs. The IgG fraction of both patients (SPS-IgG of patient 1 and 2) were purified with affinity chromatography and dissolved in ACSF after buffer exchange.

The commercially available Sandoglobulin[®] is pooled IgG of more than 1000 healthy donors and was obtained from CSL Behring (Bern, Switzerland). Even though Sandoglobulin[®] already contains the purified IgG fraction, it was again purified with affinity chromatography to achieve a better comparability to SPS-IgG. The IgG fraction of Sandoglobulin[®] was dissolved in ACSF after buffer exchange and used as control IgG.

For the experiments, all IgG fractions were used at a concentration of 40 mg/l, which represents the maximal IgG concentration in the CSF of healthy persons (Bouloukos *et al.*, 1980).

2.2 Purification of SPS-IgG and Control IgG

2.2.1 Purification of IgG with Affinity Chromatography

Plasma filtrate of two SPS patients was collected during therapeutic plasmapheresis. Plasmapheresis is a therapeutic approach used in treatment of autoimmune diseases, during which blood plasma including Abs is removed from the blood. As an autoimmune origin of SPS is supposed, plasma filtrate of SPS patients should also include specific AAbs. As the obtained plasma filtrates contained suspended solids, the plasma filtrate was filtered through a filter paper (595 1/2 folded filter; Schleicher & Schuell, Dassel, Germany). The filtered plasma filtrate was treated with ACD-A solution in a ratio of 1:3 to prevent coagulation. After 30 min, the plasma filtrate was centrifuged. The supernatant was filtered with a syringe filter (pore size 0.45 µm; Sarstedt, Nuernberg, Germany) and diluted in binding buffer (1:1).

SPS-IgG of patient 1 and 2 was purified from the supernatant using affinity chromatography. Affinity chromatography was performed with the MAbTrap[™] Kit or the HiTrap[™] Protein G HP (GE Healthcare Bio-Sciences). Both kits use the same columns packed with Protein G Sepharose[™] High Performance, except that the MAbTrap[™] Kit contained all buffers ready to use. Protein G trapped the IgG by binding to its FC region in a non-immune mechanism. The bound SPS-IgG was released from the entrapment

during elution. The purified IgG fraction of both SPS patients was dissolved in elution buffer and neutralization buffer, which neutralizes the pH level. The single steps of purification of the SPS-IgG followed the protocol enclosed by the manufacturer.

Sandoglobulin[®] was dissolved in binding buffer for affinity chromatography and treated in the same way as plasma filtrates. The obtained IgG fraction served as control IgG.

2.2.2 Buffer Exchange

The elution buffer, in which SPS-IgG and control IgG were dissolved after affinity chromatography, contained 0.1 mM glycine. As glycine acts as an inhibitory neurotransmitter, the elution buffer had to be replaced with ACSF. Therefore, the Vivaspin ultrafiltration spin columns (Vivaspin 6, 5,000 MWCO; Sartorius Stedim Biotech GmbH, Goettingen, Germany) were used, which contained a membrane only permeable for molecules smaller than 5 kDa. As the molecular mass of IgG is about 144 kDa, IgG could not pass the membrane.

The IgG solution was filled in Vivaspin columns and centrifuged (4500 U/min) at room temperature (RT; 23 to 25°C). The elution buffer including glycine, which was small enough to pass the membrane, was removed. The IgG, however, was retained and concentrated. Afterwards, the concentrated IgG solution was diluted with ACSF and again centrifuged. This procedure was repeated four times. In the first two cycles, about 50% of the fluid was exchanged. In the subsequent two cycles, about 66% of the fluid was replaced. In the end, about 97% of the elution buffer was exchanged with ACSF. For experiments, the IgG was further diluted to about 1:100. Therefore, it is unlikely that the remaining glycine influenced experiments.

2.2.3 Quantification of IgG Concentration

After buffer exchange, the concentration of the purified IgG was quantified in the department of clinical chemistry at the Max Planck Institute of Psychiatry. The IgG concentration was measured using nephelometry (BN-ProSpec[®] System; Siemens, Frankfurt am Main, Germany). This method measures the intensity of scattered light, which depends upon number, size, and surface characteristics of the particles. The concentration of the purified and buffer-exchanged IgG fractions ranged from about 2.5 g/l to 6 g/l.

2.3 Detection of Anti-GAD AAbs in Purified SPS-IgG

2.3.1 Purification of Mouse Brain Proteins

Brains of male C57Bl/6J mice obtained from Charles River Laboratories (Sulzfeld, Germany) were quick-frozen in liquid nitrogen immediately after preparation and stored at -80°C until usage. Next, brain proteins were purified using the Sample Grinding Kit (GE Healthcare Bio-Sciences) in combination with RIPA buffer. Briefly, 100 mg tissue were homogenized with 300 μl extraction buffer. The homogenized tissue was centrifuged for 30 min at 4°C (13000 U/min) and the supernatant including dissolved brain proteins was collected in a new tube.

Next, the protein concentration of the supernatant was determined using the DCTM Protein Assay (Bio-Rad Laboratories Ltd.) according to the Lowry assay (Lowry *et al.*, 1951). A standard curve for protein concentration determination was made using the Protein Assay Standard II (Bio-Rad Laboratories Ltd.). The protein concentration of our samples was determined by means of this standard curve (Dynatech MR7000 Plate Reader; Dynatech Laboratories, VA, USA).

2.3.2 Western Blots

To investigate whether Anti-GAD AAbs were present in purified SPS-IgG of patient 1 or 2, a special kind of Western Blotting using the Surf Blot approach was performed. The Surf Blot approach allows to test simultaneously several Abs on a single sheet of nitrocellulose paper by clamping liquid channels onto the surface of the blot. The Surf Blot system was obtained from Idea Scientific Company (Minneapolis, MN, USA).

A 10% acrylamide gel was poured into a CriterionTM Cassette (Bio-Rad Laboratories Ltd.). 300 μg of the extracted brain proteins were filled up to 150 μl with Laemmli Sample Buffer (Bio-Rad Laboratories Ltd.). Additionally, 15 μl NuPAGE[®] Sample Reducing Agent (10X) (Invitrogen, Carlsbad, CA, USA) was added. Proteins were denatured at 85°C for 5 min. The denatured proteins were loaded on the gel. The left lane was loaded with 5.5 μl Precision Plus Protein All Blue Standards (10 to 250 kDa; Bio-Rad Laboratories Ltd.), which served as marker. To separate the brain proteins, the gel was run at 200 V for about 1 h in running buffer. Afterwards proteins were blotted to a nitrocellulose membrane (pore size 0.45 μm ; GE Healthcare Bio-Sciences) at 100 V for 1 h in cooled transfer buffer. Afterwards, the membrane was washed with TBS-T and incubated in blocking buffer on a shaker over night at 4°C . Next day, the membrane was again washed three times with TBS-T and clamped into the Surf Blot system.

SPS-IgG of patient 1 and 2 as well as control IgG were diluted 1:30 and 1:60 in blocking buffer. The polyclonal GAD₆₅ and GAD₆₅ + GAD₆₇ Abs (ab49830 and ab11070; abcam, Cambridge, UK) were diluted 1:200 and 1:400 in blocking buffer. The diluted primary Abs/AAbs were added to the single channels of the Surf Blot system and incubated for 2 h at RT and 30 min at 4°C under continuous shaking. Afterwards, the membrane was washed three times with TBS-T for 10 min. Peroxidase-conjugated goat anti-human IgG Ab (1:10000 diluted in TBS-T; Sigma-Aldrich) was used as secondary Ab for SPS-IgG and control IgG. Peroxidase-conjugated donkey anti-rabbit IgG Ab (1:8000 diluted in TBS-T; GE Healthcare Bio-Sciences) was used as secondary Ab for the polyclonal GAD₆₅ and GAD₆₅+ GAD₆₇ Abs. The secondary Abs were incubated for 1.5 h at RT under continuous shaking. The membrane was washed three times with TBS-T and one time with dH₂O. Afterwards, ECLTM solution (GE Healthcare Bio-Sciences) was added for 2 min. A film (Fuji medical x-ray film; Fujifilm Europe GmbH, Duesseldorf, Germany) was put onto the membrane and developed in the darkroom.

2.3.3 GAD-Dot

To distinguish whether the purified SPS-IgG contained both GAD isoforms, GAD₆₅ and GAD₆₇, a GAD Dot (GA GENERIC ASSAYS GmbH, Dahlewitz, Germany) was performed, which followed the same principle as an enzyme-linked immunosorbent assay (ELISA). A color reaction indicated the presence of GAD₆₅ or GAD₆₇ AAbs in SPS-IgG. The single steps of the GAD Dot followed the protocol enclosed by the manufacturer.

2.4 Preparation of Mouse Brain Slices

2.4.1 Animals

Adult male C57Bl/6J mice and adult male Balb/cOlaHsd mice (Harlan Winkelmann GmbH; Borchon, Germany) were used for experiments. For IOS recordings, the age of animals ranged from five to nine weeks. For patch-clamp recordings, the age of animals ranged from five to eight weeks. Adult animals were chosen for several reasons. During adolescence, neuronal networks run through maturation processes refining GABA synthesis and function. A significant contribution of GAD₆₅ to total GABA content in several brain areas has been shown during early postnatal development (Hensch *et al.*, 1998), whereas in adult animals basal GABA concentration is provided by GAD₆₇ rather than GAD₆₅ (Erlander & Tobin, 1991; Esclapez *et al.*, 1994; Hensch *et al.*, 1998; Patel *et al.*, 2006). Moreover, during embryogenesis and the first week of postnatal life GABA acting via GABA_A receptors serves as an excitatory neurotransmitter due to an inverted

Cl⁻ gradient in neurons (Ben-Ari *et al.*, 1997). The animals of different experimental groups were matched according to their age to exclude the age of animals as a source of error.

2.4.2 Preparation of Coronal Brain Slices

Mice were anesthetized with isoflurane (Abbott Deutschland, Wiesbaden, Germany) before decapitation with an animal guillotine. The skull was removed by cutting from the *foramen magnum* to the forehead on both sides of the skull at the height of the basal surface of the brain with fine scissors. An additional cut between both hemispheres was made. Now the skull was carefully removed with a forceps and put aside. Using this method, the cortex of both hemispheres remained unharmed. The cleared brain was detached with a spatula and immediately cooled in chilled ACSF (4 to 6°C) saturated with carbogen. Cooling down the brain tissue reduced the metabolic rate of cells and, hence, their energy consumption, which allowed cells to survive the hypoxic period during brain slice preparation.

The brain was now put on a plexiglas dish with a filter paper (Whatman, Maidstone, Kent, UK) soaked with cooled ACSF. The filter paper prevented the brain tissue from sliding during the following dissection. With the brain lying on its basal surface, the cerebellum was removed with a razor blade (Dreaging Men; Goldhand Vertriebsgesellschaft, Duesseldorf, Germany) in an angle of 90° to obtain a plain surface. The brain was then turned by 90° so that it came to lie on the cutting plane. In this orientation, the brain was glued to the slicing stage with Histoacryl[®] (Braun). To additionally stabilize the tissue, the basal surface of the brain was leaned on an agar block (5% Agar-Agar; Roth; 0.9% NaCl), which was also glued on the slicing stage with Histoacryl[®].

The slicing stage was now mounted to the dish of the vibratome (HM 650 V; Microm international GmbH, Walldorf, Germany). The dish was filled with chilled and carbogenated ACSF, in which the brain was submerged and further cooled. Brain slices of a thickness of 300 µm (for IOS recordings) or 450 µm (for patch-clamp recordings) were made in the coronal plane with a razor blade, which was previously cleaned with ethanol and acetone to remove its oily film. Brain Slices, which included the motor cortex according to a mouse brain atlas (Paxinos & Franklin, 2001) were transferred with a Pasteur pipette into a storage beaker. The storage beaker was filled with carbogenated ACSF placed in a heating bath (GFL - Gesellschaft fuer Labortechnik mbH, Burgwedel, Germany) at a temperature of 34°C. The brain slices were carefully mounted onto a net, which was positioned halfway into the beaker and allowed both sides of the brain slices to be supplied with ACSF. This improved the support of brain slices with oxygen and nutrients and prevented the brain slices to adhere to the glass wall.

Such an incubation is known to help brain slices to recover from the preparation procedure. For recording of IOSs, the brain slices were kept for 30 min in the heating bath and additionally stored for 30 min at RT. For patch-clamp recordings, the brain slices were kept for 120 min in the heating bath and subsequently for 30 min at RT. As the patch-clamp recordings required preincubation of the brain slices with the accordant substances, these substances (2 mM SMC; 40 mg/ml SPS-IgG of patient 1 or 2; 40 mg/ml control IgG) were added to the ACSF in the storage beaker directly after brain slice preparation. Control brain slices were equally treated, but no IgG or drug was added.

2.5 IOS Recordings

IOSs were recorded using an upright microscope (Zeiss Axioskop 2 FS; Zeiss, Oberkochen, Germany) with a 2.5x Neofluar objective (N.A. 0.075). A dipping cone with a transparent cover slip was mounted on the objective and placed in the bath solution to avoid disturbing reflections at the water-air interface. The brain tissue was illuminated with a 20 W halogen lamp (Xenophot[®]; Osram, Augsburg, Germany). The light source was stabilized by the power supply (NAG stab.; Zeiss), which buffered voltage peaks of the mains supply. An optical band-pass filter (λ_{max} 780±50 nm) was inserted into the light beam to illuminate the brain slice in the near IR spectrum. A second light filter with an identical cut-off frequency was placed in the light path below the tube lens to block stray light owing to ambient illumination. The brain slice was put in the recording chamber and continuously superfused (flow rate 2 to 3 ml/min) with carbogenated ACSF by means of a peristaltic pump (Ismatec Reglo; ISMATEC SA, Labortechnik - Analytik, Glattbrugg, Switzerland). The brain slices were fixed with a grid, a platinum frame stringed with nylon thread. The ACSF was heated to 34°C with a temperature controller (TC01; Multi Channel Systems MCS GmbH, Reutlingen, Germany). Two sets of micromanipulators (Luigs & Neumann GmbH, Ratingen, Germany) allowed to move the stimulation electrode and the microscope independently from each other in all three spatial directions. Fig. 2.1 shows the main components of the IOS setup.

For electrical stimulations, a stimulator (Isolated Pulse Stimulator, Model 2100; A-M Systems, Inc., Carlsborg, WA, USA) and a monopolar tungsten electrode (Catalog# UEWLEFSEANNE; FHC, Bowdoin, ME, USA) were used. The electrode was placed at the border between white matter and cortical layer VI. Two stimulus protocols were used (100 square pulse stimuli at 50 Hz and 20 square pulse stimuli at 100 Hz). The width of stimuli was 0.2 ms. The stimulation current, which varied between 75 and 200 μ A, was adjusted in a way to trigger IOSs of about 500 to 700 μ m width and non-saturated signal intensities. IOSs were visualized using a self-made program written with Igor

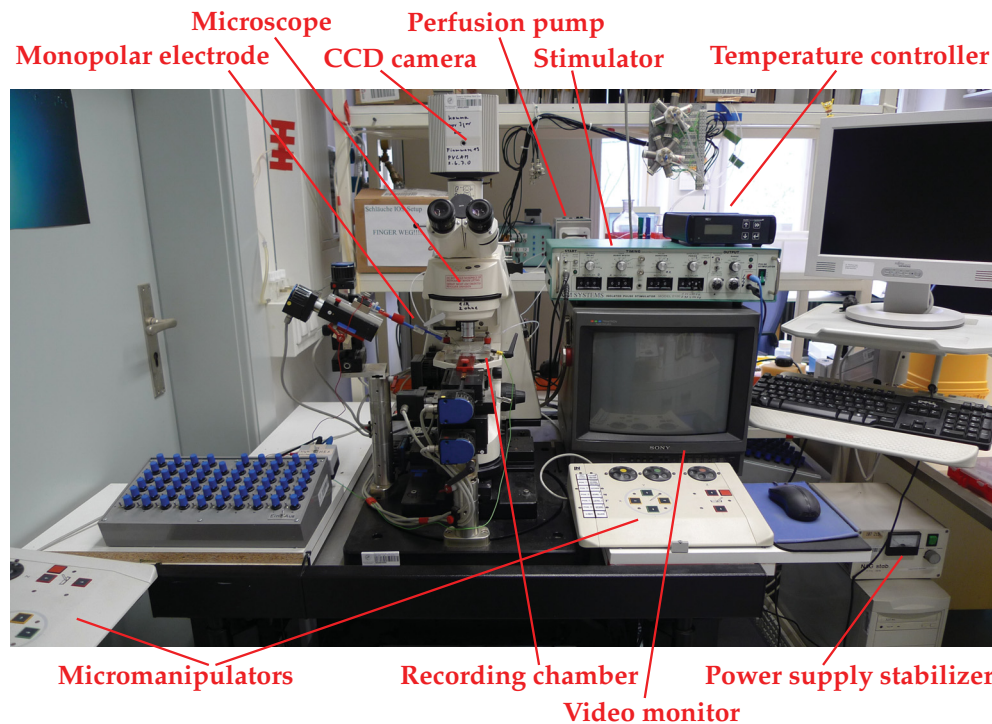


Figure 2.1: Labeled picture with the major components of the IOS setup.

programming language (Igor Pro, version 5.0; WaveMetrics, Inc., Lake Oswego, OR, USA).

The imaging system consisted of a scientific grade 12-bit charge-coupled device (CCD) camera (CoolSnapTM cf; Photometrics, Tucson, AZ, USA). Images were recorded with a 2x2 binning, which reduced the number of pixels from 1392 x 1040 pixels to 696 x 520 pixels. Just before electrical stimulation, ten images were recorded to define the baseline light intensity under resting conditions. After onset of stimulation, images were recorded at 4 Hz for 60 s. The images were stored as uncompressed 16-bit TIFF-files on a PC for further analysis.

Prior to IOS recordings, the brain slices were put in the recording chamber and equilibrated for about 30 min. The recirculation volume was 88 ml, including the volume of tubing. Brain slices were stimulated every 5 min until a stable baseline of six IOSs was achieved. Afterwards, the recirculation was changed to ACSF containing either drug-free ACSF for control experiments (sham-drug application) or 0.5 mM or 2 mM SMC, 40 mg/l SPS-IgG of patient 2 or 40 mg/l control IgG. For the application of IgG, all solutions were filtered with a syringe filter (pore size 0.45 μm). An additional filter (595 1/2 folded filter) was inserted in the perfusion system to catch aggregations of Abs and cell waste, as these particles disturbed IOS recordings. A change from ACSF recircula-

tion to open ACSF superfusion was not possible as the amount of SPS-IgG was limited. Stimulation of brain slices (every 5 min) was continued for additional 30 min for control experiments and SMC application and for 70 min for application of SPS-IgG and control IgG. Afterwards, the stimulation protocol was changed. From now on, brain slices were stimulated three times at every full hour after the beginning of drug application with an interstimulus interval of 5 min. As a strong stimulus was necessary to trigger IOSs, this lower number of stimuli presumably helped to maintain the vitality of the brain slice and to reduce a possible run-down of IOSs during long-term measurements. For wash-out, brain slices were superfused with fresh, drug-free ACSF in an open system and stimulated 30, 40, 50, and 60 min after wash-out started.

2.6 Analysis of IOSs

For data analysis, a program was developed in cooperation with Max Sperling (Max Planck Institute of Neurobiology, Martinsried) using the software MATLAB[®] (The MathWorks, Natick, MA, USA). The data analysis software is described in more detail in chapter 3.1 "Analyzing IOSs and Long-term IOS Recording", page 31.

Briefly, a 2x2 binning of images was performed, which reduced the number of pixels from 696 x 520 to 348 x 260 pixels. After the binning process, the size of one pixel was 14 x 14 μm . Subsequently, images were filtered with a moving spatial average filter (filter window size 10). The ten images taken before stimulation were averaged after the binning and filtering process. The resulting single image represented the baseline light intensity of the brain slice under resting conditions. Now $\Delta F/F$ calculation $[(F - F_0)/F_0]$ was applied with F representing the light intensity of one pixel after stimulation and F_0 the baseline light intensity of the same pixel under resting conditions. The resulting values were multiplied by 100 to obtain the percent change in light intensity.

A region of interest (ROI), in which the IOS was supposed, was automatically detected. For that purpose, a maximum intensity projection of all 240 $\Delta F/F$ -processed images was computed, in which the value of every pixel was set to its maximal change in light intensity observed after stimulation by scanning all 240 images. Now, the maximum intensity projection was binary-coded by setting pixels with changes in light intensity above the threshold of 0.75% to 1 and pixels with changes in light intensity equal or below the threshold to 0. On this binary image, a morphological opening with a structuring element in the form of a disk (radius ten pixels) was applied, which smoothed the borders of the signals. For objects larger than 300 pixels the center of mass was assigned. The object with its center of mass closest to the center of the image was defined as ROI.

Data sets, in which the automatic ROI detection failed, were excluded from further analysis.

To examine the time course of the IOS, the ROI was applied to every single $\Delta F/F$ -processed image. Within the ROI, all pixels above threshold level were detected. The number of detected pixels displayed the area of the IOS (= signal area). The values of the changes in light intensity of the detected pixels were averaged. The mean percental change in light intensity displayed the intensity of the IOS (= signal intensity). To examine changes in signal intensity and signal area, the maximum of both parameters were determined. To analyze the time course of the signal intensity, the rise time and decay time were calculated. The rise time was defined by the time period, during which the signal intensity reached its maximal amplitude after onset of stimulation. To compare the speed of signal intensity decay, the time period, during which the signal amplitude decreased from its maximum value to 80% of its maximum, was calculated. IOSs, which showed a clear upward trend in their signal traces, were discarded.

2.7 Patch-Clamp Recordings

Patch-clamp recordings were performed from layer II/III pyramidal neurons of the mouse motor cortex. Suitable neurons (tight cells with smooth membranes) were identified using an IR microscope (Zeiss Axioskop; Zeiss). The brain slices were placed into a submerged chamber and fixed with a grid. The chamber was superfused (flow rate 2 to 3 ml/min) with carbogenated ACSF using a perfusion pump (Ismatec Reglo). Recordings were conducted at RT. A total volume of 20 ml ACSF was recirculated.

A set of micromanipulators (Luigs & Neumann GmbH) allowed the recording chamber, the microscope, and the patch pipette to be independently moved in all three spatial directions to obtain maximal flexibility during the patch-clamp process. For patch-clamp recordings, borosilicate glass pipettes (Harvard apparatus, Edenbridge, Kent, UK) with an inner diameter (I.D.) of 0.86 mm and an outer diameter (O.D.) of 1.5 mm were used. Patch pipettes (open tip resistance 2 to 5 M Ω) were pulled and heat-polished with a horizontal puller (DMZ Puller; Zeitz, Martinsried, Germany), filled with intracellular solution, and electrically connected to an intracellular amplifier (SEC 10L; npi electronic GmbH, Tamm, Germany) via a silver chloride (AgCl)-coated silver electrode. The amplifier worked according to the principle of discontinuous single-electrode voltage-clamp (dSEVC), which means that the amplifier periodically switches between voltage metering and injection of compensatory current. An Ag/AgCl pellet within the bath served as reference electrode. The electrical signals were low-pass filtered at 1 kHz, digitized with an analog/digital digital/analog (AD/DA) converter (ITC 16; HEKA Elektronik

Dr. Schulze GmbH, Lambrecht/Pfalz, Germany) and stored with the software Pulse (version 8.5, HEKA Elektronik Dr. Schulze GmbH) running on a Macintosh computer.

After establishing a seal (in the range of 1 G Ω) between the tip of the pipette and the cytoplasmic membrane of the neuron, electrical access to the neuron was achieved by rupturing the cell membrane. This whole-cell configuration was used to measure the electrical activity of the neurons. Recordings of the resting membrane potential (RMP) were performed in bridge mode, all other recordings were conducted in voltage-clamp mode (holding potential -60 mV). After establishing the whole-cell configuration, 15 min elapsed before postsynaptic currents were recorded to allow a complete equilibration of the cytoplasm with the intracellular solution in the pipette. From every neuron under investigation, GABA_A Minis were recorded for 5 min and sEPSCs, due to their lower frequency, were recorded for 10 min.

To record GABA_A Minis, the NMDA receptor antagonist D-AP5 (50 μ M), the AMPA receptor antagonist NBQX (5 μ M), and the voltage-gated sodium channel blocker TTX (1 μ M) were added to the bath solution at the concentrations quoted in brackets. The remaining postsynaptic currents could be ascribed to be GABA_A receptor mediated. Control experiments showed that the remaining postsynaptic currents could completely be abolished by the addition of the GABA_A receptor antagonist BIM (10 μ M) to the bath solution. To warrant that the drugs unfolded their full potential, brain slices were incubated in the recording chamber for at least 15 min before recordings were started. As a "high-chloride" intracellular solution was used for recording GABA_A Minis, activation of the GABA_A receptor mediated negative currents, which are defined as inward currents. For recording sEPSCs, which could be attributed to both spontaneous action potential-dependent and -independent presynaptic release of excitatory neurotransmitters, no blockers were added to the ACSF. As physiological intracellular solution was used in these experiments, sEPSCs also appeared as inward currents. Depending on the experimental setting, 2 mM SMC, 40 mg/l control IgG or 40 mg/l SPS-IgG of patient 1 or 2 were additionally added to the recirculated ACSF. As GABA_A Minis and sEPSCs were compared between different groups of treatment, the age of animals and the "age of cells" (= time period between the end of the brain slice preparation and the beginning of a given whole-cell recording) were matched.

2.8 Analysis of Patch-Clamp Experiments

For data analysis, only neurons, whose RMP was between -40 and -75 mV, were included. As the serial resistance quantifies the quality of the electrical access to the cell and, hence, influences the recording of postsynaptic currents, neurons, in which the se-

rial resistance changed by more than 15% during the recording, were discarded. The serial resistance was specified by means of voltage steps (-10 mV, 100 ms). The amplitude of the fast transient was measured as an approximation of serial resistance. During recording of sEPSCs, paroxysmal depolarization shifts (PDSs), which are inward currents in the range of a few nA, or action potentials were observed in few cells. As the recorded sEPSCs were in the range of a few pA, including PDSs and action potentials would falsify the mean amplitude. Therefore, cells, which showed PDSs or action potentials during the recording time, were discarded. Moreover, cells with noisy current traces, in which GABA_A Minis or sEPSCs could not be distinguished from noise, were not included in further analysis.

The software Mini Analysis (version 6.0.9; Synaptosoft Inc., Fort Lee, NJ, USA) was used for data analysis. The sEPSC traces were filtered with a low-pass Butterworth filter (cut-off frequency 200 Hz). The GABA Mini traces were not filtered. To separate signals from noise, a threshold had to be defined. The threshold was set to five times of the root mean square (RMS) noise (calculation of the RMS noise is described on page 41). The RMS noise of GABA Mini traces was 1.04 ± 0.06 pA and, therefore, the threshold was set to 5 pA. The RMS noise of sEPSC traces was 0.8 ± 0.05 pA and the threshold was set to 4 pA. To quantify GABA_A Minis and sEPSCs, their mean amplitude and frequency was calculated.

2.9 Statistics

Statistical analysis was performed using SigmaStat (version 3.5; Systat Software, Inc., Point Richmond, CA, USA). The data were tested for normal distribution. If the data were normally distributed, a paired Student's t-test or unpaired Student's t-test was used. Otherwise a Mann-Whitney rank sum test or a Wilcoxon signed rank test was performed. Statistical significance was achieved, if the p value was equal or less than 0.05. Mean values are given with the corresponding standard error of the mean (SEM).

2.10 Index

Animals

Balb/cOlaHsd mice
C57Bl/6J mice

Harlan Winkelmann GmbH, Borchon, Germany
Charles River Laboratories, Sulzfeld, Germany

Chemicals

10% APS	Serva, Heidelberg, Germany
10% SDS	Bio-Rad Laboratories Ltd., Hercules, CA, USA
30% acrylamide/Bis	Bio-Rad Laboratories Ltd., Hercules, CA, USA
50x complete	Roche Diagnostics, Indianapolis, IN, USA
100x PMSF	Sigma-Aldrich, Munich, Germany
ACD-A solution	Klinikum Schwabing, Munich, Germany
Agar-Agar	Roth, Karlsruhe, Germany
BIM	Sigma-Aldrich, Munich, Germany
CsCH ₃ SO ₃	Sigma-Aldrich, Munich, Germany
CaCl ₂ *2H ₂ O	Merck, Darmstadt, Germany
CsCl	Merck, Darmstadt, Germany
CsOH	Sigma-Aldrich, Munich, Germany
D-AP5	Ascent Scientific, Avonmouth, Bristol, UK
DC TM Protein Assay	Bio-Rad Laboratories Ltd., Hercules, CA, USA
D(+)-glucose-monohydrate	Merck, Darmstadt, Germany
dH ₂ O/Aqua ad iniectabilia	Braun, Melsungen, Germany
ECL TM solution	GE Healthcare Bio-Sciences, Uppsala, Sweden
EDTA	Sigma-Aldrich, Munich, Germany
EGTA	Sigma-Aldrich, Munich, Germany
GAD ₆₅ Ab (ab49830)	abcam, Cambridge, UK
GAD ₆₅ + GAD ₆₇ Abs (ab11070)	abcam, Cambridge, UK
GAD Dot	GA GENERIC ASSAYS GmbH, Dahlewitz, Germany
Glycine	Sigma-Aldrich, Munich, Germany
HCl	VWR, Darmstadt, Germany
HEPES	Biomol, Hamburg, Germany
Histoacryl [®]	Braun, Melsungen, Germany
Isoflurane	Abbott Deutschland, Wiesbaden, Germany
KCl	Merck, Darmstadt, Germany
Laemmli Sample Buffer	Bio-Rad Laboratories Ltd., Hercules, CA, USA
Lidocaine <i>N</i> -ethyl chloride	Sigma-Aldrich, Munich, Germany
MABTrap TM Kit	GE Healthcare Bio-Sciences, Uppsala, Sweden
Methanol	neoLab Migge Laborbedarf-Vertriebs GmbH, Heidelberg, Germany
MgATP	Sigma-Aldrich, Munich, Germany
MgCl ₂ *6H ₂ O	Merck, Darmstadt, Germany
NaCl	VWR, Darmstadt, Germany
Na ₃ GTP	Sigma-Aldrich, Munich, Germany
NaHCO ₃	Merck, Darmstadt, Germany
NaH ₂ PO ₄ *H ₂ O	Merck, Darmstadt, Germany
Na ₂ HPO ₄ *H ₂ O	Merck, Darmstadt, Germany
NBQX disodium salt	Ascent Scientific, Avonmouth, Bristol, UK

NuPAGE [®] Sample Reducing Agent (10X)	invitrogen, Carlsbad, CA, USA
Pepstatin A	Sigma-Aldrich, Munich, Germany
Peroxidase-conjugated donkey anti-rabbit IgG Ab	GE Healthcare Bio-Sciences, Uppsala, Sweden
Peroxidase-conjugated goat anti-human IgG Ab	Sigma-Aldrich, Munich, Germany
Plasma filtrate of SPS patients	Prof. Meinck, Heidelberg University Hospital, Heidelberg, Germany
Precision Plus Protein All Blue Standards	Bio-Rad Laboratories Ltd., Hercules, CA, USA
Protein Assay Standard II	Bio-Rad Laboratories Ltd., Hercules, CA, USA
Sample Grinding Kit	GE Healthcare Bio-Sciences, Uppsala, Sweden
Sandoglobulin [®]	CSL Behring, Bern, Switzerland
SDS	Serva, Heidelberg, Germany
Skimmed milk powder	Roth, Karlsruhe, Germany
Sodium phosphate	Merck, Darmstadt, Germany
SMC hydrochloride	Sigma-Aldrich, Munich, Germany
TEMED	Serva, Heidelberg, Germany
Tris	Sigma-Aldrich, Munich, Germany
Triton [®] -X 100	Sigma-Aldrich, Munich, Germany
TTX citrate	Ascent Scientific, Avonmouth, Bristol, UK
Tween [®] 20	Sigma-Aldrich, Munich, Germany

Consumable Supplies

595 1/2 folded filter	Schleicher & Schuell, Dassel, Germany
Borosilicate glass pipettes (0.86 mm I.D., 1.5 mm O.D.)	Harvard apparatus, Edenbridge, Kent, UK
Criterion [™] Cassette	Bio-Rad Laboratories Ltd., Hercules, CA, USA
Dreaming Men razor blade	Goldhand Vertriebsgesellschaft, Duesseldorf, Germany
Filter paper	Whatman, Maidstone, Kent, UK
Fuji medical x-ray film	Fujifilm Europe GmbH, Duesseldorf, Germany
HiTrap [™] Protein G HP	GE Healthcare Bio-Sciences, Uppsala, Sweden
Monopolar tungsten electrode (Catalog# UEWLEFSEANNE)	FHC, Bowdoin, ME, USA
Nitrocellulose membrane (pore size 0.45 µm)	GE Healthcare Bio-Sciences, Uppsala, Sweden
Surf Blot System	Idea Scientific Company, Minneapolis, MN, USA
Syringe filter (pore size 0.22 µm)	Roth, Karlsruhe, Germany
Syringe filter (pore size 0.45 µm)	Sarstedt, Nuernberg, Germany
Vivaspin ultrafiltration spin columns (Vivaspin 6, 5,000 MWCO)	Sartorius Stedim Biotech GmbH, Goettingen, Germany
Xenophot [®] halogen lamp (20 W)	Osram, Augsburg, Germany

2 Materials and Methods

Equipment

BN-ProSpec [®] System	Siemens, Frankfurt am Main, Germany
CoolSnap [™] cf CCD camera	Photometrics, Tucson, AZ, USA
DMZ puller	Zeitz, Martinsried, Germany
Dynatech MR7000 Plate Reader	Dynatech Laboratories, Chantilly, VA, USA
Heating bath	GFL - Gesellschaft fuer Labortechnik mbH, Burgwedel, Germany
Ismatec Reglo	ISMATEC SA, Labortechnik - Analytik, Glattbrugg, Switzerland
Isolated Pulse Stimulator, Model 2100	A-M Systems, Inc., Carlsborg, WA, USA
ITC 16 AD/DA-converter	HEKA Elektronik Dr. Schulze GmbH, Lambrecht/Pfalz, Germany
Micromanipulators	Luigs & Neumann GmbH, Ratingen, Germany
NAG stab. power supply	Zeiss, Oberkochen, Germany
SEC 10L intracellular amplifier	npi electronic GmbH, Tamm, Germany
TC01 temperature controller	Multi-Channel Systems MCS GmbH, Reutlingen, Germany
Vibratome (HM 650 V)	Microm international GmbH, Walldorf, Germany
Zeiss Axioskop	Zeiss, Oberkochen, Germany
Zeiss Axioskop 2 FS with 2.5x Neofluar objective (N.A. 0.075)	Zeiss, Oberkochen, Germany

Software

Igor Pro, version 5.0	WaveMetrics, Inc., Lake Oswego, OR, USA
MATLAB [®]	The MathWorks, Natick, MA, USA
Mini Analysis, version 6.0.9	Synaptosoft Inc., Fort Lee, NJ, USA
Pulse, version 8.5	HEKA Elektronik Dr. Schulze GmbH, Lambrecht/Pfalz, Germany
SigmaStat, version 3.5	Systat Software, Inc., Point Richmond, CA, USA

3 Results

3.1 Analyzing IOSs and Long-term IOS Recording

3.1.1 Data Acquisition

One goal of the present work was to study the spread of stimulus-evoked neuronal network activity within the mouse motor cortex. To monitor network activity, IOS recordings, which represents an optical method to measure neuronal activity via altered light transmission based on activity-dependent cell volume changes, were performed. To elicit IOSs in cortical columns of mouse motor cortex, a monopolar tungsten stimulation electrode was placed at the border of layer VI/white matter in coronal mouse brain slices for extracellular stimulation (fig. 3.1).

Electrical stimulation triggered neuronal activity in a cortical column, which resulted in an increased light transmittance of the activated tissue. As a consequence, the light intensity of the activated cortical column rose and the column appeared brighter compared to its resting conditions. Such changes in light intensity represent IOSs. To detect IOSs, the light intensity after stimulation has to be related to baseline levels before stimulation (see page 34). For this purpose, ten images were taken before stimulation and defined as the baseline light intensity of the brain slice under resting conditions. With the onset of stimulation, 240 images were acquired at a frequency of 4 Hz.

During data acquisition, a 2x2 binning was performed for every image by the CCD camera. This means that the charge of four adjacent potential wells, which was proportional to the light intensity at this location, was summed up. This step resulted in one larger and brighter pixel. This calculation reduced the resolution from 1392 x 1040 pixels to 696 x 520 pixels. One advantage of binning is an improved signal-to-noise ratio. This was important as high noise levels disturbed the analysis of IOSs (see fig. 3.3, page 35). Additionally, binning reduces data size, which allows faster readout speeds and, therefore, higher frame rates. The reduced data size also accelerated the subsequent computer-based analysis of the IOSs. These benefits, however, come at the expense of spatial resolution. As IOSs were investigated in a whole cortical column, resolving small structures was of minor importance and this reduction in resolution was acceptable.

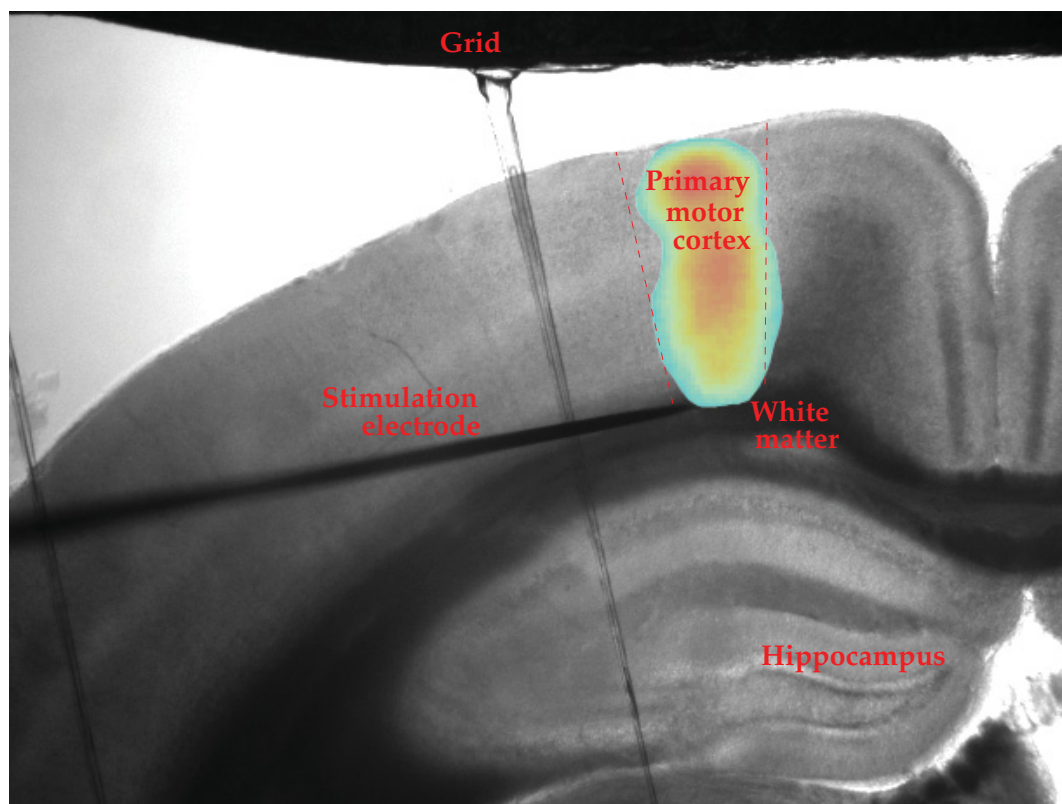


Figure 3.1: **Labeled transmission image of a coronal mouse brain slice.** The image shows a transmission image of a coronal mouse brain slice with an extracellular stimulation electrode positioned at the border of layer VI/white matter and the estimated area of the primary motor cortex. A color-coded image of an IOS was overlaid to show the typical spatial extent of IOSs. The grid served to fix the brain slice in the recording chamber.

3.1.2 Development of a Data Analysis Program for IOSs

For analyzing IOSs, a new data analysis program was developed in cooperation with Max Sperling (Max Planck Institute of Neurobiology, Martinsried). The program code was written in MATLAB[®], a software using the matrix laboratory programming language.

3.1.2.1 Binning and Filtering

The light intensity after brain slice stimulation rose just a few percent above baseline levels (fig. 3.2, fig. 3.3, A). Thus, noise, which is generated by random spatial and temporal fluctuations in pixel light intensity, independent of external stimuli, strongly impaired the analysis of stimulus-induced IOSs. The following data processing caused the spatial noise of single pixels in one image to be averaged out.

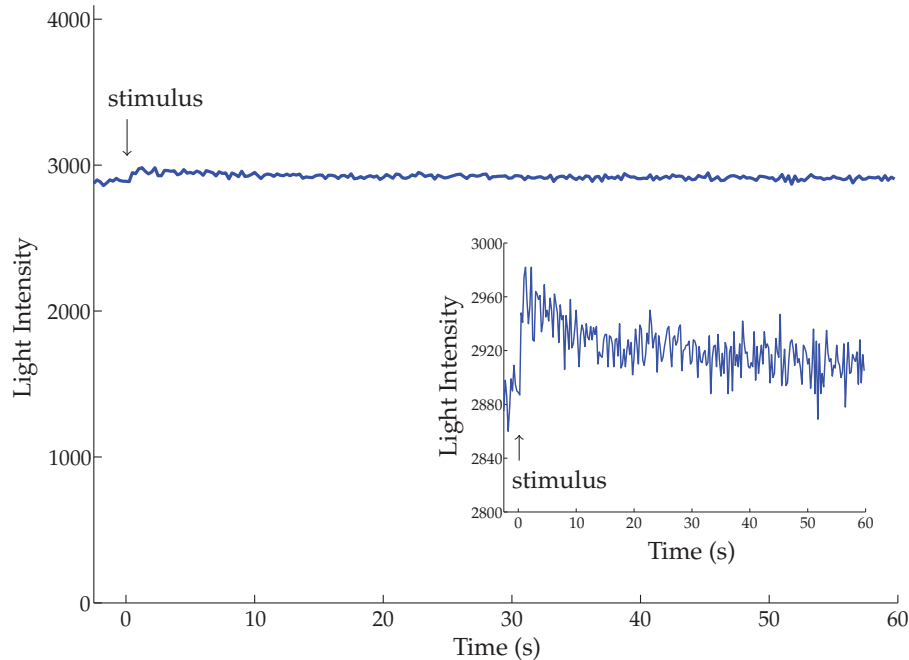


Figure 3.2: **Temporal changes in light intensity after stimulation.** The trace shows the temporal changes in light intensity of one pixel after stimulation. Light intensity rose just a few percent above baseline levels. To show the small changes in light intensity, a magnification of the trace was inserted. The arrows mark the onset of stimulation.

Binning of adjacent pixels done by the CCD camera during data acquisition was the first step to reduce noise level (see page 31). To further improve the signal-to-noise ratio, a second 2x2 binning of images was performed by the data analysis program (fig. 3.3, B). The binning procedure of the analysis program, however, differed from the binning done by the CCD camera. Compared to the binning of the camera, where the light intensity of four pixels was just summed up, the data analysis program performed an average binning. Here, the light intensity of four adjacent pixels was summed up and thereafter divided by four, resulting in one larger pixel with the average light intensity of the previous ones. This step reduced the resolution from 696 x 520 to 348 x 260 pixels. In principle, it would be possible to perform a 4x4 binning of the recorded images solely with the CCD camera during data acquisition, which would result in the same reduction in spatial resolution and noise. The summation of the light intensity of too many pixels, however, bears the risk to reach saturation levels of the camera. To avoid this, the data binning process was split between CCD camera and data analysis program.

Afterwards, a moving spatial average filter with a filter window size of ten pixels was applied to reduce noise and to smooth the signal (fig. 3.3, C). The later was important

for the automatic detection of IOSs (see page 43). For this filtering procedure, the data analysis program computed the sum of all pixels within the filter window, divided the sum by the number of summed pixels, and wrote the calculated value in the center pixel of the filter window. Afterwards, the filter window was shifted by one pixel and the computation was repeated step by step for every pixel in the image. Compared to a Gaussian filter, the moving spatial average filter has a slightly worse performance, but a markedly decreased computation time.

As it was of particular importance to keep the noise level of the baseline light intensity as low as possible (see table 3.2, page 38), the ten images taken before stimulation were additionally averaged after the binning and filtering process to reduce temporal noise, too. The resulting single image represented the baseline light intensity of the brain slice under resting conditions.

3.1.2.2 $\Delta F/F$ Calculation

During enhanced neuronal activity, more light was transmitted through the brain tissue, which caused an increase in light intensity of the corresponding pixels in the recorded images. Therefore, active regions after stimulation appeared brighter compared to their baseline levels before stimulation. To calculate changes in light intensity, which represented IOSs, the $\Delta F/F$ calculation was applied:

$$\Delta F/F = \frac{F - F_0}{F_0} \quad (3.1)$$

F represents the light intensity of one pixel after stimulation and F_0 the baseline light intensity of the same pixel under resting conditions. The $\Delta F/F$ calculation was applied to every pixel of the image. As during neuronal activity the light transmittance of brain tissue rose and, thus, the light intensity of the recorded pixels, in active areas the result of $F - F_0$ was bigger than zero. To illustrate the time course of changes in light intensity elicited by a stimulus, the $\Delta F/F$ calculation was repeated for each image taken after stimulation (figs. 3.4, 3.5). The resulting values were multiplied by 100 to obtain the percent change in light intensity relative to baseline light intensity.

F_0 in the denominator served to normalize data with regard to their baseline light intensity. This step was crucial, as the absolute changes in light intensity ($F - F_0$) correlate with the baseline light intensity, whereas the relative changes after dividing by F_0 are independent of baseline light intensity (table 3.1). In experiments lasting several hours, a decline of baseline light intensity of brain slices was observed. Therefore, it was important to normalize the data with regard to their baseline light intensity to achieve comparability of IOSs in long-term experiments (fig. 3.6).

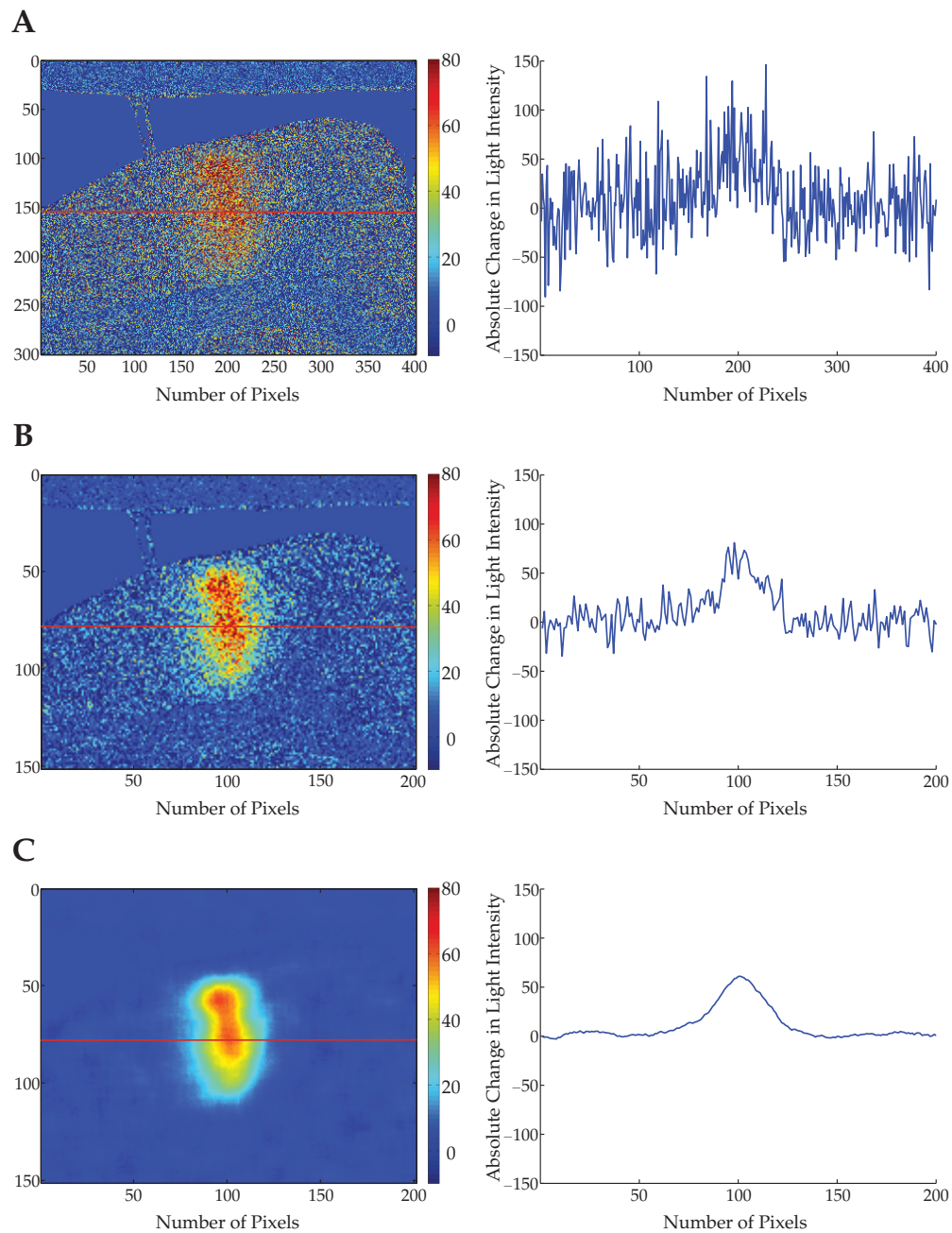


Figure 3.3: **Reduction of noise after binning and filtering.** Changes in light intensity of raw data along a line segment (red line) are shown in (A). As noise in form of random fluctuations in light intensity hampered the analysis of IOSs, a 2x2 binning of the recorded images was performed (B). The images were subsequently filtered with a moving spatial average filter by the data analysis program (C). This procedure caused the spatial noise of single pixels in one image to be averaged out; (A: before binning and filtering; B: after binning; C: after binning and filtering; Left: color-coded images of absolute changes in light intensity in a cortical column 4.75 s after stimulation, red line: position of the line segment for data plotting; Right: spatial changes in light intensity along the line segment).

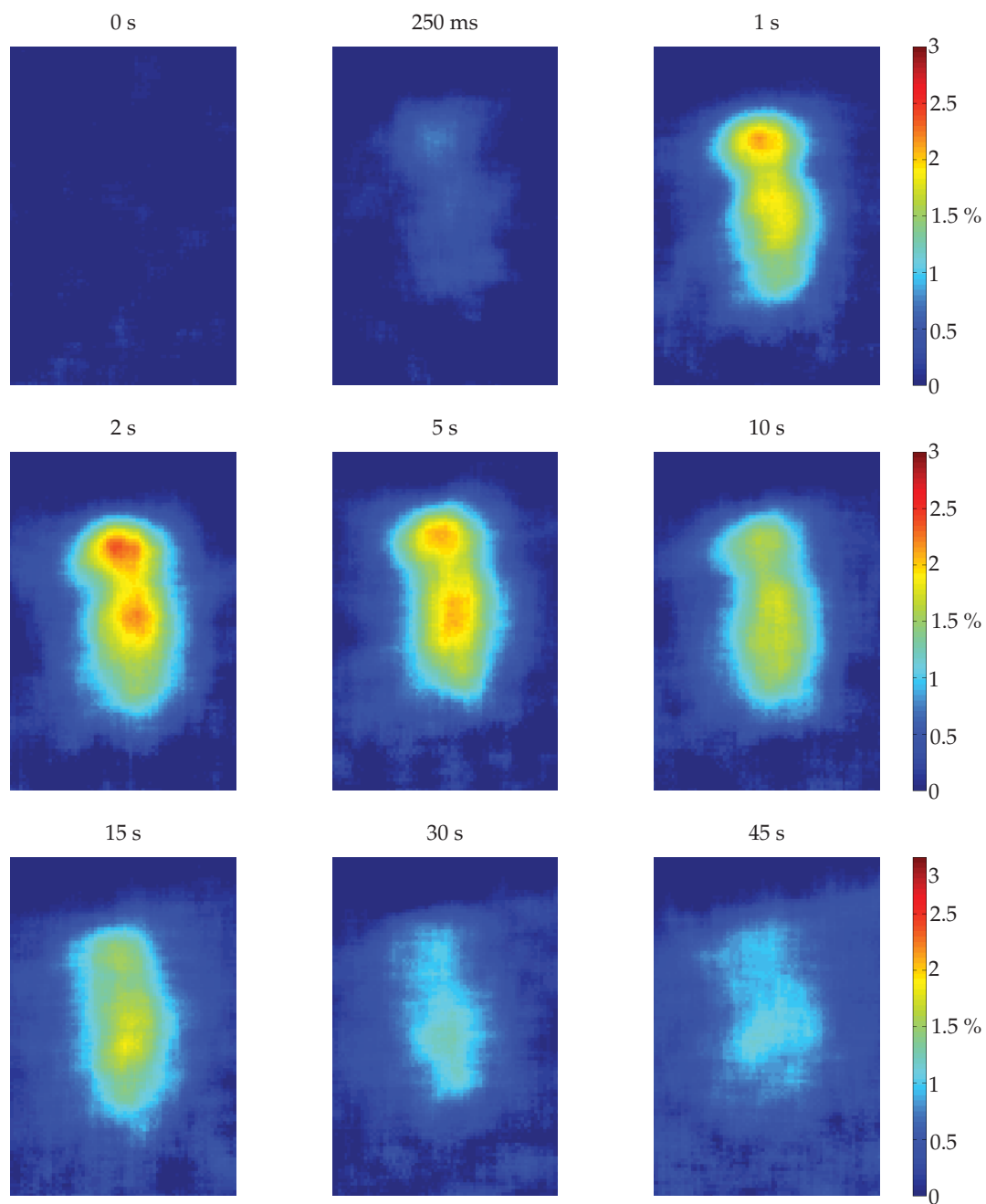


Figure 3.4: **Time course of the IOS.** The $\Delta F/F$ -processed images show the IOS time course after extracellular stimulation (onset of stimulation: 0 s). The images illustrate that the IOS peaked few seconds after stimulation and slowly declined to baseline level within tens of seconds.

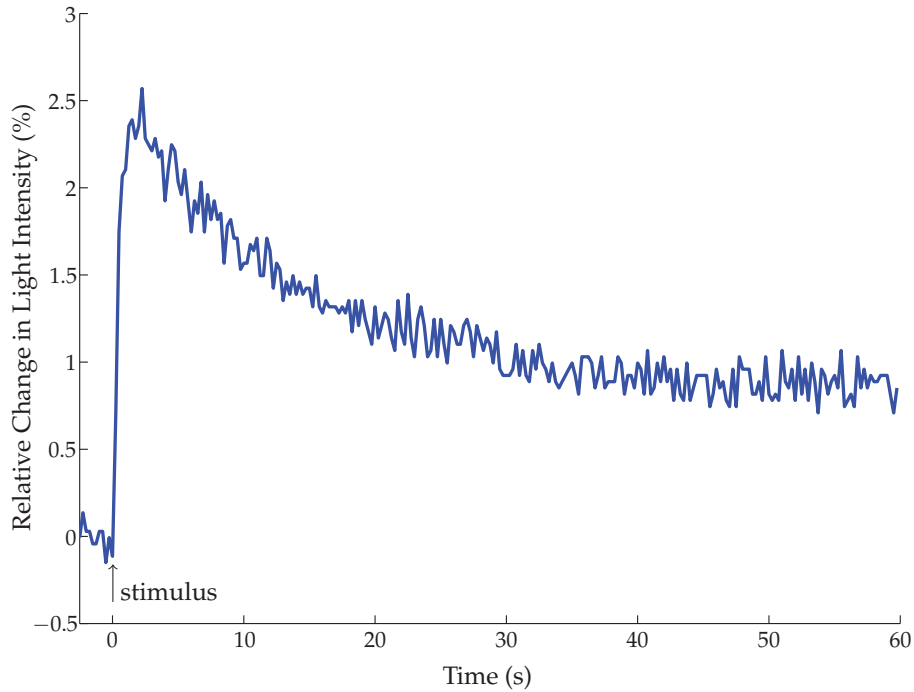


Figure 3.5: **Relative changes in light intensity after $\Delta F/F$ calculation.** $\Delta F/F$ calculation of the light intensity of one pixel allows to display its percent changes in light intensity after stimulation relative to baseline light intensity before stimulation. The arrow marks the onset of stimulation.

light intensity of one pixel		$F - F_0$	$\Delta F/F$
before stimulation	after stimulation	(absolute change)	(relative change)
1000	1100	100	10%
2000	2200	200	10%

Table 3.1: **Comparing $F - F_0$ and $\Delta F/F$ calculation.** The absolute changes in light intensity correlate with baseline light intensity, whereas the relative changes are independent from baseline light intensity.

However, the disadvantage of the $\Delta F/F$ calculation is that the resulting values can become strongly distorted by noise of the baseline light intensity as F_0 stands in the denominator (table 3.2). Hence, the noise level in the image, which represents baseline light intensity, has to be as low as possible. To reduce spatial noise, binning and filtering of the ten images recorded before stimulation were performed. Afterwards, the images were averaged to reduce temporal noise. The resulting single image represented the noise-reduced baseline light intensity of the brain slice (see page 34).

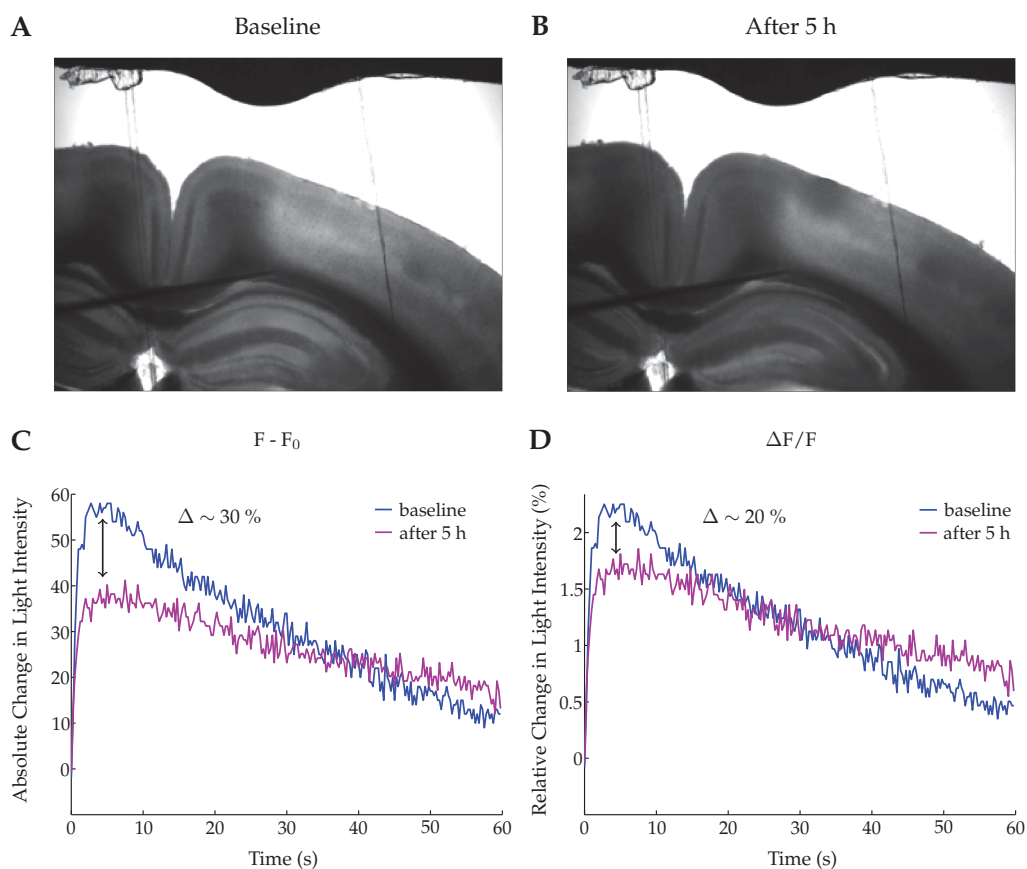


Figure 3.6: **Comparing $F - F_0$ and $\Delta F/F$ calculation after changes in baseline light intensity.** The right transmission image (B) indicates decreased baseline light intensity after 5 h of IOS recordings compared to baseline conditions on the left (A). After calculating relative changes in light intensity of one pixel, signal run-down of 20% was observed after 5 h (D). After calculating the absolute changes in light intensity, however, the signal decreased to 30% of baseline values (C). The difference of 10% between these two methods illustrates the error, which arises if no normalization to the baseline light intensity is done. Onset of stimulation was at 0 s.

	light intensity of one pixel		$F - F_0$	$\Delta F/F$
	before stimulation	after stimulation	(absolute change)	(relative change)
	2000	2200	200	0.1
higher baseline noise	2100	2200	100	0.048
reduction:			50%	52%

Table 3.2: **Susceptibility of $\Delta F/F$ calculation to noise of baseline light intensity.** As F_0 stands in the denominator, normalization of changes in light intensity increases the susceptibility of $\Delta F/F$ calculation to noise of baseline light intensity.

3.1.2.3 Automatic Detection of a ROI and Calculation of Signal Traces

The binning and filtering procedure (see page 32) and the subsequent calculation of $\Delta F/F$ (see page 34) revealed changes in light intensity after extracellular stimulation, which represented IOSs. Each patch of pixels with increased light intensity, however, cannot be regarded as a stimulus-evoked IOS as noise may cause random, stimulus-independent increases in light intensity. Data binning and filtering are capable of reducing spatial noise of single pixels (see page 32), but fail to do so if several adjacent pixels show the same behavior. This can be due to vibrations of the electrode and the grid. These vibrations enhance the noise level of several adjacent pixels and, therefore, may be mistaken for an IOS. To exclude those sources of interference in further data analysis, a ROI was selected, in which the stimulus-induced IOSs were supposed. Only within this ROI, the changes in light intensity were further analyzed. In the data analysis program an automatic ROI detection was performed, which simplified the time-consuming analysis of optical imaging data.

Defining a Threshold One challenging step in analyzing optical data sets was the separation of signal and noise as the transition from noise to signal was smooth. Therefore, a threshold had to be defined. Changes of light intensity above the threshold were regarded as IOSs, changes beyond as noise. To define a threshold, three approaches are possible:

- fraction of signal maximum
- a multiple of noise level
- fixed threshold

Defining the threshold as a fraction of the signal maximum was sometimes used for analyzing the area of IOSs (Holthoff *et al.*, 1994; Dodt *et al.*, 1996; D'Arcangelo *et al.*, 1997; Becker *et al.*, 2005). In most cases, a maximally activated area was chosen by eye. The changes in light intensity of the pixels within this area were defined as signal maximum and the threshold was set to 50% of this maximum. The area of IOSs was constituted by the number of pixels with changes in light intensity above threshold. With this approach, however, the threshold rises if changes in light intensity increase (fig. 3.8). In this case, a different range of percent changes in light intensity is included in signal analysis. Consequently, signal area may be distorted as only pixels with higher changes in light intensity are included. This approach is also unsuitable for analyzing the amplitude of changes in light intensity. As pixels with lower light intensity changes are neglected, the average changes in light intensity of the included pixels could rise. The opposite

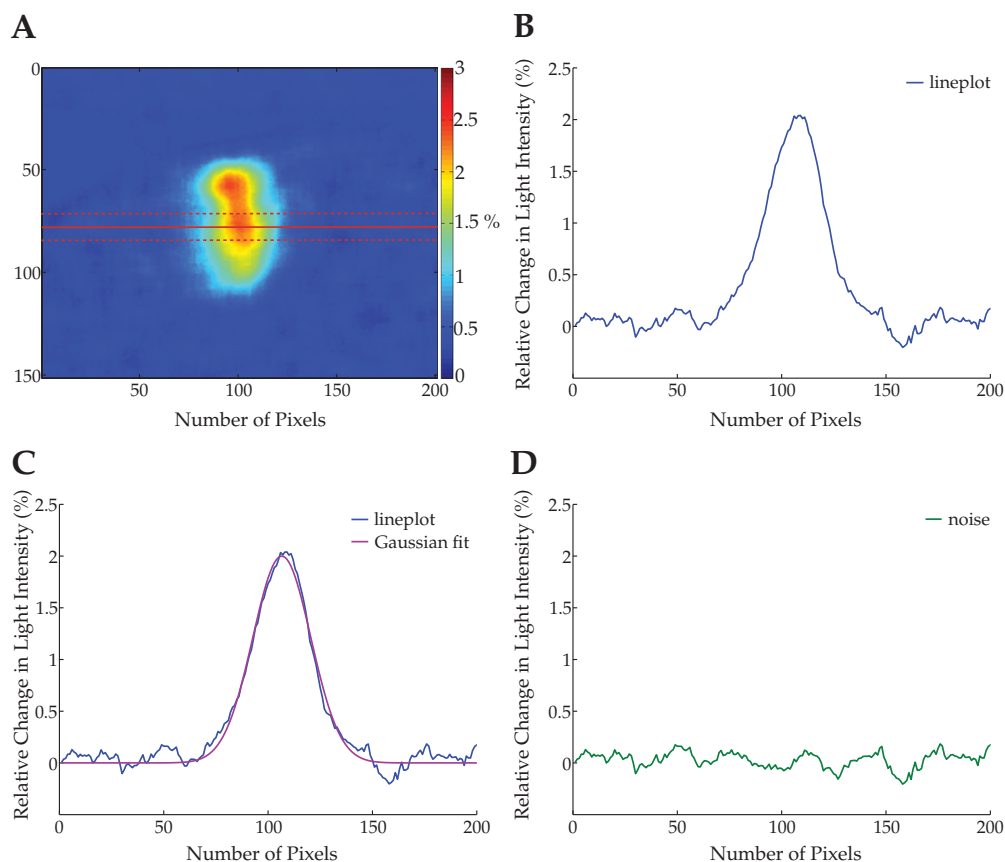


Figure 3.7: **Noise extraction.** The position of one line segment (continuous red line) in a color-coded image after $\Delta F/F$ calculation is shown in (A). Along this line segment the intensity profile was plotted (B). A Gaussian curve fit was applied (C) and subtracted from the intensity profile. The resulting trace was regarded as noise (D). Per IOS recording noise extraction was repeated for another two line segments (dashed red lines).

effect is observed with decreased changes in light intensity. As this approach bears the risk to distort signal area and to boost signal intensity of stimulus-induced IOSs, it was rejected.

For the other approaches, defining the noise level is necessary. Therefore, an intensity profile along a line segment including the center of signal was plotted after $\Delta F/F$ calculation (fig. 3.7). Towards the center of the signal, light intensity increased with a profile resembling a Gaussian distribution. A Gaussian curve fit was applied, which showed a good approach to data distribution [$R^2 = 0.9684 \pm 0.0034$; $n = 15$ intensity profiles (five brain slices with three line segments per slice)]. The fitted Gaussian curve was subtracted from the intensity profile of the line segment. The resulting trace was regarded as noise. The intensity profiles were determined in images recorded 4.75 s after stimulation. At that time point, the signal approximately reached its maximum amplitude, which facilitated the Gaussian fit.

IOS recording	1	2	3	4	5	6
intensity profile 1	0.0773	0.0746	0.1300	0.0958	0.1200	0.0875
intensity profile 2	0.0988	0.0948	0.1200	0.1100	0.1400	0.1100
intensity profile 3	0.0866	0.0858	0.1100	0.0953	0.1200	0.0879

Table 3.3: **RMS noise of one brain slice.** To figure out temporal and spatial differences of noise levels within a brain slice, the RMS noise was calculated in six different IOSs recordings and along three different line segments per IOS recording. The table shows a high variance of temporal and spatial RMS noise even within a single brain slice.

Noise is assumed to be distributed equally in the direction of increased and decreased light intensities. Therefore, calculating the mean of the random fluctuations in light intensity would cause them to cancel each other out. To avoid this problem, the RMS noise was calculated, which squares the values before summing them up.

$$RMS\ noise = \sqrt{\frac{x_1^2 + x_2^2 + \dots + x_n^2}{n}} \quad (3.2)$$

The RMS noise was determined in five brain slices. To investigate if the temporal and spatial noise levels differ within the same brain slice, the RMS noise was calculated in six different IOS recordings per slice and along three different line segments per IOS recording. This resulted in 18 RMS noise values per brain slice. Averaging all RMS noise values of five brain slices gave a mean RMS noise of $0.1078 \pm 0.0029\%$ ($n = 90$ RMS noise values). The RMS noise of one brain slice is displayed in table 3.3.

As shown in table 3.3, the RMS noise varied between different IOS recordings and between different locations in the brain slice. Therefore, defining the threshold of every single stimulation time point as a multiple of its RMS noise would cause high variations of threshold levels even within a single experiment. This approach bears the same risk of distorting IOS area and IOS intensity as setting the threshold to 50% of the maximum signal (see page 39).

Taken together, a fixed threshold was assumed as the best method to separate signal from noise. The value of the threshold is often set to five times of the RMS value. A threshold of 0.5%, however, failed to separate signal from noise in some experiments with higher noise levels. If the threshold was increased to 0.75%, it excluded noise more reliably and resulted in a ROI with the expected form and size of cortical columns (fig. 3.8). Therefore, the threshold was set to 0.75% and changes in light intensity above this level were regarded as stimulus-induced IOSs.

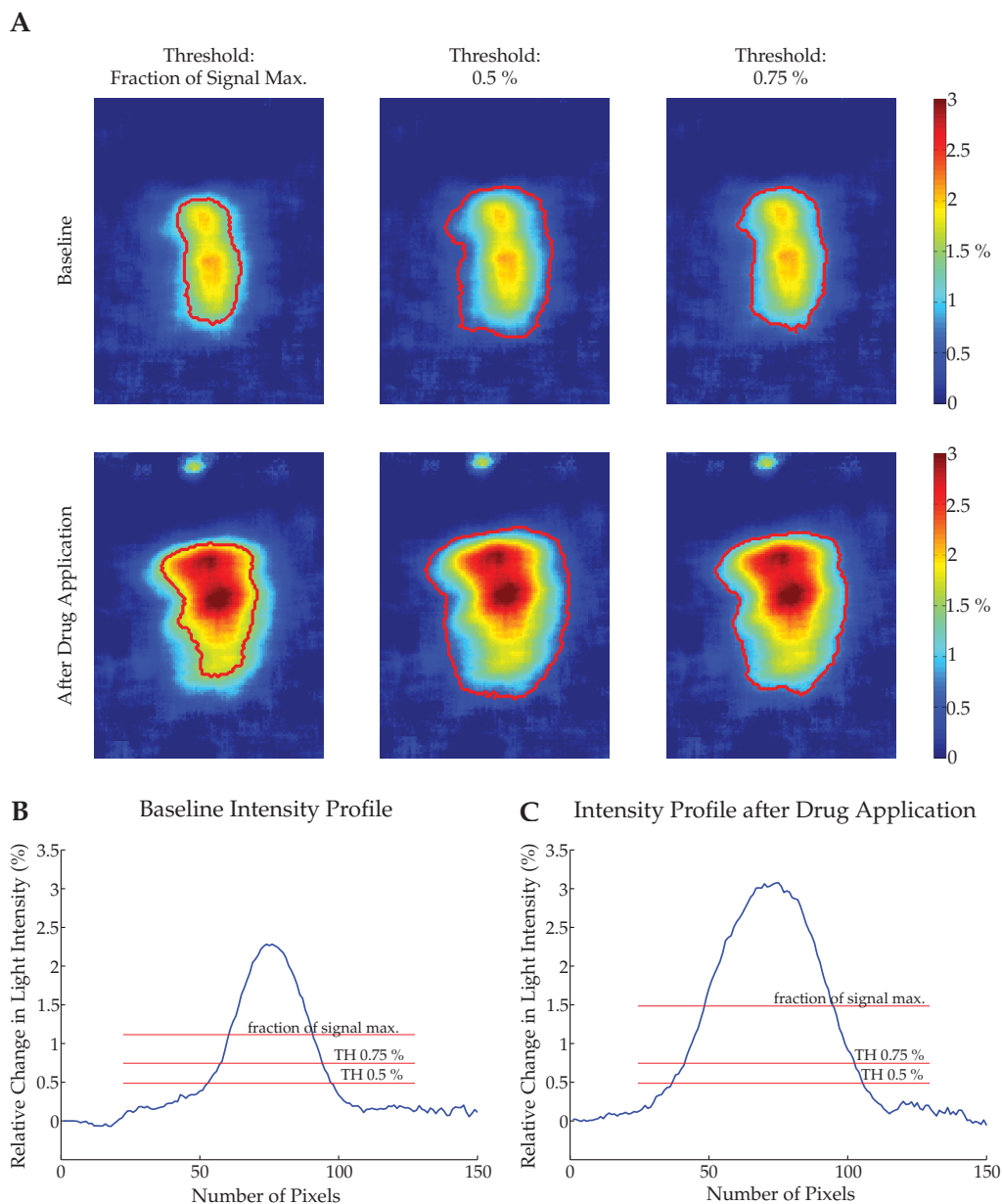


Figure 3.8: **Different approaches for defining a threshold.** Color-coded images after $\Delta F/F$ calculation are shown in (A). The upper line of images was recorded during baseline conditions, the images underneath after application of a drug, which increased IOSs. The images approximately show the maximum magnitude of the signal, which was detected 2.75 s (baseline condition) and 3.5 s (drug application) after onset of stimulation. The red lines illustrate the threshold level and enclose pixels above threshold. The enclosed areas represent IOSs. First, the threshold was defined as a fraction of the signal maximum. The threshold was set to 50% of signal maximum, which is 1.14% for baseline condition and 1.53% after drug application. Next, two fixed thresholds of 0.5% and 0.75% were applied. Underneath, line plots of the intensity profile during baseline conditions (B) and after drug application (C) were plotted. The red lines illustrate the different threshold levels (TH = threshold). The areas above the lines represent the signal. The plots illustrate the risk of distorting IOS area and intensity if setting the threshold to 50% of the signal maximum, as a different range of percent changes in light intensity is included. Defining a fixed value as threshold level avoids this risk.

Automatic Detection of a ROI So far, the program calculated the relative changes in light intensity for every pixel in an image and for all 240 images recorded after stimulation (see page 34). For the automatic detection of the ROI, in which the IOS was assumed, a maximum intensity projection of all 240 $\Delta F/F$ -processed images was computed (fig. 3.10, A). In this maximum intensity projection the value of every pixel was set to its maximum change in light intensity observed after stimulation by scanning all 240 images. Therefore, in the maximum intensity projection all pixels, which reached changes in light intensity above threshold level at any time after stimulation, could be detected.

As the amplitude of changes in light intensity was negligible for the ROI detection, the changes in light intensity were divided in two subsets: changes above threshold (1) and changes below threshold (0). In the maximum intensity projection, pixels with a value of changes in light intensity greater than the threshold were set to 1, while pixels with a value equal or below the threshold were set to 0. This resulted in a binary image, in which each pixel was restricted to a value of either 0 or 1 (fig. 3.10, B). Areas filled up with 1's included the stimulus-induced IOSs and were further regarded for the automatic detection of the ROI.

Next, the morphological opening, a technique for analysis and processing of geometric binary images, was applied on the binary image (figs. 3.9; 3.10, C). A disk with a radius of ten pixels was chosen as a structuring element. All pixels with 1's, which could be covered by the entire structuring element, were preserved. However, all pixels with the value of 1, which could not be covered by the structuring element without parts of the element also covering 0's, were set to 0 and not further regarded. Hence, boundaries of large objects were smoothed by removing small appendices while preserving shape and size of the objects.

As IOSs were assumed to be large, only objects with a minimum size of 300 pixels were further included in the automatic ROI detection. Afterwards, the center of mass was assigned for the remaining objects. The center of mass describes the point of an object where all of its mass can be considered to be concentrated. When an object is supported at its center of mass, it is balanced as there is no net torque acting on the body. Brain slices were positioned in the recording chamber in a way that the stimulated cortical columns were largely centered in the field of view, the object with its center of mass nearest to the center of the image was defined as ROI, which enclosed the IOS (fig. 3.10, D).

Data sets, in which the automatic ROI detection failed, were excluded from further analysis. Failure of automatic ROI detection occurred if stimulation did not trigger a signal above noise level. In this case, no ROI could be detected. Furthermore, the auto-

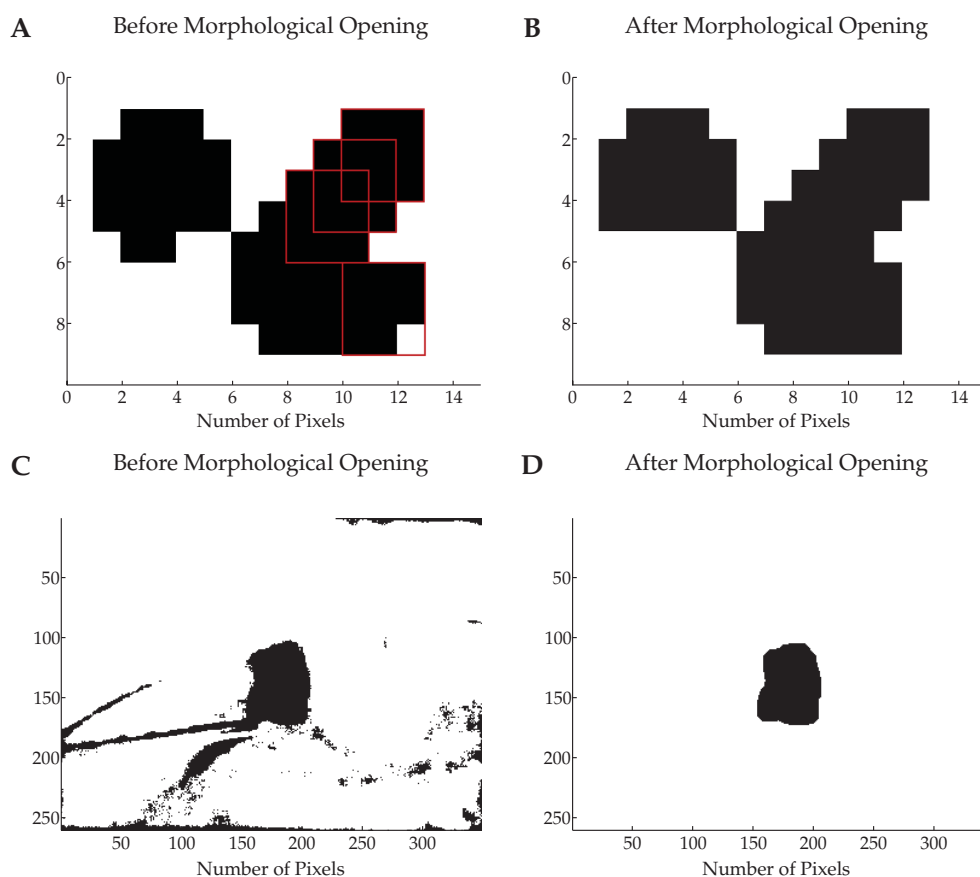


Figure 3.9: **Morphological opening.** During morphological opening, small objects and small appendices of large objects are removed. This results in smoothed boundaries of large objects, while preserving shape and size of the objects. The upper images illustrate the principle of morphological opening with the help of an example. Both images are binary images (white = 0, black = 1) before (A) and after morphological opening (B) with a structuring element of a square of 3×3 pixels. The red squares in (A) symbolize the structuring element, which moved along the borders of the object. All black pixels, which could be covered by the entire structuring element, were preserved. Black pixels, which could not be covered by the structuring element without parts of the elements also covering white pixels, were deleted as seen in the lower right square. The images underneath show the binary images of the maximum intensity projection (white = 0, black = 1) after $\Delta F/F$ calculation of a brain slice with high noise level and a vibrating electrode. As the IOSs were expected to exhibit round boundaries, a structuring element in form of a disk (radius ten pixels) was applied. Before the morphological opening (C), it is impossible to clearly detect the boundaries of the IOS. After morphological opening (D), the noise caused by the vibrating electrode as well as other small noisy regions were removed and the boundaries of the IOS became clearly visible.

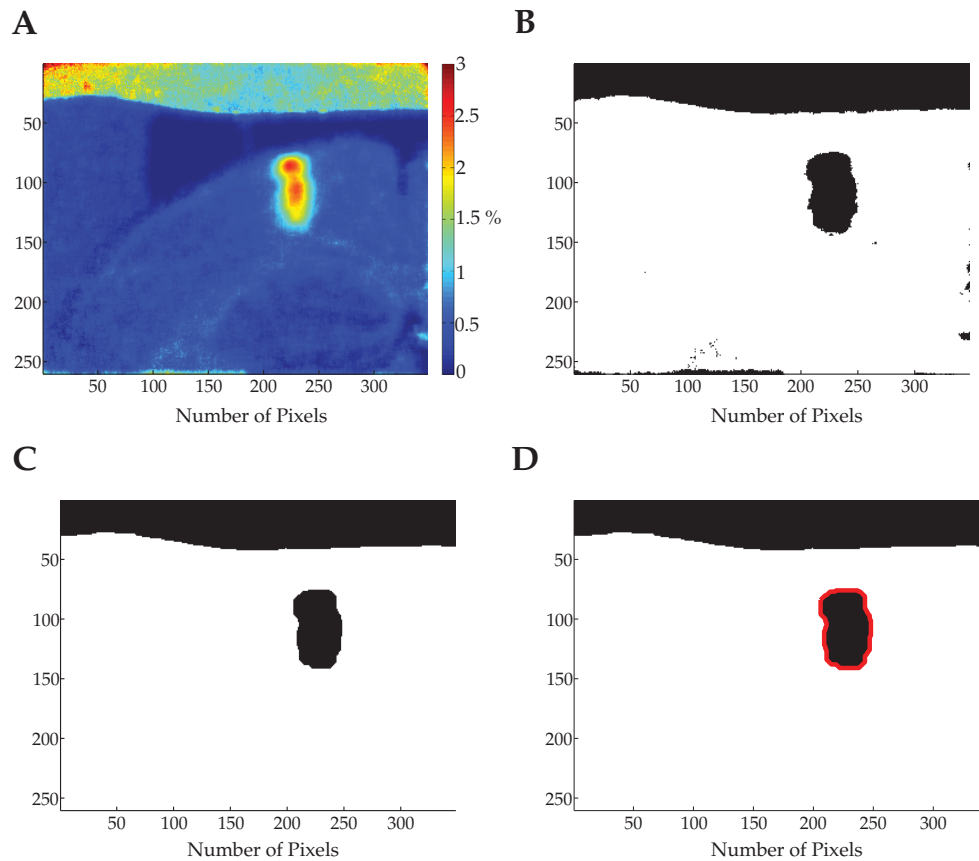


Figure 3.10: **Automatic ROI detection.** After $\Delta F/F$ calculation of all 240 images recorded after stimulation, a maximum intensity projection of the $\Delta F/F$ -processed images was computed (A). In the maximum intensity projection, every pixel value was set to its maximal change in light intensity observed after stimulation by scanning all 240 processed images. This process enabled the detection of all pixels, which reached changes in light intensity above threshold level at any time after stimulation. The maximum intensity projection illustrates that especially dark structures, e.g. the grid on top of the image, are susceptible to noise. As the baseline light intensity is very low in dark structures, even small fluctuations in light intensity cause high relative changes in light intensity after $\Delta F/F$ calculation and can be misinterpreted as IOSs. The maximum intensity projection was afterwards binary-coded (B). Therefore, pixels with changes in light intensity above threshold were set to 1 (black), pixels with changes equal or below threshold were set to 0 (white). Black areas might represent IOSs. In this binary image, the morphological opening was applied (fig. 3.9) to smooth the boundaries of the signal (C). Afterwards, only objects larger than 300 pixels were further included in the automatic ROI detection. The object with its center of mass nearest the center of the image was defined as ROI (red line), which enclosed the IOS.

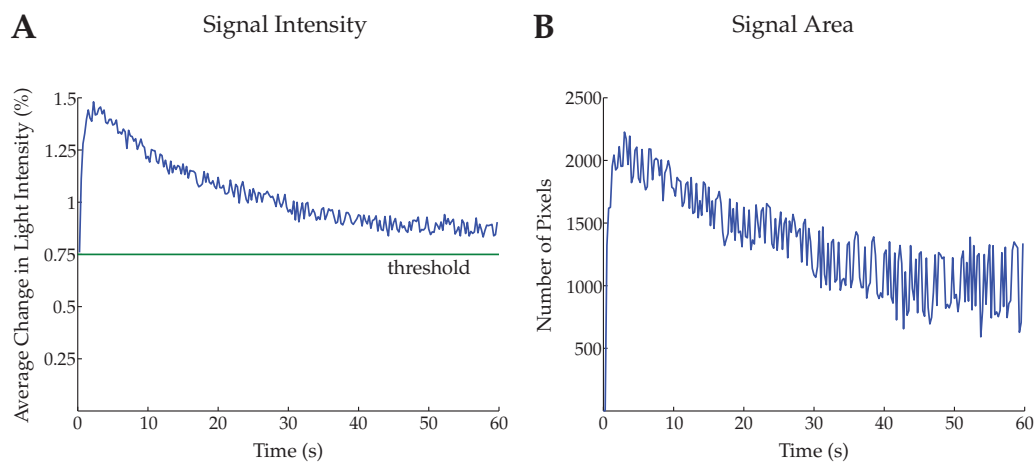


Figure 3.11: **Time course of signal intensity and signal area.** Within the ROI, pixels above threshold level were regarded as IOS. To illustrate the time course of IOSs, pixels within the ROI and above threshold level were detected in every $\Delta F/F$ -processed image recorded after stimulation. The number of detected pixels displays the area of the IOS (= signal area, *B*). The changes in light intensity of detected pixels were averaged. The mean percent change in light intensity displays the intensity of the IOS (= signal intensity, *A*). As for the signal intensity, changes in light intensity of many pixels were averaged, the trace of signal intensity was smoother compared to the trace of the signal area. Onset of stimulation was at 0 s.

matic ROI detection failed in data sets with extreme high noise levels. In these data sets, a much too large ROI was detected as the border of the ROI could not be set reliably.

Calculating Signal Traces The ROI included all pixels, which displayed changes in light intensity above threshold in at least one of the 240 $\Delta F/F$ -processed images recorded after stimulation. Pixels within the ROI and with changes in light intensity above threshold level were now regarded as IOS. As the ROI illustrated the maximum possible size of the signal, it was now possible to restrict further data analysis to the area enclosed by the ROI. To examine the time course of the IOS, the ROI was applied on every single $\Delta F/F$ -processed image. Within the ROI, all pixels above threshold level were detected. The number of detected pixels display the area of the IOS (= signal area) and specify the size of the stimulus-activated area. Changes in signal area were most likely caused by changes in the lateral extension of IOSs as the vertical extension of IOSs nearly spanned the full height of cortical columns under control conditions. The values of changes in light intensity of the detected pixels were averaged. The mean percent change in light intensity display the intensity of the IOS (= signal intensity) and mirror the strength of neuronal activation (fig. 3.11).

Up to now, most published data restricted the analysis of IOSs to changes in signal intensity. With the new data analysis program developed here, it was possible to extend the data analysis to changes in area and time course of IOSs. To examine changes in

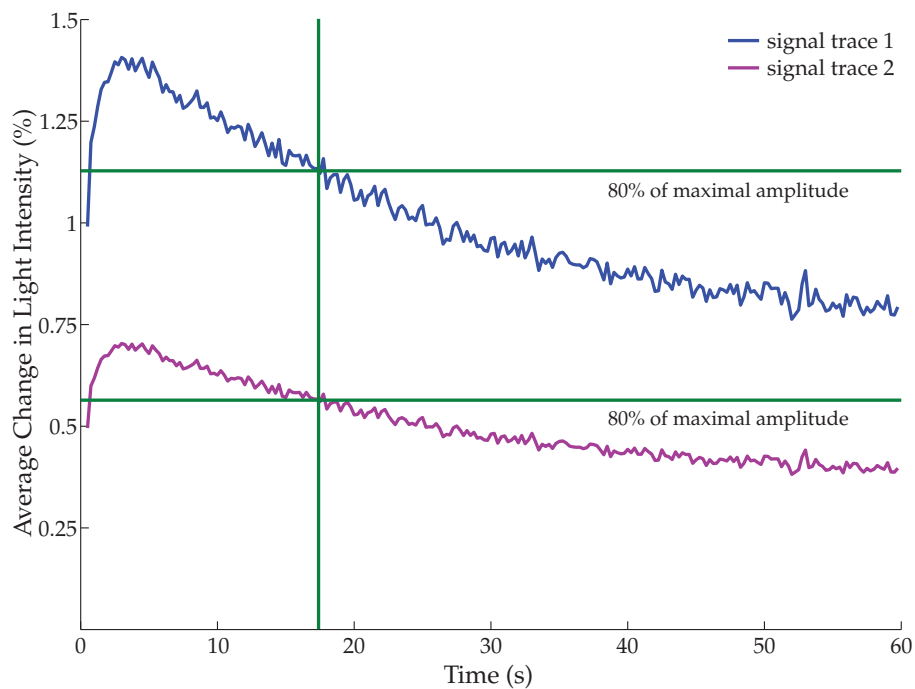


Figure 3.12: **Changes in time course of signal intensity.** To detect changes in time course of IOSs, time periods, during which the signal intensity reached certain levels of its maximum amplitude, were assigned. The speed of signal decay was investigated by calculating the time period, during which the signal amplitude decreased from its maximum value to 80% of its maximum (green lines). Signal trace 2 was produced by dividing signal trace 1 by two. Even if both signal traces differ in their maximal amplitude, they follow the same time course and decay from their maximum amplitudes to 80% within about 18 s. The onset of stimulation was at 0 s.

signal intensity and signal area, the maximum amplitudes of these two parameters were determined. As the signal intensity displays mean changes in light intensity of many pixels, it is less susceptible to temporal noise compared to the signal area, which is the total number of pixels above threshold at a certain time point (fig. 3.11). Therefore, the time course of IOSs was only regarded on the basis of the time course of stimulus-induced changes in signal intensity. To analyze the time course, the time periods, during which the signal reached certain levels of its maximum amplitude, were assigned. The rise time was defined by the time period, during which the signal intensity reached its maximum amplitude after onset of stimulation. To compare the speed of signal intensity decay, the time period, during which the signal amplitude decreased from its maximum value to 80% of its maximum, was calculated. This approach allows to compare the time course of signal traces even if their maximum amplitudes vary (fig 3.12).

In few cases, a biphasic decay of IOSs could be observed (fig. 3.13, A). As this pattern was also described in other publications (Holthoff *et al.*, 1994), a biphasic decay

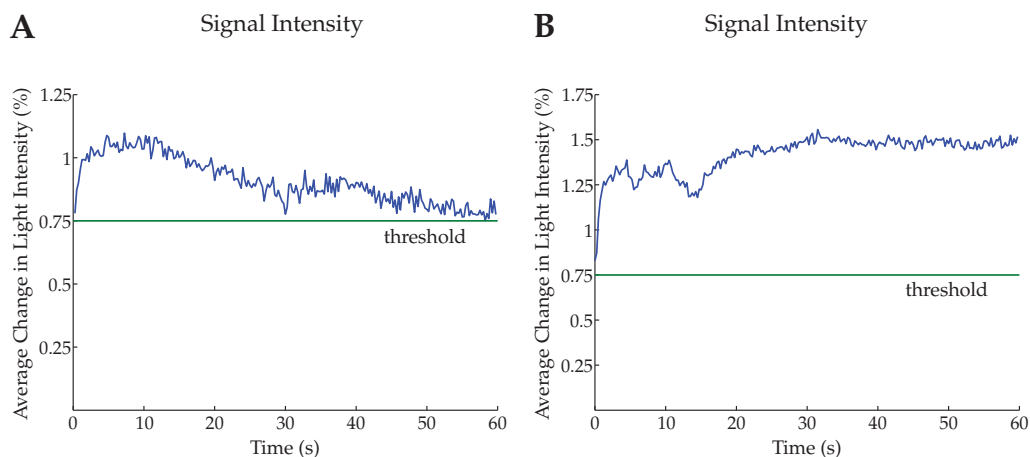


Figure 3.13: **Abnormalities in signal decay.** In some cases, a biphasic decay of the signal could be observed (A). This pattern, however, was regarded as a natural variant of signal decay. Data sets were excluded, however, if signal traces exhibited a clear upward trend, because this may influence the value and temporal position of the maximum signal intensity (B). Onset of stimulation was at 0 s.

of the signal was regarded as a natural variant. Sometimes, signal traces exhibited a clear upward trend (fig. 3.13, B). As such a time course influenced value and temporal appearance of the maximum amplitude, these data sets were excluded from further analysis.

3.1.3 Long-term IOS Recording

In contrast to optical signals generated by fluorescence dyes (voltage- and Ca^{2+} -sensitive dyes), IOSs are not impaired by bleaching or wash-out effects during long-term experiments. Furthermore, during IOS recordings no pharmacological side effects or photodynamic damages occur (Grinvald *et al.*, 1986; Holthoff & Witte, 1996; Takashima *et al.*, 2001). These advantages of IOS recordings suggests that intrinsic optical imaging possibly constitutes a technique for long-term recordings of neuronal network activity. Therefore, the next goal was to test whether IOS recordings are capable of monitoring neuronal network activity for several hours. This was of particular importance, as the uptake of drugs inhibiting GAD activity and the depletion of preexisting GABA pools was thought to be slow.

A typical stimulation protocol for eliciting IOSs consists of 100 square pulse stimuli applied at 50 Hz and a stimulus duration of 0.2 ms (Holthoff *et al.*, 1994; Dodt *et al.*, 1996; D'Arcangelo *et al.*, 1997; Holthoff & Witte, 1997, 1998; Witte *et al.*, 2001; Becker *et al.*, 2005; Holthoff *et al.*, 2007). This stimulation protocol, however, is close to protocols, which can induce synaptic plasticity, even in cat or rat motor cortex (Keller *et al.*, 1991; Aroniadou

3.1 Analyzing IOSs and Long-term IOS Recording

	typical stimulation protocol	adapted stimulation protocol
mean max. signal intensity	1.92±0.09%	1.10±0.05%
mean max. signal area	3775.80±251.22 pixels	1668.30±245.64 pixels
mean rise time	6.65±1.02 s	6.31±0.78 s
mean decay time	24.55±1.72 s	35.50±4.30 s

Table 3.4: **Comparison of stimulation protocols.** Different parameters of the IOS were compared with respect to different stimulation protocols (typical stimulation protocol: 100 square pulse stimuli, 50 Hz, stimulus duration 0.2 ms, stimulation current 100 μ A; adapted protocol: 20 square pulse stimuli, 100 Hz, stimulus duration 0.2 ms, stimulation current 100 μ A; typical stimulation protocol: n = 5 brain slices, adapted stimulation protocol n = 4 brain slices).

& Keller, 1995). Moreover, repeated strong stimulation is supposed to impair brain slice physiology during long-term experiments. Due to these reasons, it was hypothesized that reduced stimulation strength facilitates long-term IOS recordings. Pilot experiments indicated that, at higher stimulation frequencies, less stimulation pulses were necessary to trigger IOSs. Therefore, brain slice stimulation was reduced to 20 square pulse stimuli at 100 Hz and a stimulus duration of 0.2 ms. A lower stimulation frequency (20 square pulse stimuli at 10 Hz and a stimulus duration of 0.2 ms) failed to induce IOSs at a moderate stimulation strength.

Compared to the typical stimulation protocol described above (100 square pulse stimuli, 50 Hz, stimulus duration 0.2 ms), the adapted protocol (20 square pulse stimuli, 100 Hz, stimulus duration 0.2 ms) triggered IOSs which were roughly half in size, but with similar kinetics (table 3.4). When a stimulation current of 100 μ A was used, the changes in light intensity were $1.1\pm 0.05\%$ (n = 4 brain slices). In relation to the mean RMS noise of 0.1078% (see page 41), the signal-to-noise ratio was still about 1:10 with the new more gentle stimulation protocol.

3.1.3.1 Reproducibility of IOSs

The maximum signal intensity and signal area showed a high reproducibility during repetitive stimulation performed at an interstimulus interval of 5 min (fig. 3.14, A, B). This was important as high fluctuations would have made it impossible to accurately determine changes of these parameters. The time course of the signal intensity, however, showed a higher variability (fig. 3.14, C, D).

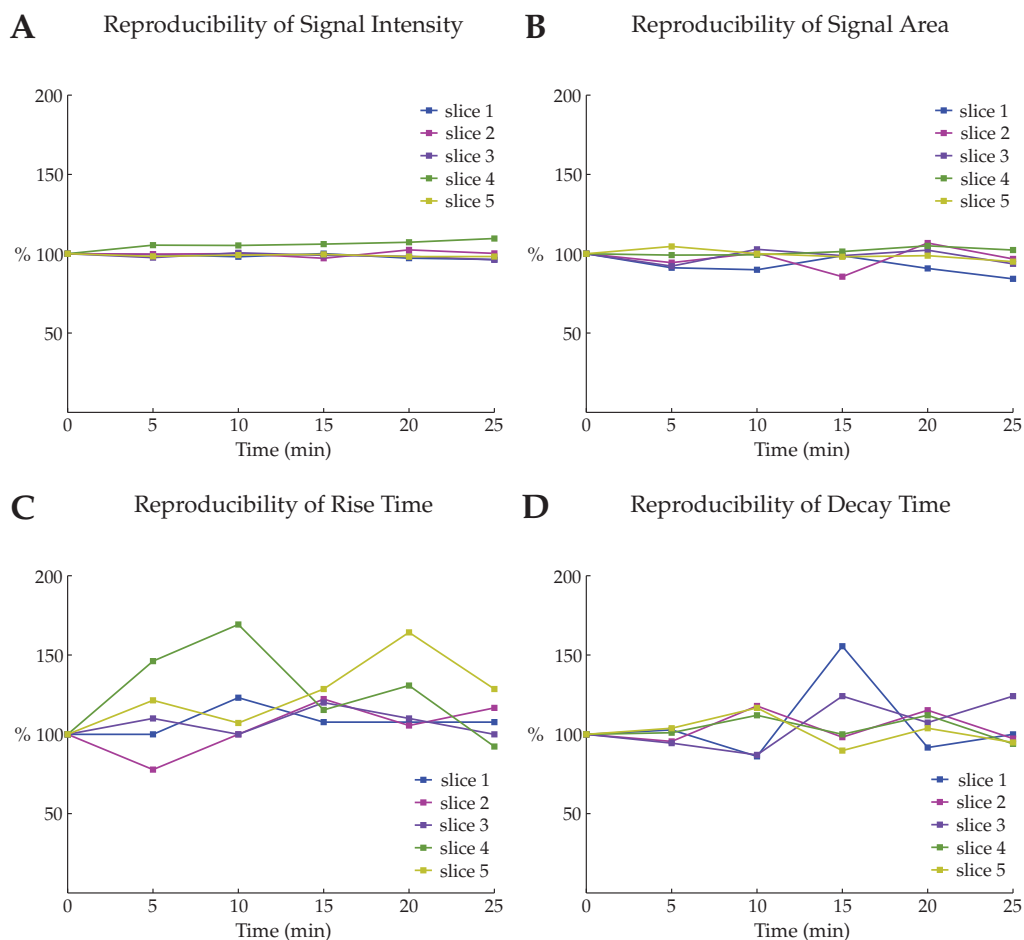


Figure 3.14: **Reproducibility of IOSs.** The reproducibility of signal parameters was investigated with repetitive stimulations (interval between stimulations: 5 min). The maximal signal intensity and signal area as well as the rise time and the decay time were normalized to the first signal, which was set to 100%. The maximal signal intensity (A) showed the highest reproducibility over time. Compared to the signal intensity, the size of the signal area (B) was less stable. The degree of reproducibility of IOS time course (C, D) differed between single brain slices; (n = 5 brain slices).

3.1.3.2 Correlation of IOSs with Stimulation Strength

With increasing stimulation currents, both signal intensity and signal area increased in a linear manner as shown by a linear fit of the data (fig. 3.15). Compared to the signal intensity, the signal area was more sensitive to an increase in stimulation current as shown by the higher slope of the linear fit. As higher stimulation currents cause stronger activation of the neuronal network, these results demonstrate that it is possible to display changes in neuronal network activity by means of IOSs.

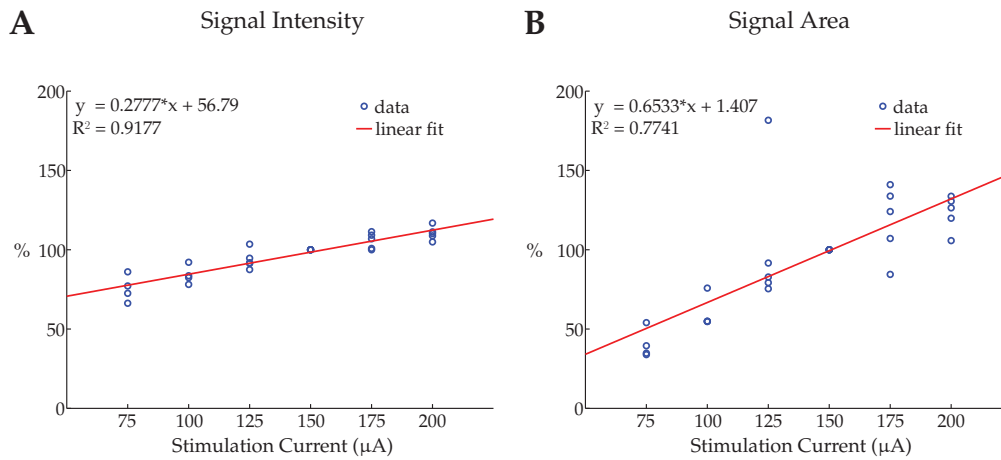


Figure 3.15: **Correlation of IOSs with stimulation strength.** With increasing stimulation currents, the maximum of both signal intensity (A) and signal area (B) increased in a linear manner as shown by a linear fit of the data of five brain slices. Compared to the signal intensity, the signal area was more sensitive to an increase in stimulation current as shown by the higher slope of the linear fit. As higher stimulation currents cause stronger activation of the neuronal network, these results demonstrate that IOSs are capable of displaying changes in network activity; [n = 5 brain slices; normalized to signal size after stimulation with 150 μ A (100%)].

3.1.3.3 Long-term Measurements

To investigate a possible run-down of IOSs during long-term experiments, long-term measurements of about 7 h were performed. Long-term measurements with drug-free ACSF followed the same protocol, which was later applied for long-term drug application (see page 23).

During long-term measurements, a run-down in both signal intensity and signal area was observed (fig. 3.16). The signal intensity declined to about 85% of its starting value after about 6 h (fig. 3.16, A; n = 6 brain slices). The decrease of the signal area to about 70% of its starting size indicates that this parameter was more susceptible to run-down (fig. 3.16, B; n = 6 brain slices). Both signal parameters did not recover to baseline levels even after applying fresh ACSF during wash-out. The good reproducibility shown above (see page 49) worsened during the course of experiments. The maximum signal area and signal intensity during sham-drug application were of higher variability as during baseline conditions at the beginning of the experiments. Therefore, the results of the six IOS recordings performed during baseline conditions and the results of the three IOS recordings done every full hour during sham-drug application were averaged for statistical analysis. Statistical analysis revealed that both mean signal intensity and mean signal area significantly declined to $91.93 \pm 1.27\%$ ($p = 0.001$, paired Student's t-test, n = 6 brain slices) and $83.38 \pm 1.13\%$ ($p < 0.001$, paired Student's t-test, n = 6 brain slices) of baseline levels after 60 min of sham-drug application and remained at

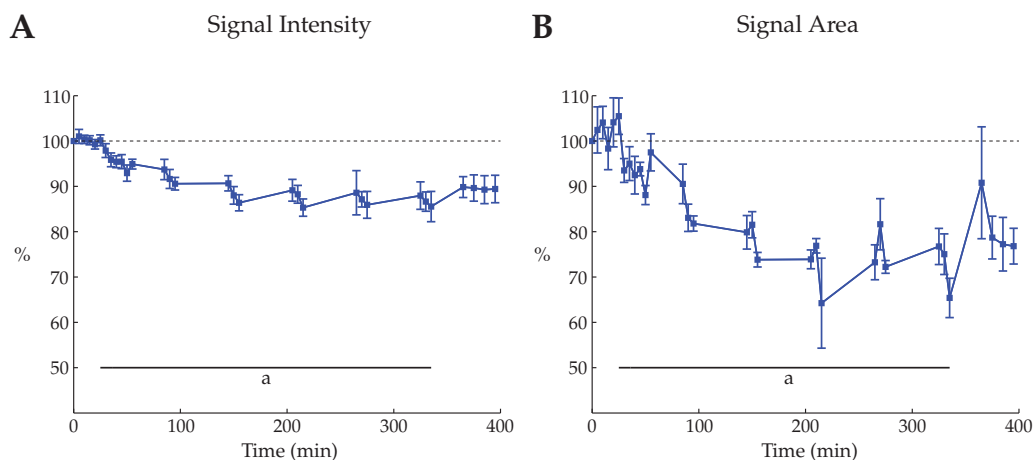


Figure 3.16: **Changes in signal intensity and signal area during long-term measurements.** Run-down of both signal area and signal intensity could be observed during long-term measurements under drug-free ACSF recirculation. The signal intensity declined to about 85% of its starting size. The signal area was even more susceptible to run-down as it was reduced to 70% of its starting size. Both parameters did not recover after simulated wash-out with fresh ACSF; [n = 6 brain slices; normalized to first baseline recording (100%); a = sham-drug application].

a significantly lower level during the further course of experiments [signal intensity after 300 min of sham-drug application: $86.55 \pm 2.00\%$ ($p = 0.001$, paired Student's t-test, $n = 6$ brain slices); signal area after 300 min of sham-drug application: $71.89 \pm 3.18\%$ ($p < 0.001$, paired Student's t-test, $n = 6$ brain slices); signal intensity after 60 min wash-out: $89.24 \pm 2.76\%$ ($p = 0.011$, paired Student's t-test, $n = 6$ brain slices); signal area after 60 min wash-out: $74.93 \pm 2.81\%$ ($p < 0.001$, paired Student's t-test, $n = 6$ brain slices)] (fig. 3.17).

Examining the time course of IOSs, a change in rise time and decay time could be observed. Both rise time and decay time nearly doubled after 5 h of sham-drug application, but returned to baseline levels after wash-out with fresh ACSF (fig. 3.18). The high SEM values, however, indicate a high variability between single experiments. Additionally, the time period, after which first signals could be detected, increased from 0.31 ± 0.02 s (baseline conditions) to 0.50 ± 0.06 s (300 min of sham-drug application) after onset of stimulation and decreased to 0.42 ± 0.05 s after wash-out with fresh ACSF ($n = 6$ brain slices). Altogether these results imply that neuronal network physiology changes during long-term measurements, presumably caused by ACSF recirculation (e.g. under-supply with nutrients and ions, accumulation of degradation products etc.). Together with the observation that the reproducibility of IOSs time course was poor in some brain slices under baseline conditions (see page 49), changes in time course of IOSs were not regarded as a suitable parameter to describe IOSs during long-term experiments. Additionally, these findings show that it is important to detect the maximum signal intensity

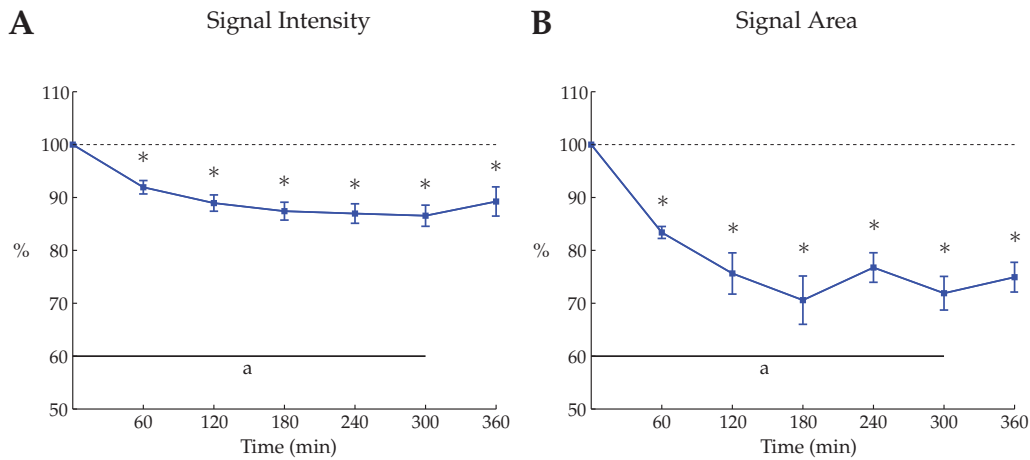


Figure 3.17: **Run-down during long-term measurements.** For statistical analysis, the results of six IOS recordings under baseline conditions and the results of the three IOS recordings at every full hour of sham-drug application were averaged. This reveals that both signal intensity and signal area were significantly reduced after 60 min of sham-drug application. Both signal intensity and signal area remained at significantly low levels during the further course of experiments even after applying fresh ACSF during wash-out (360 min = after 60 min wash-out); [n = 6 brain slices; normalized to baseline conditions (100%); a = sham-drug application; *p < 0.05].

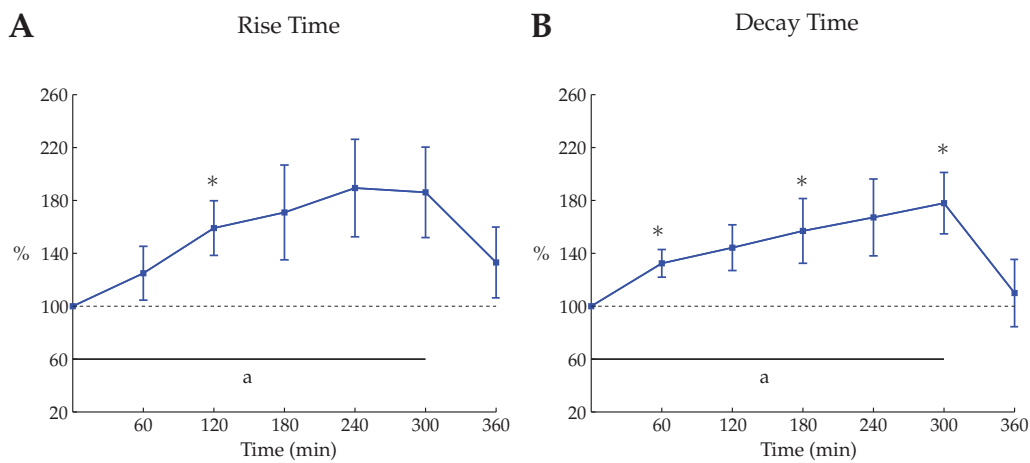


Figure 3.18: **Changes in rise and decay time of signal intensity during long-term measurements.** Both rise time and decay time were prolonged during long-term IOS measurements, but returned to baseline levels after applying fresh ACSF during wash-out (360 min = after 60 min wash-out). The high SEM values indicate a high variability between single experiments; [n = 6 brain slices; normalized to baseline conditions (100%); a = sham-drug application; *p < 0.05].

and signal area independent of the time course of the signal. If the IOSs are examined after a fixed time point (e.g. 3 s after stimulation), which was often done in previous studies (Dodt *et al.*, 1996; D'Arcangelo *et al.*, 1997; Becker *et al.*, 2005), the maximum signal intensity or area might not be correctly determined.

The significant decrease in signal area and signal intensity over time during long-term measurements may require to correct IOSs by run-down to reveal changes after application of slow-acting drugs. Most likely, run-down could be reduced by an open ACSF superfusion of brain slices. Nevertheless, for good comparability of data, all experiments in the present study were done with ACSF recirculation, which was necessary due to the small amounts of available SPS-IgG.

3.1.4 Effects of BIM on IOSs

BIM is a competitive antagonist of GABA_A receptors and is known to enhance IOSs in brain slices (Dodt *et al.*, 1996; Kohn *et al.*, 2000). Experiments with application of 5 μ M BIM to mouse brain slices were carried out to examine the effect of an impaired GABAergic system on IOSs as it was intended to block GABA synthesis in further experiments.

Application of 5 μ M BIM increased the signal area, but had no effect on the signal intensity (fig. 3.19). The signal area started to increase about 10 min after beginning of BIM application, reached its maximal size after about 30 min and remained constant until wash-out (fig. 3.19, B). The results of the six stimulations under baseline conditions were averaged and set to 100%. The mean signal area after 60 min of BIM application was significantly increased to $176.83 \pm 7.58\%$ of baseline conditions ($p < 0.001$, paired Student's t-test, $n = 5$ brain slices) and decreased to baseline levels after 60 min of wash-out ($102.69 \pm 3.92\%$; $p = 0.583$, paired Student's t-test, $n = 4$ brain slices) (fig. 3.19, D). The signal intensity, however, was not statistically significantly affected after 60 min of BIM application ($94.15 \pm 4.94\%$; $p = 0.302$, paired Student's t-test, $n = 5$ brain slices) (fig. 3.19, A, C).

3.2 Effects of SMC on Motor Cortical Neuronal Network Activity

Up to now, the influence of the GAD inhibitor SMC on neuronal network activity has not been investigated. To close this gap, IOS recordings and patch-clamp experiments were performed in motor cortical brain slices in the absence and presence of SMC.

3.2.1 Effects of SMC on IOSs

3.2.1.1 Effects of Different SMC Concentrations on IOSs

To investigate effects of SMC on neuronal network activity within the motor cortex, SMC was first applied via the bath solution at two concentrations (0.5 and 2 mM) to

3.2 Effects of SMC on Motor Cortical Neuronal Network Activity

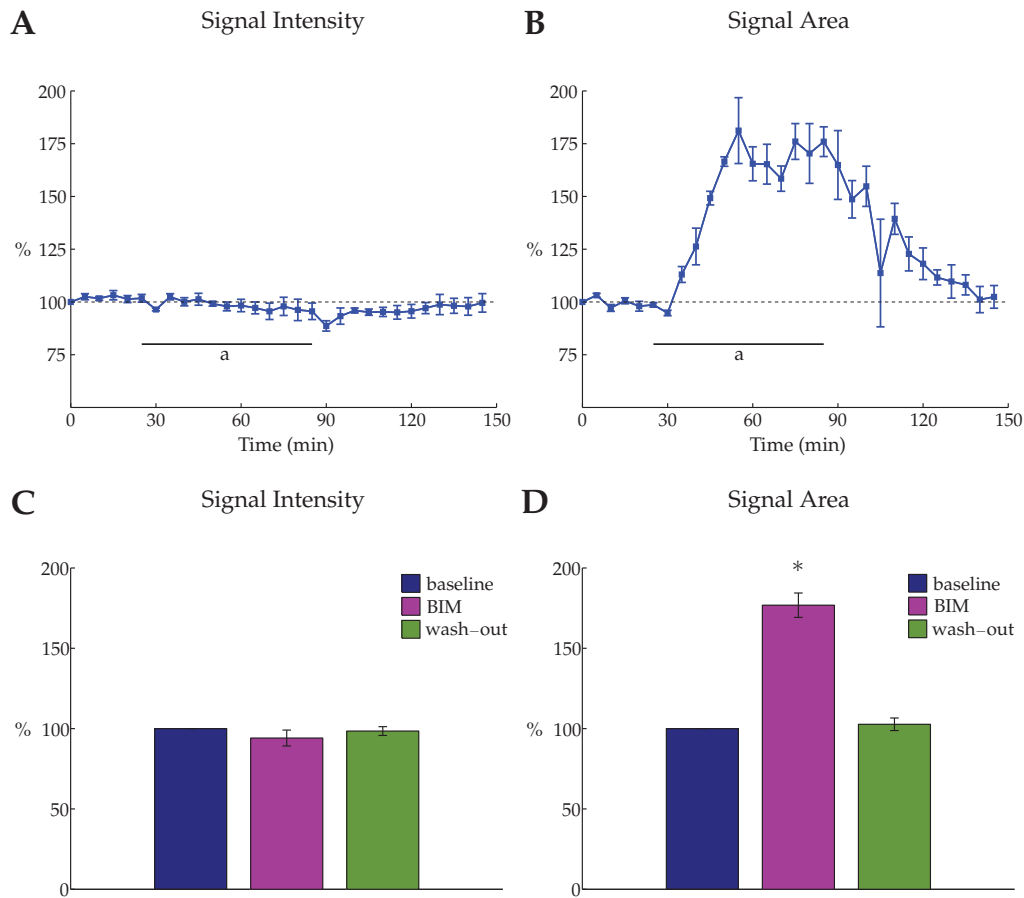


Figure 3.19: Changes in signal intensity and signal area during BIM application. About 10 min after beginning of BIM application, the signal area started to increase, reached its maximum size after about 30 min and remained constant until wash-out (B). After 60 min of BIM application, this increase was significant compared to baseline conditions (D). During wash-out, the signal area decreased to baseline levels (B, D). The signal intensity, however, was not affected by BIM application (A, C); [baseline/BIM application: $n = 5$ brain slices; wash-out: $n = 4$ brain slices; normalized to baseline conditions (100%); a = 5 μM BIM application; * $p < 0.05$].

brain slices obtained from Bl/6 mice. For control, sham-drug application with drug-free ACSF was performed following the same protocol as for SMC application. Statistical analysis was performed by comparing the values of sham-drug application with those of SMC treatment. SMC, applied at a concentration of 0.5 mM, showed no effect on signal intensity and signal area during an application period of 5 h (fig. 3.20).

In contrast to 0.5 mM SMC, long-term application of 2 mM SMC increased both signal intensity and signal area. During the first 30 min of SMC application, however, a decrease rather than an increase in signal intensity and signal area was observed [signal intensity: $96.80 \pm 2.16\%$; signal area: $95.93 \pm 3.47\%$ ($n = 6$ brain slices)]. A stable increase in both signal intensity and signal area was not apparent before an application time of

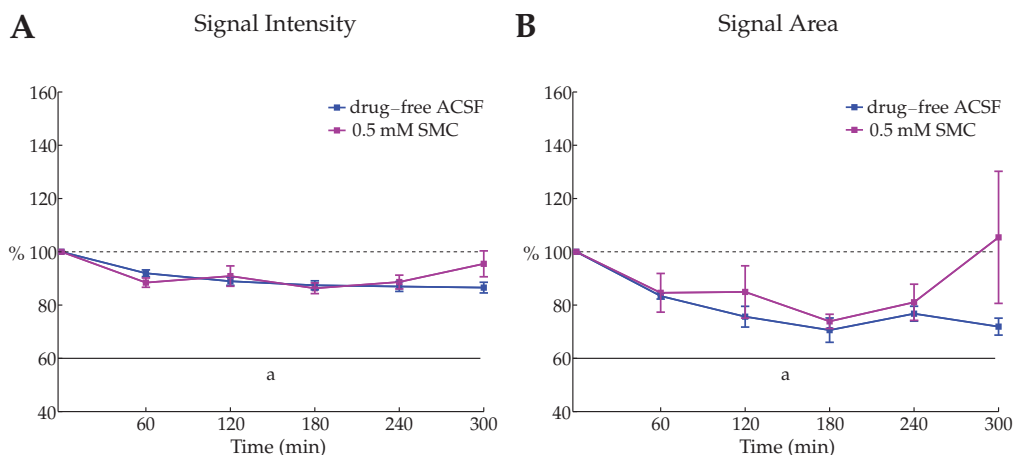


Figure 3.20: Comparison of IOSs during sham-drug application and during 0.5 mM SMC application in Bl/6 mouse brain slices. Application of 0.5 mM SMC was not sufficient to increase signal intensity and signal area compared to sham-drug application (control); [sham-drug application (control): $n = 6$ brain slices; 0.5 mM SMC application: $n = 6$ brain slices; normalized to mean signal intensity and mean signal area of first six IOS recordings (100%); a = sham-drug application/0.5 mM SMC application].

2 h [signal intensity after 120 min of application: sham-drug $88.94 \pm 1.54\%$ ($n = 6$ brain slices); 2 mM SMC $101.31 \pm 4.58\%$ ($n = 6$ brain slices); $p = 0.028$, unpaired Student's t-test; signal area after 120 min of application: sham-drug $75.63 \pm 3.90\%$ ($n = 6$ brain slices); 2 mM SMC $99.36 \pm 4.89\%$ ($n = 6$ brain slices); $p = 0.004$, unpaired Student's t-test; signal intensity after 300 min of application: sham-drug $86.55 \pm 2.00\%$ ($n = 6$ brain slices); 2 mM SMC $118.25 \pm 7.22\%$ ($n = 6$ brain slices); $p = 0.004$, Mann-Whitney rank sum test; signal area after 300 min of application: sham-drug $71.89 \pm 3.18\%$ ($n = 6$ brain slices); 2 mM SMC $129.08 \pm 11.38\%$ ($n = 6$ brain slices); $p < 0.001$, unpaired Student's t-test] (fig. 3.21). These results show that the long latent period of SMC could not be shortened by applying SMC directly on the brain slice. After a subsequent open ACSF superfusion of slices (wash-out), signal intensity and signal area were statistically no more different compared to control conditions [signal intensity after wash-out: sham-drug $89.24 \pm 2.76\%$ ($n = 6$ brain slices); 2 mM SMC $106.00 \pm 8.93\%$ ($n = 4$ brain slices); $p = 0.110$, unpaired Student's t-test; signal area after wash-out: sham-drug $74.93 \pm 2.81\%$ ($n = 6$ brain slices); 2 mM SMC $91.12 \pm 16.71\%$ ($n = 4$ brain slices); $p = 0.257$, Mann-Whitney rank sum test].

3.2.1.2 Effects of SMC in Different Mouse Strains

As mentioned before, one project of the present study was to test whether SPS-IgG containing Anti-GAD AAbs is capable of affecting neuronal network activity within the motor cortex. As it was considered that effects of SPS-IgG on IOSs might be small, an utmost sensitive assay was aimed for. One possibility to reach this goal was to investigate

3.2 Effects of SMC on Motor Cortical Neuronal Network Activity

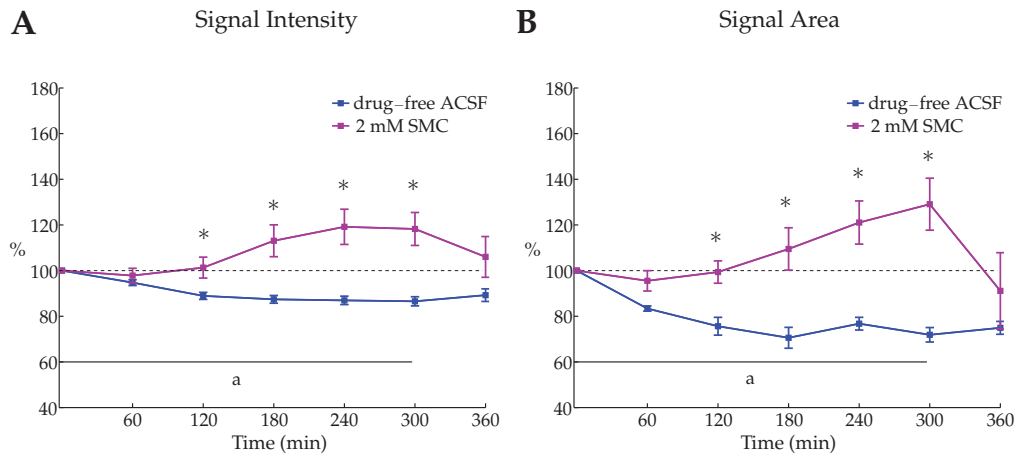


Figure 3.21: Comparison of IOSs during sham-drug application and during application of 2 mM SMC in Bl/6 mouse brain slices. The temporal changes in signal intensity and signal area were compared between sham-drug application (control) and application of 2 mM SMC. This comparison indicates that application of 2 mM SMC counteracted run-down of signal intensity and signal area observed during sham-drug application. After 120 min of 2 mM SMC application, both signal intensity and signal area were significantly increased compared to control conditions. These effects lasted over the whole time period of SMC application and were abolished by wash-out of SMC (360 min = after 60 min wash-out); [sham-drug application (control): n = 6 brain slices; 2 mM SMC application: n = 6 brain slices/ wash-out 2 mM SMC: n = 4 brain slices; normalized to mean signal intensity and mean signal area of first six IOS recordings (100%); a = sham-drug application/2 mM SMC application; *p < 0.05].

different mouse strains regarding their sensitivity to display SMC effects on IOSs. This idea is based on findings by Tunncliffe and colleagues, who observed differences in the GAD activity between different mouse strains (Tunncliffe *et al.*, 1973). The lowest GAD activity was observed in Bl/6 mice, whereas Balb/c mice showed the highest GAD activity of all mouse strains investigated. It was therefore hypothesized that in brain slices from Balb/c mice GAD inhibition would be compensated to a higher extent compared to Bl/6 mice. To possibly provide physiological evidence for this scenario and, if so, to show that brain slices from Bl/6 mice were more suitable for the SPS-IgG experiments, effects of 2 mM SMC on neuronal network activity were additionally examined in brain slices from Balb/c mice.

Indeed, compared to brain slices obtained from Bl/6 mice, statistically significant effects of SMC on signal intensity and signal area occurred after a longer application of SMC, i.e. after 4h of SMC application [signal intensity after 240 min of application: sham-drug $88.63 \pm 1.45\%$ (n = 3 brain slices); 2 mM SMC $105.97 \pm 1.57\%$ (n = 5 brain slices); p = 0.036, Mann-Whitney rank sum test; signal area after 240 min of application: sham-drug $89.19 \pm 2.23\%$ (n = 3 brain slices); 2 mM SMC $108.67 \pm 3.05\%$ (n = 5 brain slices); p = 0.004, unpaired Student's t-test] (fig. 3.22). These findings suggest that brain

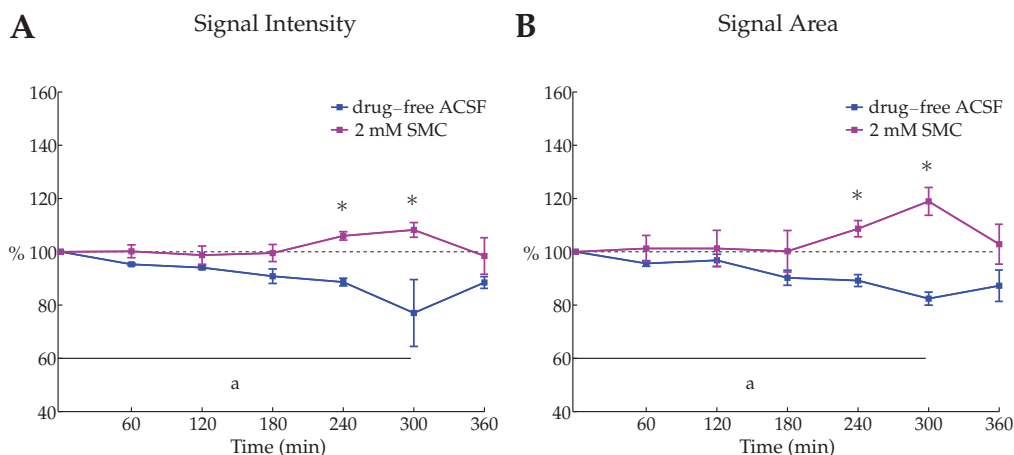


Figure 3.22: Comparison of IOSs during sham-drug application and during application of 2 mM SMC in Balb/c mouse brain slices. The temporal changes in signal intensity and signal area were compared between sham-drug application (control) and SMC application (2 mM). This comparison indicates that application of 2 mM SMC counteracted run-down of signal intensity and signal area observed during sham-drug application. After 240 min of 2 mM SMC application, both signal intensity and signal area were significantly increased compared to control conditions. These effects lasted over the whole time period of SMC application and were abolished by wash-out of SMC (360 min = after 60 min wash-out); [sham-drug application (control): $n = 3$ brain slices; 2 mM SMC application: $n = 5$ brain slices; normalized to mean signal intensity and mean signal area of first six IOS recordings (100%); a = sham-drug application/2 mM SMC application; * $p < 0.05$].

slices from Bl/6 mice were more sensitive to GAD inhibition. Therefore, all further experiments were conducted in brain slices from Bl/6 mice.

3.2.2 Effects of SMC on Synaptic Transmission

As shown above, SMC increased signal intensity and signal area of evoked motor cortical IOSs and, thus, enhanced neuronal network excitability. To detail the mechanisms by which SMC exerted this effect, whole-cell patch-clamp recordings from motor cortical layer II/III pyramidal neurons were performed to investigate actions of SMC on synaptic transmission. Layer II/III pyramidal neurons were chosen as these cells receive high GABAergic synaptic inputs via various inter- and intralaminar connections (Helmstaedter *et al.*, 2008, 2009) and, therefore, are appropriate to examine SMC effects on GABA_A receptor-mediated neurotransmission.

IOS recordings, however, revealed a long latent period of at least 2 h until first SMC-induced changes could be observed (see page 55). As it is difficult to achieve stable whole-cell recordings for more than 2 h, brain slices were preincubated with 2 mM SMC for 2 h before postsynaptic currents of layer II/III pyramidal neurons were recorded, while brain slices preincubated in drug-free ACSF served as control. Afterwards, whole-cell recordings were established and spontaneous postsynaptic currents were recorded.

Generated by spontaneous neurotransmitter release, these currents served to investigate SMC effects on synaptic transmission. Moreover, the investigated spontaneous postsynaptic currents in a neuron typically result from synaptic transmission at numerous synapses innervating this neuron and, consequently, mirror the activity of the presynaptic network.

3.2.2.1 Effects of SMC on GABA_A Minis

GABA_A Minis are the result of action potential-independent GABA release at GABAergic synapses and can be used to unravel pre- vs. postsynaptic effects of a particular drug on these synapses (Nusser *et al.*, 1997; Zhou *et al.*, 2000; Kilman *et al.*, 2002). As it was suggested that SMC reduces the presynaptic GABA content in the brain slice preparation used and, in this way, led to the increased motor cortical network excitability as observed in IOS recordings (see page 55), it was hypothesized that SMC would reduce the amplitude of GABA_A Minis in layer II/III pyramidal neurons. These postsynaptic currents were pharmacologically isolated by the addition of NBQX, D-AP5, and TTX to the ACSF to block AMPA and NMDA receptors as well as voltage-gated sodium channels. GABA_B receptor-mediated Minis were blocked by the cesium-based intracellular solution. The remaining postsynaptic currents could be completely abolished by BIM application (data not shown, see page 26).

Consistent with a reduced GABA content within presynaptic vesicles, the mean amplitude of GABA_A Minis recorded over a time period of 5 min was statistically significantly decreased in SMC-treated brain slices compared to control brain slices [control 13.95 ± 0.96 pA (n = 14 cells/7 animals); 2 mM SMC preincubation 9.39 ± 0.64 pA (n = 13 cells/7 animals); $p < 0.001$, unpaired Student's t-test] (fig. 3.23, A, B, D). In the same experiments, 2 mM SMC diminished the frequency of GABA_A Minis [control 4.12 ± 0.37 Hz (n = 14 cells/7 animals); 2 mM SMC preincubation 1.96 ± 0.69 Hz (n = 13 cells/7 animals); $p = 0.001$, Mann-Whitney ranks sum test] (fig. 3.23, A, C, E). The reduced frequency of GABA_A Minis was most likely a secondary effect of the reduced GABA_A Mini amplitudes as smaller events could not be distinguished from noise.

3.2.2.2 Effects of SMC on sEPSCs

It is likely that the reduced strength of GABAergic inhibition by SMC, as evident by its effects on GABA_A Minis (see above), leads to increased neuronal network activity. Presumably in this way SMC enhanced the signal intensity and signal area of evoked IOSs (see page 55). To possibly reveal consistent effects at the level of spontaneous neuronal activity, the action of SMC on sEPSCs, which represent action potential-dependent and -independent excitatory postsynaptic currents, was investigated. These experiments

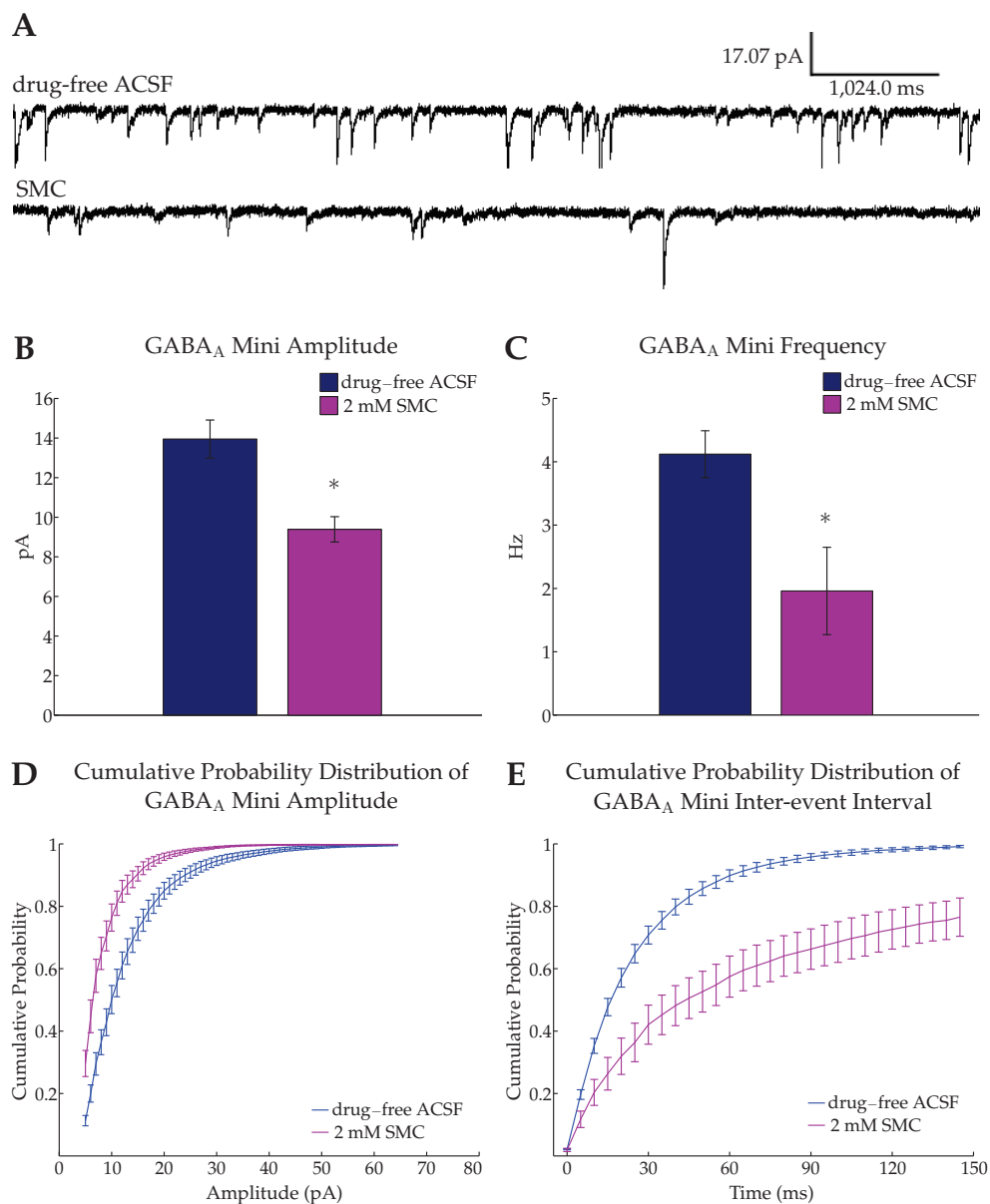


Figure 3.23: **Effects of SMC preincubation of brain slices on amplitude and frequency of GABA_A Minis.** Representative current traces recorded under control conditions and after SMC preincubation are shown in (A). Preincubation of brain slices with 2 mM SMC significantly reduced the mean GABA_A Minis amplitude and mean GABA_A Minis frequency (B, C). This is also evident from the shift of the cumulative probability distribution of GABA_A Minis amplitudes to the left and of inter-event intervals (= time interval between GABA_A Minis detected) to the right after SMC preincubation. This indicates that the probability of smaller GABA_A Minis amplitudes and of longer time intervals between single events was increased (D, E); (control: 14 cells/7 animals; 2 mM SMC preincubation n = 13 cells/7 animals; *p < 0.05)

were performed without any additional pharmacological treatment of brain slices. However, neither the amplitude nor the frequency of sEPSCs differed between control and SMC-preincubated brain slices [mean amplitude of sEPSCs: control 6.57 ± 0.25 pA (n = 15 cells/6 animals); 2 mM SMC preincubation 6.43 ± 0.22 pA (n = 13 cells/7 animals); mean frequency of sEPSCs: control 3.47 ± 0.58 Hz (n = 15 cells/6 animals); 2 mM SMC preincubation 3.00 ± 0.50 Hz (n = 13 cells/7 animals)] (fig. 3.24).

3.3 Effects of SPS-IgG on Motor Cortical Neuronal Network Activity

SPS represents a neurological disorder characterized by alterations in motor behavior and elevated Anti-GAD AAbs levels. Up to now, however, it is still a matter of debate, whether Anti-GAD AAbs contribute to the development and/or appearance of SPS symptoms or are merely a marker for disease. Therefore, the final aim of this study was to investigate potential effects of IgG derived from SPS patients on motor cortical neuronal network activity. This investigation was intended to be also conducted by a combination of IOS recordings and patch-clamp measurements in the motor cortex. Subsequent comparison of the results with those obtained by application of the well-known GAD inhibitor SMC may help to reveal an effect of SPS-IgG on GAD activity and to suggest a possible mechanism of SPS-IgG action on neuronal network activity.

3.3.1 Detection of Anti-GAD AAbs in Purified SPS-IgG

Plasma filtrates of two SPS patients were collected during therapeutic plasmapheresis. As an autoimmune origin of SPS is supposed, the plasma filtrates obtained should include potentially pathogenic AAbs. The IgG fraction (SPS-IgG) was purified from SPS patients' plasma filtrates by affinity chromatography (see page 17). Sandoglobulin[®], pooled IgG of over 1000 healthy donors, was treated in the same way as the plasma filtrates. The obtained IgG fraction served as control IgG.

First, Western Blots were used to prove whether both patients' SPS-IgG included AAbs directed against GAD. As shown in fig. 3.25 (A), SPS-IgG of both patients contained AAbs directed against a protein in the range of 65 kDa (patient 1: band 4; patient 2: band 5). Similar bands were found with polyclonal Abs against GAD₆₅ (band 1) and polyclonal Abs against both GAD₆₅ and GAD₆₇ (band 2). With control IgG no immunoreactivity against GAD₆₅ and/or GAD₆₇ could be observed (band 3). These results show that SPS-IgG of both patients contained Anti-GAD AAbs, which were not present in control IgG. As during immunoblotting proteins are denaturated, the results

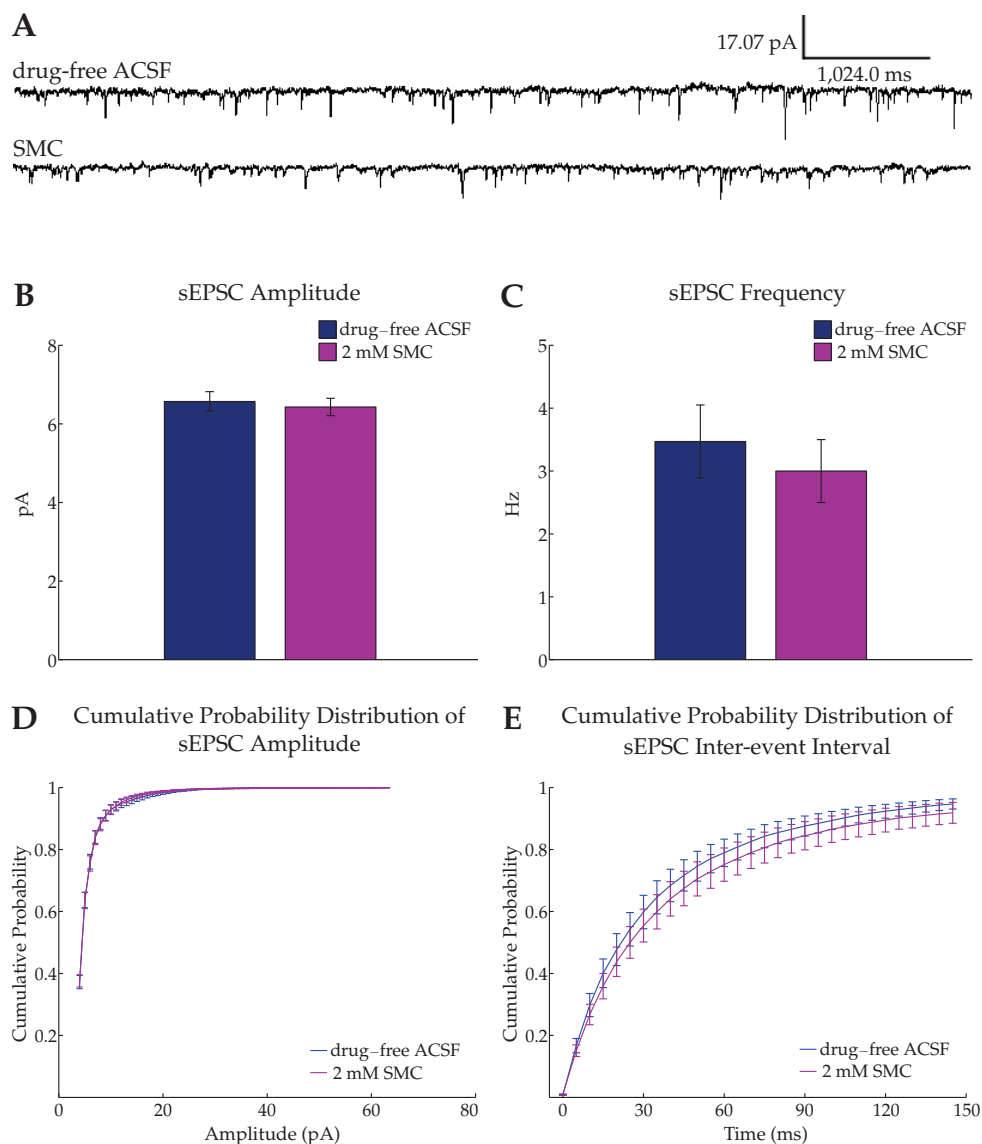


Figure 3.24: **Effects of SMC preincubation of brain slices on amplitude and frequency of sEPSCs.** Representative current traces recorded under control conditions and after SMC preincubation are shown in (A). Preincubation with 2 mM SMC did not alter mean sEPSC amplitude (B). A smaller mean sEPSC frequency could be observed in SMC-preincubated brain slices compared to control brain slices, but this difference was statistically not significant (C). The cumulative probability distribution of sEPSC amplitudes and inter-event intervals was similar in control and SMC-preincubated brain slices (D, E); (control: 15 cells/6 animals; SMC preincubation n = 13 cells/7 animals)

further indicate that at least a subset of the Anti-GAD AAbs of both patients were directed against a linear GAD epitope. The double band of the polyclonal Abs against GAD₆₅ and GAD₆₇ showed that both GAD isoforms lie close together. Therefore, it was not possible to clearly discern against which isoform the patients' Anti-GAD AAbs were directed.

To answer this question, an immunodot (GAD Dot) was used (fig. 3.25, B). One test stripe contained two control fields (negative and positive control) and two test fields with fixed antigens (GAD₆₅ and GAD₆₇). A violet staining of the test field, which had to be stronger than the staining of the negative control field, indicated the presence of AAbs against the according isoform. The GAD Dot revealed that both patients' SPS-IgG contained only AAbs against GAD₆₅ (patient 1: stripe 2; patient 2: stripe 3). No immunoreactivity of SPS-IgG with GAD₆₇ could be observed. As expected, the control IgG showed no immunoreactivity neither against GAD₆₅ nor against GAD₆₇ (stripe 1).

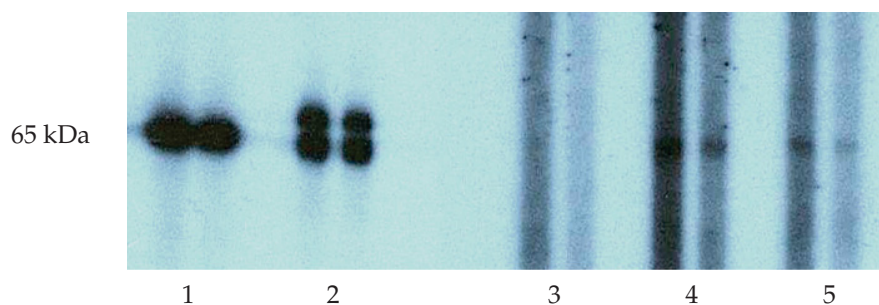
3.3.2 Effects of SPS-IgG on IOSs

To investigate effects of SPS-IgG on neuronal network activity within the mouse motor cortex, SPS-IgG of patient 2 and control IgG were applied via the bath solution at a concentration of 40 mg/l to brain slices obtained from Bl/6 mice. This concentration equals the maximal IgG concentration in the CSF of healthy persons (Bouloukos *et al.*, 1980). As additional control experiment, sham-drug application with IgG-free ACSF was performed following the same protocol as for IgG application. Statistical analysis was done by comparing the results of control IgG application with those of SPS-IgG application as well as the results of sham-drug application with those of control IgG and SPS-IgG application.

SPS-IgG caused no statistically significant effect on signal intensity or signal area compared to control IgG during an application time of 5 h (fig. 3.26).

When comparing the IOSs recorded every full hour during sham-drug application with those recorded during SPS-IgG and control IgG application, the run-down of signal intensity and signal area was significantly decelerated for 1 and 2 h, respectively [signal intensity after 60 min of application: sham-drug $91.93 \pm 1.27\%$ (n = 6 brain slices); SPS-IgG $100.52 \pm 1.96\%$ (n = 5 brain slices); p = 0.004, unpaired Student's t-test; signal intensity after 120 min of application: sham-drug $88.94 \pm 1.54\%$ (n = 6 brain slices); control IgG $93.90 \pm 1.14\%$ (n = 5 brain slices); p = 0.034, unpaired Student's t-test; signal area after 120 min of application: sham-drug $75.63 \pm 3.90\%$ (n = 6 brain slices); control IgG $93.23 \pm 3.15\%$ (n = 5 brain slices); SPS-IgG $99.43 \pm 6.55\%$ (n = 5 brain slices); sham-drug vs. control IgG: p = 0.008, unpaired Student's t-test; sham-drug vs. SPS-IgG: p = 0.010, unpaired Student's t-test] (fig. 3.27). After 2 h of both control IgG and SPS-IgG appli-

A



B

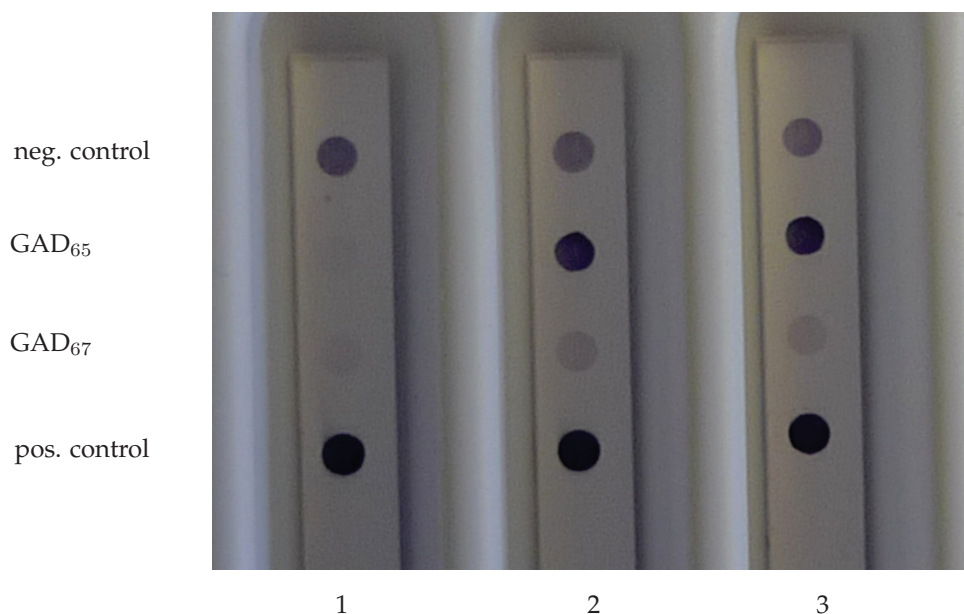


Figure 3.25: **Detection of Anti-GAD AAbs in purified IgG of SPS patients.** Western Blots (A) revealed that SPS-IgG of both patients contained AAbs directed against a protein in the range of 65 kDa (patient 1: band 4, dilution 1:30 and 1:60; patient 2: band 5, dilution 1:30 and 1:60). Similar bands were found with polyclonal Abs against GAD₆₅ (band 1, dilution 1:200 and 1:400) and polyclonal Abs against GAD₆₅ and GAD₆₇ (band 2, dilution 1:200 and 1:400). No immunoreactivity could be observed with control IgG (band 3). The immunodot (GAD Dot) (B) showed that Anti-GAD AAbs of both patients were only directed against the GAD₆₅ isoform as no reactivity with GAD₆₇ was detected (patient 1: stripe 2; patient 2: stripe 3). The control IgG reacted with neither GAD₆₅ nor GAD₆₇ (stripe 1).

3.3 Effects of SPS-IgG on Motor Cortical Neuronal Network Activity

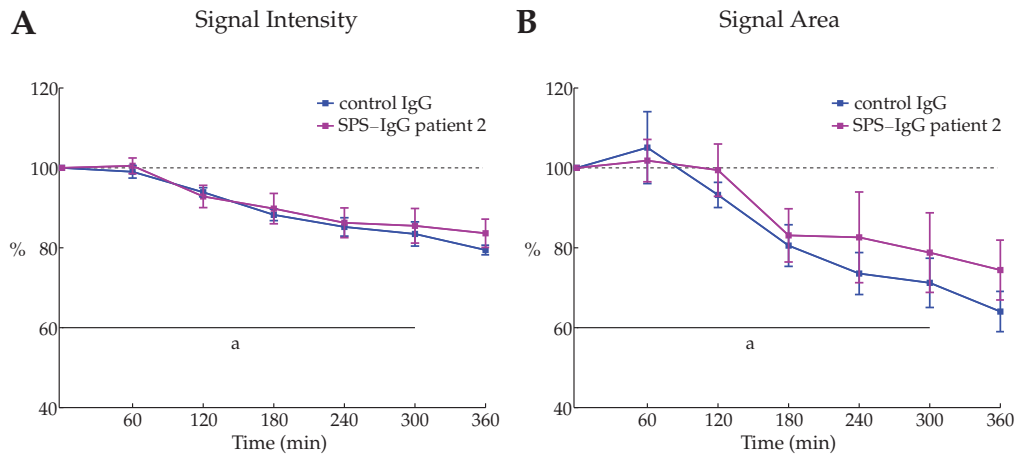


Figure 3.26: **Comparison of IOSs during application of 40 mg/l control IgG and 40 mg/l SPS-IgG of patient 2 in B1/6 mouse brain slices.** The temporal changes in signal intensity and signal area were compared between application of 40 mg/l control IgG and 40 mg/l of SPS-IgG of patient 2. SPS-IgG did not significantly alter IOSs compared to control IgG. However, after 240 and 300 min of application, signal area was slightly bigger in SPS-IgG treated brain slices. Both signal area and signal intensity did not recover after wash-out (360 min = after 60 min wash-out); [control IgG application: n = 5 brain slices; application of SPS-IgG patient 2: n = 5 brain slices; normalized to mean signal intensity and mean signal area of first six IOS recordings (100%); a = control IgG application/application of 40 mg/l SPS-IgG patient 2].

cation, however, the run-down of IOSs accelerated in IgG-treated brain slices. After 3 h of IgG application, no significant difference to sham-drug application was found. Moreover, no recovery of signal intensity and signal area was observed in any group after 60 min wash-out.

3.3.3 Effects of SPS-IgG on Synaptic Transmission

As IOS recordings did not reveal different effects of control IgG and SPS-IgG on neuronal network activity (see page 63), whole-cell patch-clamp recordings, which might be more sensitive to detect SPS-IgG effects than IOS recordings, were performed on motor cortical layer II/III pyramidal neurons. As done with SMC (see page 58), brain slices were preincubated for 2 h in IgG-free ACSF or ACSF containing either 40 mg/l SPS-IgG of patient 1 or 2 or 40 mg/l control IgG. Using the same preincubation protocol allowed to compare potential effects of SPS-IgG with those exerted by SMC. This may help to reveal possible mechanisms of SPS-IgG action and the role of Anti-GAD AAbs in alterations of neuronal network activity.

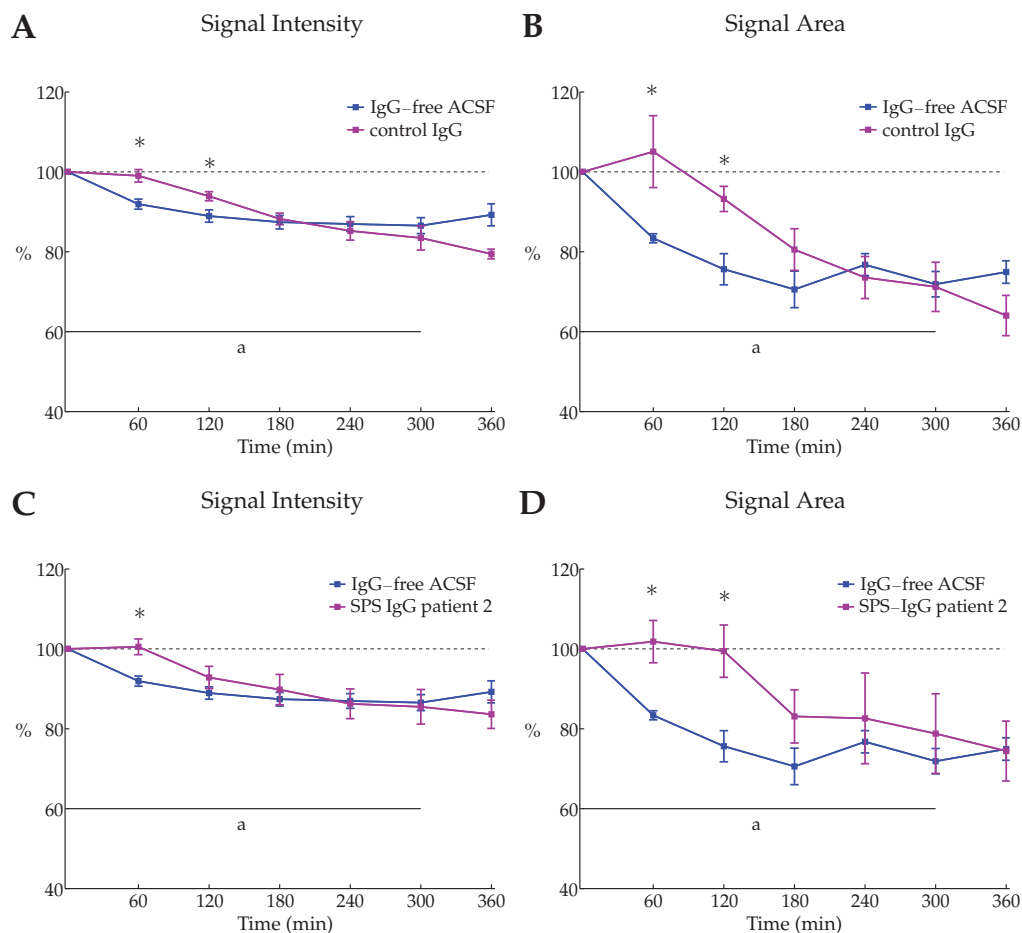


Figure 3.27: **Comparison of IOSs during sham-drug application, during application of 40 mg/l control IgG and during application of 40 mg/l SPS-IgG.** The temporal changes in signal intensity and signal area were compared between sham-drug application with IgG-free ACSF and application of 40 mg/l control IgG or application of 40 mg/l SPS-IgG. This comparison showed that both control IgG and SPS-IgG significantly decelerated the run-down for 60 and 120 min, respectively. Subsequently, the run-down of IOSs accelerated in IgG-treated brain slices. After 180 min of IgG application, no significant difference to sham-drug application was found. Moreover, no recovery of signal intensity and signal area was observed after wash-out (360 min = after 60 min wash-out); [sham-drug application: n = 6 brain slices; control IgG application: n = 5 brain slices; application of SPS-IgG patient 2: n = 5 brain slices; normalized to mean signal intensity and mean signal area of first six IOS recordings (100%); *p < 0.05].

3.3.3.1 Effects of SPS-IgG on GABA_A Minis

Recording of GABA_A Minis after preincubation of brain slices with SPS-IgG and control IgG as well as IgG-free ACSF followed the same protocol as for SMC preincubation (see page 59).

To possibly reveal unspecific effects of IgG preincubation, the mean amplitude and frequency of GABA_A Minis recorded in brain slices preincubated either in IgG-free ACSF or ACSF containing control IgG were compared. The mean GABA_A Mini amplitude

was slightly smaller in brain slices preincubated with control IgG [12.40 ± 0.77 pA (n = 16 cells/6 animals)] compared to brain slices preincubated in IgG-free ACSF [13.95 ± 0.96 pA (n = 14 cells/7 animals)], but this difference was not significant (fig. 3.28, A, B, D). The mean GABA_A Mini frequency, too, did not differ between brain slices preincubated with IgG-free ACSF [4.12 ± 0.37 Hz (n = 14 cells/7 animals)] and with control IgG [4.59 ± 0.46 Hz (n = 16 cells/6 animals)] (fig. 3.28, A, C, E).

Similar to SMC (see page 59), SPS-IgG attenuated GABA_A Mini amplitude even though this effect was not significant for all settings. GABA_A Mini amplitude in brain slices preincubated with SPS-IgG [SPS-IgG patient 1: 11.06 ± 0.57 pA (n = 15 cells/7 animals); SPS-IgG patient 2: 11.62 ± 0.89 pA (n = 13 cells/7 animals)] tended to be slightly smaller compared to those recorded in brain slices preincubated with control IgG [12.40 ± 0.77 pA (n = 16 cells/6 animals)] (fig. 3.29, A, B, D). This effect, however, was not statistically significant. Compared to mean GABA_A Mini amplitude recorded in brain slices preincubated with IgG-free ACSF [13.95 ± 0.96 pA (n = 14 cells/7 animals)], a significantly decreased mean GABA_A Mini amplitude was only observed in brain slices preincubated with SPS-IgG of patient 1 (p = 0.014, unpaired Student's t-test) but not in brain slices preincubated with SPS-IgG of patient 2 (fig. 3.30, A, B).

The mean frequency of GABA_A Minis was significantly reduced in brain slices preincubated with SPS-IgG [SPS-IgG patient 1: 2.58 ± 0.30 Hz (n = 15 cells/7 animals); SPS-IgG patient 2: 2.52 ± 0.35 Hz (n = 13 cells/7 animals)] compared to brain slices preincubated with control IgG [4.59 ± 0.46 Hz (n = 16 cells/6 animals); control IgG vs. SPS-IgG patient 1: p < 0.001, Mann-Whitney rank sum test; control IgG vs. SPS-IgG patient 2: p = 0.002, Mann-Whitney rank sum test] (fig. 3.29, A, C, E) as well as compared to brain slices preincubated with IgG-free ACSF [4.12 ± 0.37 Hz (n = 14 cells/7 animals); IgG-free ACSF vs. patient 1: p = 0.002, Mann-Whitney rank sum test; IgG-free ACSF vs. patient 2: p = 0.004, Mann-Whitney rank sum test] (fig. 3.30, A, C).

3.3.3.2 Effects of SPS-IgG on sEPSCs

Even though the results of IOS recordings did not corroborate an effect of SPS-IgG on evoked neuronal network activity (see page 63), whole-cell patch-clamp recordings of GABA_A Minis revealed a reduction in GABAergic inhibition (see above). As this effect potentially increases neuronal network activity at the level of spontaneous neuronal activity, the action of SPS-IgG on sEPSCs was investigated.

As done for the recordings of GABA_A Minis, sEPSCs recorded in brain slices preincubated with control IgG or in IgG-free ACSF were analyzed with respect to unspecific IgG effects. The mean amplitude of sEPSCs did not differ between both groups [IgG-free ACSF: 6.57 ± 0.25 pA (n = 15 cells/6 animals); control IgG: 6.79 ± 0.27 pA (n = 14 cells/7

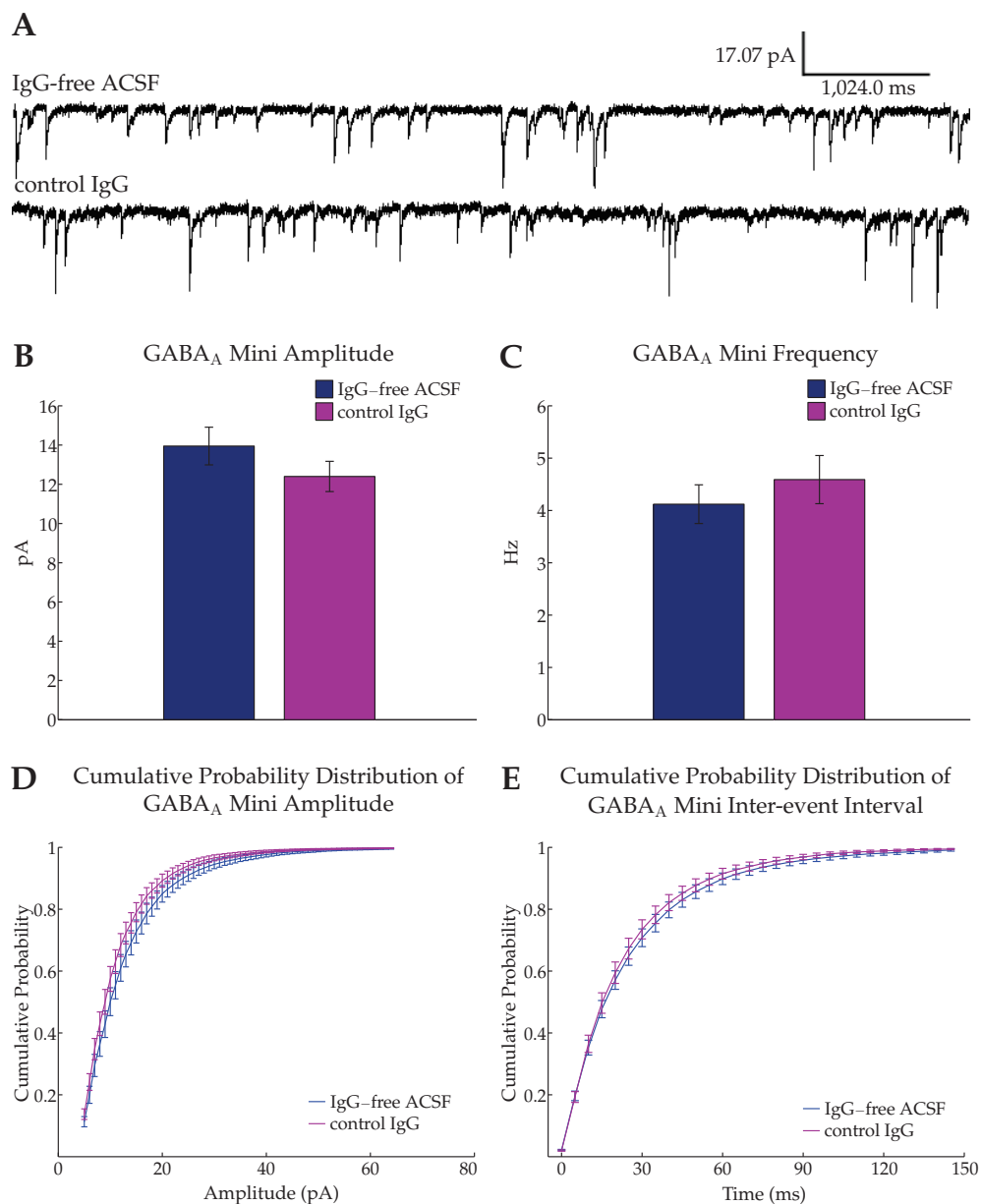


Figure 3.28: Effects of control IgG preincubation of brain slices on amplitude and frequency of GABA_A Minis. Representative current traces recorded under control conditions (preincubation in IgG-free ACSF) and after control IgG preincubation are shown in (A). Preincubation with 40 mg/l control IgG did not alter mean GABA_A Mini amplitude and mean GABA_A Mini frequency (B, C), excluding a possible unspecific IgG effect on GABA_A Minis. Consistent with these results, the cumulative probability distribution of GABA_A Mini amplitudes and GABA_A Mini inter-event intervals (= time interval between GABA_A Minis detected) did not differ between brain slices preincubated in control IgG or preincubated in IgG-free ACSF (D, E); (IgG-free ACSF: 14 cells/7 animals; control IgG: n = 16 cells/6 animals).

3.3 Effects of SPS-IgG on Motor Cortical Neuronal Network Activity

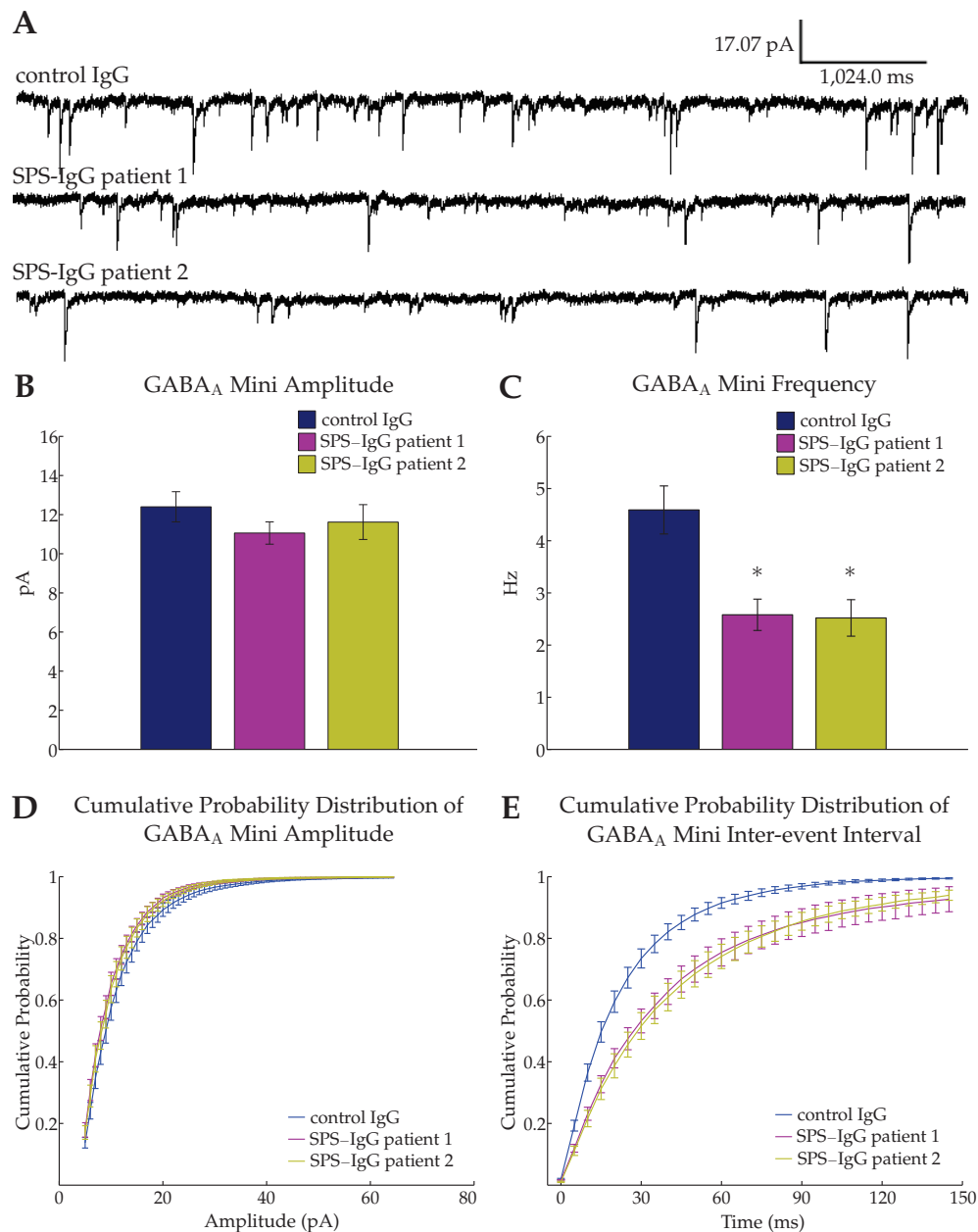


Figure 3.29: Effects of SPS-IgG preincubation of brain slices on amplitude and frequency of GABA_A Minis compared to control IgG. Representative current traces recorded after control IgG preincubation and after preincubation with SPS-IgG of patient 1 and patient 2 are shown in (A). Mean GABA_A Mini amplitude tended to be slightly smaller in brain slices preincubated with 40 mg/l SPS-IgG of both patients (B). Mean GABA_A Mini frequency (C), however, was significantly decreased in SPS-IgG-preincubated brain slices. The cumulative probability distribution of GABA_A Mini amplitudes did not differ between control IgG- and SPS-IgG-preincubated brain slices (D). The cumulative probability distribution of the inter-event intervals (= time interval between GABA_A Minis detected) was shifted to the right after SPS-IgG preincubation indicating a longer time interval between single events and, hence, a reduced frequency of GABA_A Minis (E); (control IgG: 16 cells/6 animals; SPS-IgG patient 1: n = 15 cells/7 animals; SPS-IgG patient 2: n = 13 cells/7 animals; *p < 0.05).

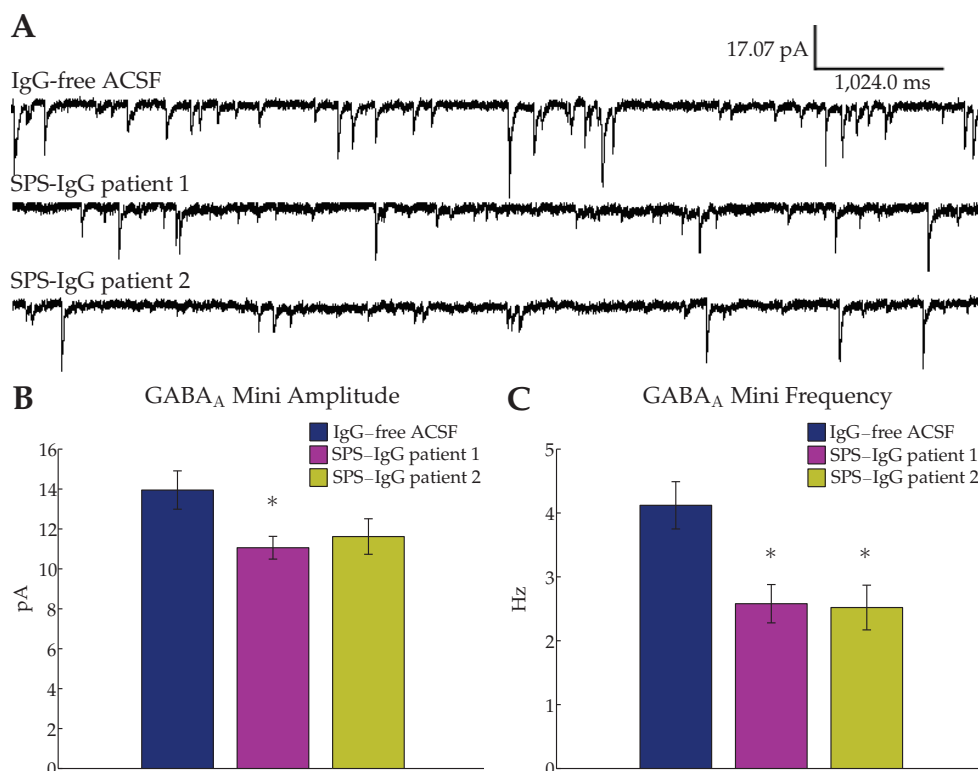


Figure 3.30: **Effects of SPS-IgG preincubation of brain slices on amplitude and frequency of GABA_A Minis compared to brain slices preincubated in IgG-free ACSF.** Representative current traces recorded after preincubation of brain slices in IgG-free ACSF and in SPS-IgG of patient 1 and patient 2 are shown in (A). Preincubation of brain slices in ACSF containing 40 mg/l SPS-IgG reduced mean GABA_A Mini amplitude, but this effect was only significant for SPS-IgG of patient 1 (B). Mean GABA_A Mini frequency was significantly decreased after preincubation of brain slices with SPS-IgG of patient 1 and patient 2 (C); (IgG-free ACSF: 14 cells/7 animals; SPS-IgG patient 1: n = 15 cells/7 animals; SPS-IgG patient 2: n = 13 cells/7 animals; *p < 0.05).

animals)] (fig. 3.31, A, B, D). The mean frequency of sEPSCs, however, was significantly reduced in brain slices preincubated with control IgG [IgG-free ACSF: 3.47 ± 0.58 Hz (n = 15 cells/6 animals); control IgG: 1.92 ± 0.31 Hz (n = 14 cells/7 animals); p = 0.031, Mann-Whitney rank sum test] suggesting an unspecific effect of control IgG on the release of excitatory neurotransmitters (fig. 3.31, A, C, E).

SPS-IgG preincubation did not affect the mean sEPSC amplitude [IgG-free ACSF: 6.57 ± 0.25 pA (n = 15 cells/6 animals); control IgG: 6.79 ± 0.27 pA (n = 14 cells/7 animals); SPS-IgG patient 1: 6.36 ± 0.14 pA (n = 14 cells/7 animals); SPS-IgG patient 2: 6.68 ± 0.24 pA (n = 14 cells/7 animals)], thus contradicting postsynaptic effects of SPS-IgG (figs. 3.32, A, B, D; 3.33, A, B).

When the mean frequency of sEPSCs was compared between brain slices preincubated with control IgG and SPS-IgG, mean frequency was significantly increased in SPS-

3.3 Effects of SPS-IgG on Motor Cortical Neuronal Network Activity

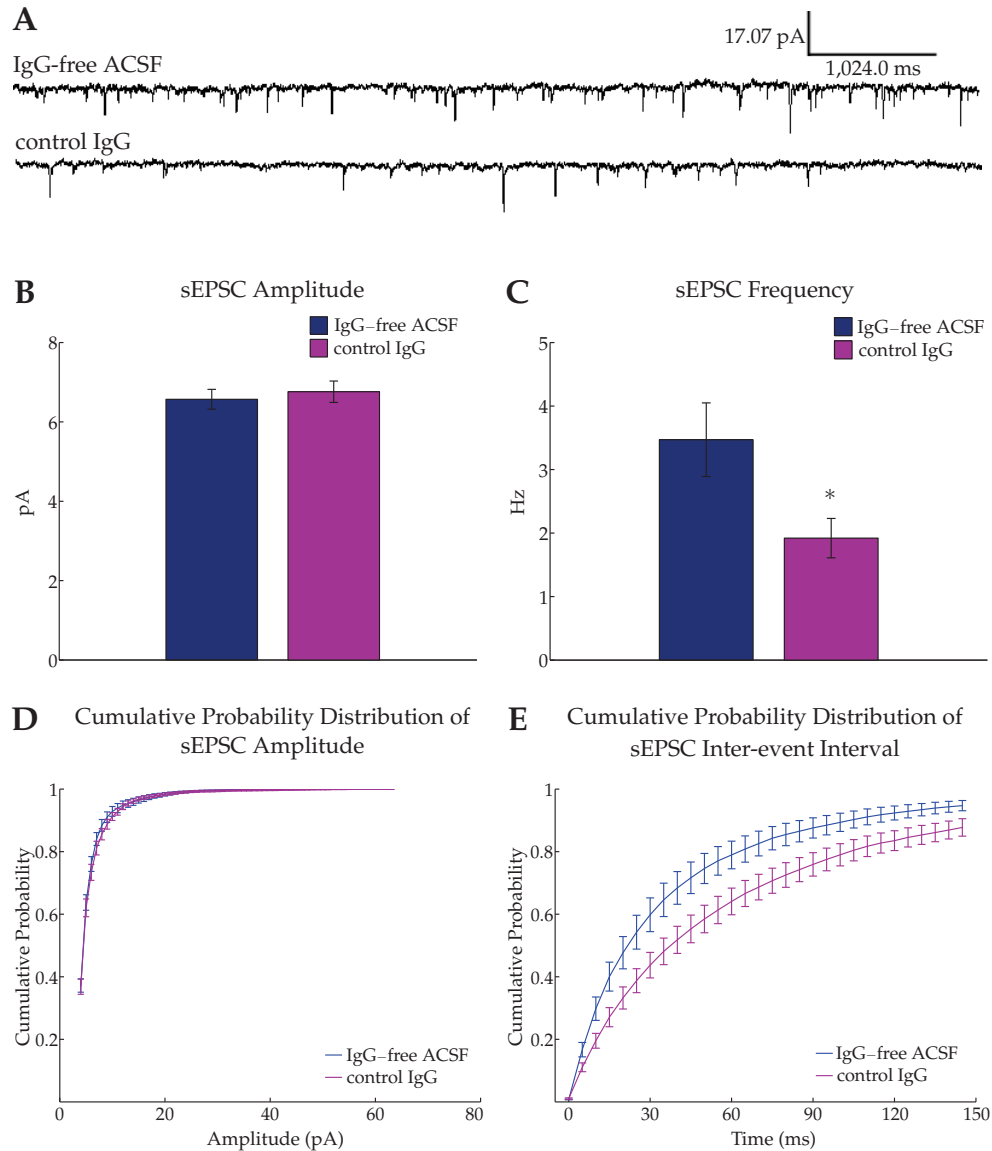


Figure 3.31: **Effects of control IgG preincubation of brain slices on amplitude and frequency of sEPSCs.** Representative current traces recorded under control conditions (preincubation in IgG-free ACSF) and after control IgG preincubation are shown in (A). Preincubation with 40 mg/l control IgG did not alter mean sEPSC amplitude (B). The mean frequency of sEPSCs, however, was significantly reduced in control IgG-preincubated brain slices (C). The cumulative probability distribution of sEPSC amplitude was similar in IgG-free ACSF- and control IgG-preincubated brain slices (D). The cumulative probability distribution of sEPSC inter-event intervals, however, was shifted to the right after control IgG preincubation as the probability of longer time intervals between single events was increased (E); (IgG-free ACSF: 15 cells/6 animals; control IgG: n = 14 cells/7 animals; *p < 0.05).

3 Results

IgG-preincubated brain slices [control IgG: 1.92 ± 0.31 Hz ($n = 14$ cells/7 animals), SPS-IgG patient 1: 4.41 ± 0.63 Hz ($n = 14$ cells/7 animals); SPS-IgG patient 2: 4.17 ± 0.59 Hz ($n = 14$ cells/7 animals); control IgG vs. SPS-IgG patient 1: $p = 0.001$, Mann-Whitney rank sum test; control IgG vs. SPS-IgG patient 2: $p = 0.002$, Mann-Whitney rank sum test] (fig. 3.32, A, C, E). This increase in mean sEPSC frequency, however, was not significant if compared to the mean frequency of sEPSCs recorded in brain slices preincubated in IgG-free ACSF [IgG-free ACSF: 3.47 ± 0.58 Hz ($n = 15$ cells/6 animals)] (fig. 3.33, A, C).

3.3 Effects of SPS-IgG on Motor Cortical Neuronal Network Activity

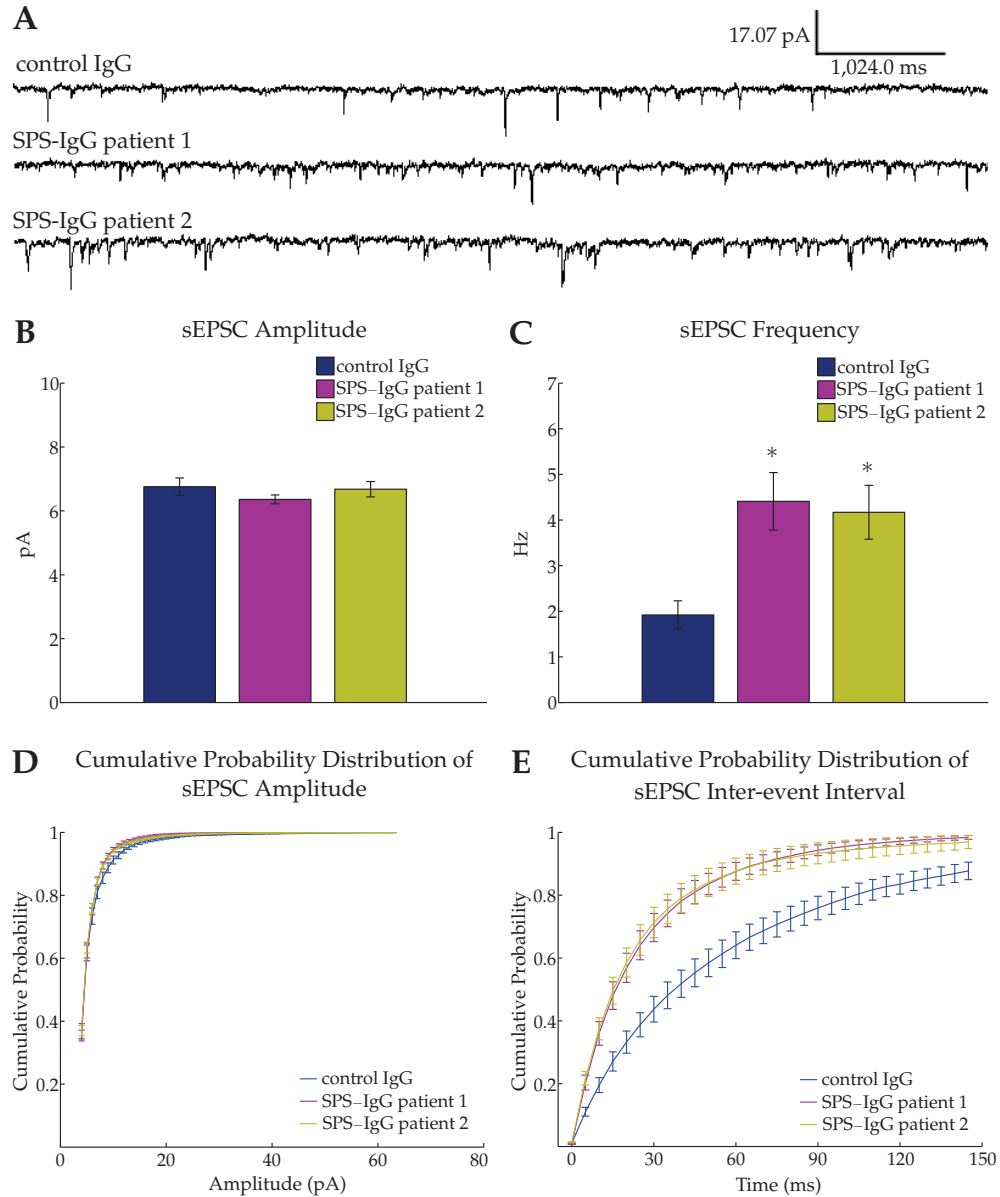


Figure 3.32: Effects of SPS-IgG preincubation of brain slices on amplitude and frequency of sEPSCs compared to control IgG. Representative current traces recorded after control IgG and SPS-IgG preincubation are shown in (A). Preincubation with 40 mg/l SPS-IgG did not alter mean sEPSC amplitude in brain slices compared to control IgG preincubation (B). The recorded frequency of sEPSCs, however, was significantly increased in SPS-IgG-preincubated brain slices (C). The cumulative probability distribution of sEPSC amplitudes was similar in control IgG- and SPS-IgG-preincubated brain slices (D). The cumulative probability distribution of sEPSC inter-event intervals, however, was shifted to the left for SPS-IgG-preincubated brain slices, indicating an increased sEPSC frequency (E); (control IgG: n = 14 cells/7 animals; SPS-IgG patient 1: n = 14 cells/7 animals; SPS-IgG patient 2: n = 14 cells/7 animals; *p < 0.05).

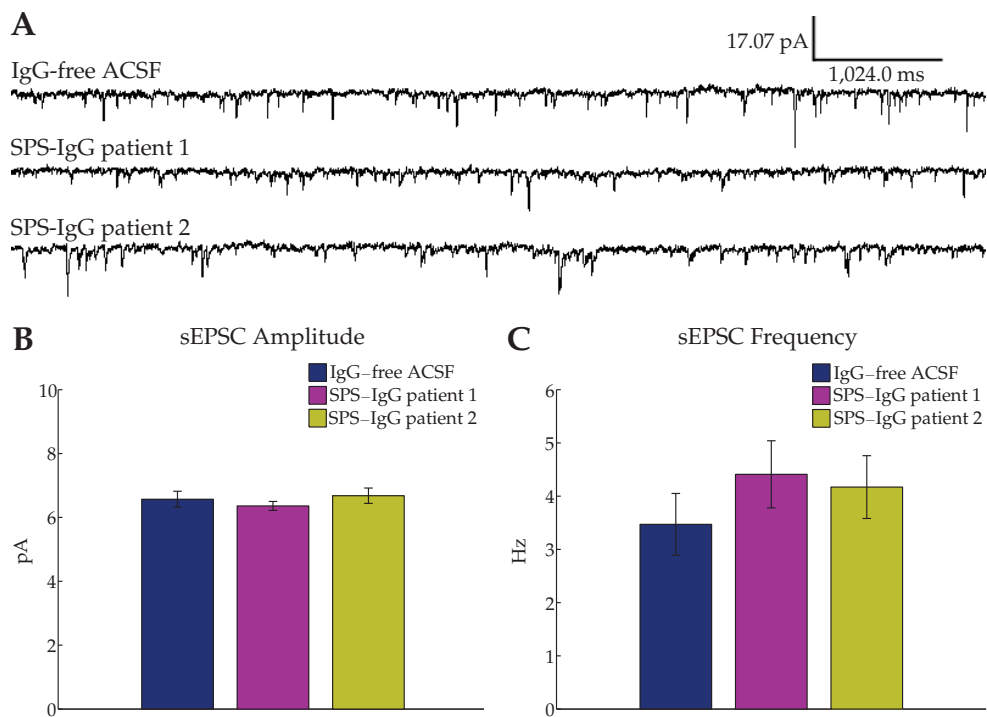


Figure 3.33: **Effects of SPS-IgG preincubation of brain slices on amplitude and frequency of sEPSCs compared to brain slices preincubated in IgG-free ACSF.** Representative current traces recorded after preincubation of brain slices in IgG-free ACSF and with SPS-IgG of patient 1 and patient 2 are shown in (A). Preincubation with 40 mg/l SPS-IgG did not alter mean sEPSC amplitude (B). The frequency of sEPSCs, however, was slightly increased in SPS-IgG-preincubated brain slices (C), but this increase was not significant; (IgG-free ACSF: n = 15 cells/6 animals; SPS-IgG patient 1: n = 14 cells/7 animals; SPS-IgG patient 2: n = 14 cells/7 animals).

4 Discussion

4.1 IOS Recordings

4.1.1 Physiological Interpretations of IOSs

IOSs can be used to investigate spread and strength of stimulus-evoked neuronal network activity as these signals represent activity-dependent changes in the optical properties of brain tissue. In particular, IOSs evoked within the cerebral cortex nearly span the whole area of cortical columns and, thus, are suitable to study cortical network activity. One question, however, that arises concerns the physiological interpretation of changes in IOSs as observed in this PhD study within the murine primary motor cortex.

The cerebral cortex consists of cortical columns, which are made up of six histologically discernible layers of different cell types (Rockel *et al.*, 1980; Rakic, 2008). The different layers are numbered consecutively from the outside pial surface (layer I) to the inside white matter (layer VI). A columnar pattern of the cortex was previously shown using the [¹⁴C]deoxyglucose technique. The concentration of this compound in tissue closely reflects that tissue's rate of glucose utilization or energy metabolism (Kennedy *et al.*, 1975; Sokoloff, 1981). The pattern of [¹⁴C]deoxyglucose incorporation observed in the rat barrel cortex after stroking the C3 vibrissa is similar to the pattern of IOSs (Kossut & Hand, 1984a,b). Placing the stimulation electrode in different cortical layers or cortical areas causes changes in the spatial characteristics of IOSs indicating that IOSs reflect functional properties of interlaminar connectivity of the cortex and allow to determine activation patterns (Grinvald *et al.*, 1986; Haglund *et al.*, 1992a; Kohn *et al.*, 2000; Holthoff *et al.*, 2007).

A study by Holthoff *et al.* (2007), mapping IOSs in different cortical areas, showed the strongest IOS intensities in layer II/III and layer V of the motor cortex. No signal could be detected in layer I (Holthoff *et al.*, 1994; Holthoff & Witte, 1996, 1997; Holthoff *et al.*, 2007). The shape of IOSs observed in this PhD study matched these previous findings (see fig. 3.4, page 36). Small variations in signal shape may be attributed to small differences in the plane of cutting during brain slice preparation.

IOSs show a weak correlation with strength, spatial distribution, and time course of changes in extracellular K⁺ concentrations, which can serve as a marker for neuronal

activity (Holthoff & Witte, 1996, 1998; Witte *et al.*, 2001). Moreover, inhibiting synaptic transmission blocks IOSs (MacVicar & Hochman, 1991; Dodt *et al.*, 1996) and IOSs correlate with the amplitude as well as spatial distribution of field potentials (Federico *et al.*, 1994; Holthoff *et al.*, 1994; Dodt *et al.*, 1996; Holthoff & Witte, 1997; Kohn *et al.*, 1997; Cerne & Haglund, 2002). A more detailed analysis, however, showed that the lateral distribution of field potentials is narrower than the lateral distribution of IOSs (Cerne & Haglund, 2002). A strong correlation between the amplitudes of field potentials and IOSs can be observed in the center of the IOS column, but such a correlation is missing at the edge of the IOSs (Holthoff & Witte, 1997; Cerne & Haglund, 2002). The edge of the evoked column seems to reflect primarily the sub-threshold excitatory synaptic activity (Das & Gilbert, 1995; Toth *et al.*, 1996; Cerne & Haglund, 2002). These findings show that, although occurring with a certain delay and slow kinetics, IOSs nicely reflect neuronal activity, but cannot be used to discern between action potentials and sub-threshold depolarizations.

In this PhD study, a new program for the analysis of IOSs has been developed. This program allowed to monitor changes in the signal intensity (see fig. 3.11, A, page 46), which represented the strength of stimulus-induced activation, and in the signal area (see fig. 3.11, B, page 46), which represented the lateral extent of the signal. With increasing stimulation currents, both signal intensity and signal area increased (see fig. 3.15, page 51). As higher stimulation currents cause stronger activation of the neuronal network, these results demonstrate that it is possible to display changes in neuronal network activity by means of IOSs.

Compared to the signal intensity, however, the signal area was more sensitive to an increase in stimulation current, reached its almost maximum size at intermediate stimulation intensities, and was only weakly affected by a further increase in stimulation strength (see fig. 3.15, B, page 51). Previous studies came to similar results, showing that the lateral extent of IOSs is independent of stimulation intensities if brain slices are stimulated with intermediate stimulation intensities (Holthoff *et al.*, 1994; Kohn *et al.*, 1997, 2000), whereas signal intensity exhibits a linear relationship to stimulation strength (Holthoff *et al.*, 1994). These observations imply that the lateral spread of IOSs within the cortex is restricted by anatomical borders and that the borders of IOSs roughly match the borders of functional columns.

4.1.2 Long-term IOS Recording

Recording of IOSs is not hampered by bleaching, wash-out, pharmacological side effects, and photodynamic damage as frequently observed with voltage and ion-sensitive dyes (Grinvald *et al.*, 1986; Holthoff & Witte, 1996; Takashima *et al.*, 2001). As these ad-

vantages of IOS recording suggest that intrinsic optical imaging presumably constitutes a technique for long-term recordings of neuronal network activity, one goal of this PhD thesis was to test whether IOS recordings are capable of monitoring neuronal network activity for several hours. This was of particular importance as the uptake of drugs inhibiting GAD activity and the depletion of preexisting GABA pools was thought to be slow and as the high variability of IOSs between different brain slices made it necessary to measure relative changes within one brain slice.

To facilitate long-term IOS recordings, the stimulation strength was reduced as it was hypothesized that repeated strong stimulations impair brain slice physiology (see page 48). Moreover, a typical stimulation protocol for triggering IOSs (Holthoff *et al.*, 1994; Dodt *et al.*, 1996; D'Arcangelo *et al.*, 1997; Holthoff & Witte, 1997, 1998; Witte *et al.*, 2001; Becker *et al.*, 2005; Holthoff *et al.*, 2007) is close to protocols, which can induce synaptic plasticity in cat or rat motor cortex (Keller *et al.*, 1991; Aroniadou & Keller, 1995). The adapted stimulation protocol was capable of eliciting IOSs with a sufficient signal-to-noise ratio of about 1:10 and with a good reproducibility of signal intensity and signal area during subsequent stimulations within the same brain slice (see fig. 3.14, page 50).

Pilot experiments indicated that, at higher stimulation frequencies, less stimulus pulses were necessary to trigger IOSs. These results are in line with previous studies showing stronger IOSs at higher stimulation frequencies (MacVicar & Hochman, 1991; Federico *et al.*, 1994; Kohn *et al.*, 2000). In the present study, however, much slower kinetics of IOSs were observed (see tab. 3.4, page 49) compared to those described in previous work (Holthoff *et al.*, 1994; Holthoff & Witte, 1996). There are many explanations for this difference in IOS kinetics, e.g. the use of different stimulation protocols, of different methods of data analysis, and of animals of different age.

Long-term measurements with drug-free ACSF following the same protocol, which was later applied for long-term drug application, were conducted over a time period of 7 h. As a strong stimulus is typically necessary to trigger IOSs, a low number of IOS acquisitions may help to maintain the vitality of the brain slice and to reduce run-down of IOSs during long-term measurements. Therefore, the stimulation protocol was changed during the course of experiment, i.e. a reduction to three IOS acquisitions at every full hour during sham-drug/drug application (see page 23).

Nevertheless, both signal intensity and signal area significantly declined, reached a stable plateau after about 3 h and did not recover to their baseline level during wash-out with fresh ACSF (see fig. 3.16, page 52 and fig. 3.17, page 53). The run-down was more pronounced for the signal area ($\approx 30\%$) compared to the signal intensity ($\approx 15\%$). This effect can best be explained by a decrease in neuronal network activity over time, which,

as stated before (see page 76), should cause a stronger reduction in signal area than in signal intensity.

Another observation during IOS recordings was that the reproducibility of signal intensity and signal area worsened with increasing recording time (see fig. 3.16, page 52). The differences in signal intensity between the three stimulations, however, were small, whereas the signal area showed a higher variability in subsequent stimulations. The signal intensity declined in a more linear fashion during the three IOS recordings at every full hour possibly because the brain slices could not recover so effectively between the three subsequent stimulations after a certain recording time under ACSF recirculation. To compensate for this effect, the results of the six IOS recordings performed during baseline conditions and the results of the three IOS recordings done every full hour during sham-drug/drug application were averaged.

The time course of IOSs also changed during long-term measurements. The rise time, decay time, and the time period, after which first signals could be detected, were nearly doubled after 5 h of sham-drug application, but returned to baseline levels during wash-out with fresh ACSF (see fig. 3.18, page 53). Due to these changes in IOS kinetics and the observation that the variability of IOS kinetics was high under baseline conditions even in the same brain slice (see fig. 3.14, page 50), IOS kinetics were not regarded suitable to characterize IOSs during long-term experiments. These findings show that it is essential to accurately detect the maximum signal intensity and signal area independent of the time course of the signal. If the IOSs are examined after a fixed time point (e.g. 3 s after stimulation), which was often done in previous studies (Dodt *et al.*, 1996; D'Arcangelo *et al.*, 1997; Becker *et al.*, 2005), the maximum signal intensity and/or area may not be correctly determined.

In conclusion, the results presented above show that, under certain experimental conditions, long-term IOS recordings (at least up to 7 h) can be performed in the motor cortex in brain slices. Even if such experiments have to be conducted under ACSF recirculation (due to small amounts of substances available to be investigated) and under these conditions IOSs do not remain constant over time, pharmacological effects on IOSs can be revealed, as shown later, by comparing the putative run-down effects during sham-drug application on IOSs with the effects on IOSs occurring during drug application.

4.1.3 Effects of BIM on IOSs

BIM, a competitive antagonist of the GABA_A receptor, was applied to mouse brain slices to examine the effects of an impaired GABAergic system on IOSs. Consistent with the observations that IOSs mirror neuronal network activity, previous studies found an in-

crease in IOS area after application of 10 μM bicuculline (Dodt *et al.*, 1996; Kohn *et al.*, 2000). In the present study, a lower BIM concentration of 5 μM was used. Nevertheless, signal area increased to approximately 200% after about 30 min of BIM application and remained at this level until wash-out started (see fig. 3.19, page 55). After 60 min wash-out, the signal area decreased to baseline levels. These results suggest that the tangential extent of IOSs within the motor cortex is constrained by stimulus-triggered GABAergic inhibition. In contrast to Kohn *et al.* (2000), however, no increase in signal intensity was observed. This discrepancy may be due to different methods used for quantification of signal intensity.

4.2 Effects of SMC on Motor Cortical Neuronal Network Activity

The hydrazide SMC is a known GAD inhibitor. SMC blocks GAD activity by interacting with the GAD cofactor PLP and, in this way, reduces brain GABA levels (Roberts & Frankel, 1951a; Killam & Bain, 1957; Maynert & Kaji, 1962; Bell & Anderson, 1972; Banna, 1973; Yamashita, 1976; Abe & Matsuda, 1979; Hoshino *et al.*, 1979; Yamashita & Hirata, 1979; Sakurai *et al.*, 1981; Matsushima *et al.*, 1986). These reduced GABA levels are believed to cause the tonic and clonic convulsions as well as the running fits observed after a long latent period of one hour or more after systemic administration of SMC in rodents (Jenney & Pfeiffer, 1958; Yamashita, 1976; Yamashita & Hirata, 1977, 1979). Even though SMC is widely used to induce fear behavior in rats (Di Scala & Sandner, 1989; Nobre *et al.*, 2003; Borelli *et al.*, 2005; Brandao *et al.*, 2005) and is found in several food products (de la Calle & Anklam, 2005), effects of SMC on neuronal network activity have not yet been investigated. To close this gap, IOS recordings and patch-clamp experiments were performed in the present PhD study in motor cortical brain slices in the absence and presence of SMC.

4.2.1 Effects of SMC on IOSs

As previous studies have been shown that in the presence of 2 mM SMC GAD activity is inhibited to almost half the normal level (Matsushima *et al.*, 1986), IOSs recordings were performed during the bath application of 2 mM SMC. Under these conditions, SMC increased both signal intensity and signal area of IOSs in the mouse motor cortex. If compared to the values of sham-drug application with drug-free ACSF, a stable increase in both signal intensity and signal area was observed after an application time of 2 h (see fig. 3.21, page 57). After a subsequent open ACSF superfusion of brain slices (wash-

out), signal intensity and signal area were statistically no more different from control conditions.

These results are partially contrary to the observed effects of the GABA_A receptor antagonist BIM, which enhanced only signal area and left signal intensity unchanged. Previous studies have been shown that GABAergic neurons shape the flow of excitation within the barrel cortex and that the spatial distribution of these cells is related to the organization of the barrel field (Lin *et al.*, 1985; Lübke & Feldmeyer, 2007). GABAergic neurons are therefore assumed to restrict the lateral spread of the IOSs. As BIM and most likely also SMC diminished GABAergic inhibition, IOSs broadened after application of these drugs. The increase in signal intensity after SMC application implies that SMC enhances the strength of neuronal network activity. As this effect is not apparent after BIM application, the SMC-induced increase in signal intensity was presumably not mediated by a reduced GABAergic inhibition. As SMC influences not only GAD but also several other enzymes (see page 82), it cannot be excluded that SMC enhances the strength of neuronal network activity via another mechanism.

SMC shows a long latent period of one to several hours if it is systemically applied (Jenney & Pfeiffer, 1958; Yamashita, 1976; Yamashita & Hirata, 1977, 1979), possibly because hydrazides have a low oil/water partition coefficient and, therefore, are expected to penetrate only slowly into the brain (Schanker, 1961). Consistently, other studies have been shown a much shorter latent period of about 10 min if SMC is directly injected in the lateral ventricle or superior colliculus *in vivo* (Yamashita, 1976; Yamashita & Hirata, 1977). Therefore, bath application of SMC to brain slices was thought to overcome the long latent period of systemic administration. The effects of SMC on IOSs, however, were apparent after an application time of 2 h (see fig. 3.21, page 57). This may be explained by the well-known lower spontaneous neuronal activity in acute brain slices compared to *in vivo* conditions and the long interval of 5 min between stimulations. The later fits well to a study by Grafstein (1963) showing that the latent period of Thio-SMC to cause stimulus-evoked epileptiform activity within the neocortex corresponds to the rate of stimulations. With lower stimulation frequencies, the effects of Thio-SMC establish later, most likely as it takes longer to exhaust preexisting GABA pools.

To find an utmost sensitive assay for detecting changes in neuronal network activity due to GAD inhibition, two mouse strains were investigated regarding their sensitivity to display SMC effects on IOSs. This idea is based on findings by Tunnicliff *et al.* (1973), who observed differences in the GAD activity between different mouse strains. The lowest GAD activity was observed in Bl/6 mice (0.415 µg/mg protein/h), whereas Balb/c mice showed the highest GAD activity (0.477 µg/mg protein/h) of all mouse strains investigated. SMC in a concentration of 2 mM has been shown to reduce GAD

activity by about 50% *in vitro* (Matsushima *et al.*, 1986). Therefore, a residual pool of active GAD is still able to produce GABA during SMC application though at a lower level. As the GAD activity is higher in Balb/c mice, these mice may compensate GAD inhibition better than Bl/6 mice. Indeed, compared to brain slices obtained from Bl/6 mice, statistically significant effects of SMC on signal intensity and signal area occurred after a longer application of SMC, i.e. after 4 h of SMC application (see fig. 3.22, page 58). Additionally, Yilmazer-Hanke *et al.* (2003) detected a high GABA_A receptor density in Balb/c mice compared to Bl/6 mice, which possibly increases the probability of the remaining GABA to bind to and, hence, activate GABA receptors. These findings suggest that brain slices from Balb/c mice are less sensitive to GAD inhibition and, hence, less appropriate to investigate changes in GABAergic inhibition due to GAD-inhibitory substances.

4.2.2 Effects of SMC on Synaptic Transmission

To potentially detail the mechanisms by which SMC exerted its effect on IOSs, also whole-cell patch-clamp recordings from motor cortical layer II/III pyramidal neurons were performed to directly investigate actions of SMC on synaptic transmission.

4.2.2.1 Effects of SMC on GABA_A Minis

First, GABA_A Minis were recorded, which can be attributed to spontaneous action potential-independent presynaptic GABA release. A reduction in both GABA_A Mini amplitude ($\approx 35\%$) and GABA_A Mini frequency ($\approx 50\%$) in SMC preincubated brain slices was observed (see fig. 3.23, page 60). At first glance, the reduced GABA_A Mini amplitude would suggest that SMC affects functioning of postsynaptic GABA_A receptors (Nusser *et al.*, 1997; Kilman *et al.*, 2002). However, the validity of this common interpretation requires that the vesicle content remains constant. As SMC is expected to diminish GABA vesicle content, the decreased GABA_A Mini amplitude rather speaks in favor of a presynaptic effect. Such an effect was also observed by Zhou *et al.* (2000), who investigated how a reduced vesicular filling influences synaptic transmission. In this study, neurons were treated with bafilomycin A1 (Baf), which is a blocker of the vacuolar-type (V-type) ATPase and, thus, eliminates the driving force for uptake of both glutamate and GABA into synaptic vesicles. After incubation of brain slices with Baf, both GABA_A Mini amplitude and GABA_A Mini frequency were reduced. Similar to SMC, Baf affected GABA_A Mini frequency stronger than GABA_A Mini amplitude. Zhou *et al.* suggested that these findings indicate a diminished vesicular GABA content, which causes

a reduced activation of postsynaptic receptors and, hence, a reduced GABA_A Mini amplitude.

The observed reduction in GABA_A Mini frequency after Baf and SMC incubation may arise from a lowered release probability of insufficiently filled synaptic vesicles as suggested by Golan & Grossman (1996). Zhou *et al.*, however, provided evidence against this scenario. Therefore, the mechanisms involved in controlling the release of synaptic vesicles seem to be completely oblivious to the state of vesicle filling. The reduced GABA_A Mini frequency was presumably a consequence of reduced GABA_A Mini amplitude since some events fell below threshold for detection.

It was concluded that SMC impairs GABA synthesis by blocking GAD activity and, hence, cause a reduced GABA content in vesicles. Consequently, less GABA is released in the synaptic cleft leading to a weaker activation of postsynaptic GABA_A receptors and, therefore, to a diminished GABA_A Mini amplitude. The reduced frequency of GABA_A Minis is most likely a secondary effect of the reduced GABA_A Mini amplitudes since smaller events cannot be distinguished from noise.

4.2.2.2 Effects of SMC on sEPSCs

It is feasible to assume that a reduced strength of GABAergic inhibition by SMC, as evident from its effects on GABA_A Minis, causes an increased neuronal network activity as observed during IOS recordings. To possibly reveal consistent effects at the level of spontaneous neuronal activity, the action of SMC on sEPSCs, which represent action potential-dependent and -independent excitatory postsynaptic currents, was investigated. In virtue of the fast kinetic of detected sEPSCs, most of the events could be attributed to AMPA receptor-mediated postsynaptic currents elicited by presynaptic glutamate release. SMC preincubation, however, increased neither sEPSC amplitude nor frequency (see fig. 3.24, page 62).

The absent effect of SMC on sEPSCs may be explained by other actions of SMC on synaptic transmission. As the GAD cofactor PLP, a derivative of vitamin B6 (Roberts & Frankel, 1951a), is the cofactor of over 100 enzyme-catalyzed reactions, including syntheses or catabolism of several neurotransmitters (Dakshinamurti *et al.*, 1990; Ebadi *et al.*, 1990; Clayton, 2006), SMC also influences other PLP-dependent enzymes. In vitamin B6-deficient rats, a prolonged time course of dopamine release and decay (Tang & Wei, 2004) and reduced NMDA receptor function (Guilarte, 1989) were observed. Moreover, abnormal brain neurotransmitter concentrations and abnormal endogenous release of amino acids were detected in vitamin B6-deficient juvenile rats (Guilarte, 1989, 1991). This also included reduced brain glutamate levels and reduced potassium-induced glutamate release in the cortex, whereas the basal glutamate efflux remained unchanged.

This suggests that SMC may also impair glutamate synthesis. The enzyme aspartate aminotransferase, an enzyme localized in mitochondria, is involved in the synthesis of glutamate (Balázs *et al.*, 1966). As aspartate aminotransferase depends on the cofactor PLP, this enzyme is possibly also inhibited by SMC. SMC, however, scarcely penetrates organella suggesting that SMC does not influence the activity of PLP-dependent intra-mitochondrial enzymes (Sakurai *et al.*, 1981). Moreover, no reduction in glutamate concentration was found in brain extracts of adult SMC-treated rats (Killam & Bain, 1957) and even a slight increase in whole brain glutamate concentration could be detected in suckling rats from dams fed a B6-deficient diet after parturition (Kurtz *et al.*, 1972). *In vivo*, no increase in spontaneous convulsive activity was found in the dorsal and ventral root after SMC application (Bell & Anderson, 1972). Similar to the slightly reduced sEPSC frequency observed in the present study (see fig. 3.24, page 62), SMC also decreases frequency of spontaneous action potentials in neuronal cultures (Vlasova *et al.*, 1980).

Altogether, the absent increase in spontaneous neuronal activity cannot be ascribed to reduced glutamate synthesis as this would decrease sEPSC amplitude. SMC application more likely reduces presynaptic vesicle release in general. It is known that in vitamin B6-deficient suckling rats cerebral sphingolipids are reduced (Kurtz *et al.*, 1972). Sphingolipids are involved in vesicle exocytosis (Martin, 2000b; Salaün *et al.*, 2004) and their reduction possibly impairs spontaneous vesicle release. This might also contribute to the reduced GABA_A Mini frequency in SMC-preincubated brain slices.

4.2.3 Possible Effects of SMC on Human Health

SMC is assumed to have carcinogenic properties as it belongs to the chemical class of hydrazides, a group that has been proven to have carcinogenic effects (Mori *et al.*, 1960; Parodi *et al.*, 1981) and/or genotoxic properties in animals (Parodi *et al.*, 1981). However, whether this holds true is still a matter of debate since SMC shows mild carcinogenic effects *in vitro* (Hayatsu *et al.*, 1966; Hayatsu & Ukita, 1966; Parodi *et al.*, 1981), but *in vivo* data are inconsistent (Toth *et al.*, 1975; Abramsson-Zetterberg & Svensson, 2005; Vlastos *et al.*, 2009). In animal models, high SMC concentrations induce osteochondral and vascular lesions due to an impaired cross-linking reactions of collagen and elastin (Ramamurti & Taylor, 1959; Langford *et al.*, 1999; Dawson *et al.*, 2002; Mercier *et al.*, 2007; Takahashi *et al.*, 2009). In addition, teratogenic effects such as induction of cleft palate and aortic aneurysms have been reported (Steffek *et al.*, 1972; de la Fuente & del Rey, 1986; Gong *et al.*, 2006). In SMC-fed rats (up to 140 mg/kg per day), a marked alteration of motor and exploratory behavior was described, showing an increase of open rearing and grooming during exploration of a novel environment (Maranghi *et al.*, 2009). This

may indicate an enhanced arousal and an ineffective modulation of response to novelty. Moreover, SMC acts as an endocrine disruptor altering the homeostasis of the endocrine system (Maranghi *et al.*, 2010). As small amounts of SMC (up to 1200 ppb) can be found in various food products (see page 5), an additional goal of this PhD thesis was to assess if an SMC concentration under 2 mM is also capable of modulating neuronal network activity and, therefore, potentially harmful to human health.

To do so, IOS recordings were performed during application of 0.5 mM SMC. This SMC concentration did not increase network activity (see fig. 3.20, page 56). An SMC concentration of 0.5 mM is equivalent to 55.77 mg/kg or 55770 ppb. This implies that high SMC concentrations are necessary to induce a detectable harmful effect. However, humans seem to react more sensitive to SMC as the convulsant dose is only about one third of the convulsant dose in mice (Jenney & Pfeiffer, 1958). Additionally, SMC exhibits a relatively high half-life of about 15 days in muscle and 7 days in liver or kidney tissue (Cooper *et al.*, 2005b,a). This suggests that SMC ingested by food might accumulate in the brain to much higher concentrations as found in food products. Therefore, possible harmful effects of SMC on humans should further be investigated and the concentration of SMC in food products be kept as low as possible.

4.3 Effects of SPS-IgG on Motor Cortical Neuronal Network Activity

4.3.1 SPS - an Immunopathy?

SPS is a rare movement disorder characterized by fluctuating muscle stiffness, disabling spasms and a heightened sensitivity to external as well as internal stimuli (Moersch & Woltman, 1956; Lorish *et al.*, 1989; Meinck *et al.*, 1994; Dalakas *et al.*, 2000; Meinck & Thompson, 2002). About 60 to 98% of SPS patients exhibit Anti-GAD AAbs (Solimena *et al.*, 1990; Walikonis & Lennon, 1998; Meinck *et al.*, 2001). *In vitro*, sera and CSF as well as purified IgG fractions of SPS patients are capable of inhibiting GAD activity (Dinkel *et al.*, 1998; Raju *et al.*, 2005). SPS patients show decreased GABA levels in the sensorimotor cortex and posterior occipital cortex (Levy *et al.*, 2005) as well as in the CSF (Dalakas *et al.*, 2001), hyperexcitability of the motor cortex (Sandbrink *et al.*, 2000; Koerner *et al.*, 2004) and the brainstem (Molloy *et al.*, 2002) as well as a continuous background firing of motor-units despite the patient's attempt of muscle relaxation (Levy *et al.*, 1999). Cell loss was only described in few cases (Warich-Kirches *et al.*, 1997; Ishizawa *et al.*, 1999; Saiz *et al.*, 1999b; Warren *et al.*, 2002; Guardado Santervas *et al.*, 2007; Ishida *et al.*, 2007). Drugs enhancing the strength of GABAergic transmission, e.g. benzodiazepines, val-

proate, vigabatrin, tiagabine, gabapentin, and baclofen, improve symptoms (Lorish *et al.*, 1989; Vasconcelos & Dalakas, 2003; Dalakas, 2009). Plasmapheresis and intravenous Ig infusions, classical methods in the treatment of autoimmune diseases, provide an additional benefit (Dalakas *et al.*, 2001; Vasconcelos & Dalakas, 2003; Dalakas, 2006, 2009; Rossi *et al.*, 2009). Taken together, these results suggest an autoimmune origin of SPS possibly mediated by Anti-GAD AAbs.

Anti-GAD AAbs are also found in several other neurological diseases, e.g. ataxia or some forms of epilepsy (Abele *et al.*, 1999; Honnorat *et al.*, 2001; Vianello *et al.*, 2003; McKnight *et al.*, 2005; Vulliemoz *et al.*, 2007). It is, however, unclear until now whether Anti-GAD AAbs are causally involved in the pathophysiology of these disorders and, if so, why AAbs directed against the same enzyme are able to cause different symptoms. Moreover, Anti-GAD AAbs were detected in healthy persons even though at much lower levels than in SPS patients (Burns *et al.*, 2003). It is also unknown how an autoimmune response is triggered against an intracellular enzyme and how Anti-GAD AAbs are able to inhibit the activity of such an enzyme.

The pathogenic role of AAbs in peripheral autoimmune diseases is typically proven by passive transfer studies, in which patient-IgG is injected in mice or rats to induce characteristic symptoms, or by maternal passive transfer of AAbs from mother to child during pregnancy. In a case study, an infant from a mother suffering from SPS during pregnancy was asymptomatic after birth despite its elevated Anti-GAD AAb titer (Burns *et al.*, 2005). A passive transfer study in animals is still missing.

In conclusion, the origin of SPS and the role of Anti-GAD AAbs in this disease are insufficiently understood. Therefore, the final aim of this study was to investigate potential effects of IgG derived from SPS patients on motor cortical neuronal network activity.

4.3.2 Detection of Anti-GAD AAbs in Purified SPS-IgG

The IgG fraction of two SPS patients (SPS-IgG), which should also include potentially pathogenic AAbs, was purified from plasma filtrates (see page 17). The sample size of only two IgG fractions may appear low, but SPS is a highly rare condition with about one to two newly diagnosed SPS patients in a population of one million people per year (Meinck & Thompson, 2002). Moreover, as SPS-IgG was applied via the bath solution, relatively high quantities of raw material were required, which was only available from few patients.

Sandoglobulin[®], pooled IgG of over 1000 healthy persons, was treated in the same way as plasma filtrates and, afterwards, served as control IgG (see page 17). As this control IgG included a huge number of different IgG molecules targeted against a broad spectrum of antigens, it should help to unravel possible unspecific effects of human IgG

on mouse brain slices. As SPS is a noninflammatory disease, IgG of patients with inflammatory diseases, e.g. multiple sclerosis (MS), would provide another possible source for control IgG. Even though this approach is sometimes used, pooled IgG from healthy donors was preferred in the present study, as potentially pathogenic AAbs, which possibly mimics the effect of SPS-IgG, could not be excluded in MS patients.

First, SPS-IgG was tested for the presence of Anti-GAD AAbs. Western Blots revealed a clear reaction against a protein in the range of 65 kDa, the molecular weight of GAD (see fig. 3.25, A, page 64). As during immunoblotting proteins are denaturated, the results further indicate that at least a subset of the Anti-GAD AAbs of both patients were directed against linear GAD epitopes as seen in previous studies (Solimena & De Camilli, 1991; Giometto *et al.*, 1996; Dalakas *et al.*, 2001; Vianello *et al.*, 2006). This band was not observed for control IgG indicating that this reaction was specific for SPS-IgG. No further bands were detected, which differed between SPS-IgG and control IgG, even though some unspecific binding was observed for SPS-IgG, control IgG as well as for both polyclonal Abs against GAD₆₅ and GAD₆₅/GAD₆₇ used for control. As in some SPS patients AAbs against both GAD isoforms, GAD₆₅ and GAD₆₇, are present (Daw *et al.*, 1996; Meinck *et al.*, 2001), an immunodot (GAD Dot) was performed to elucidate against which isoform Anti-GAD AAbs were directed. Both patients had produced Anti-GAD AAbs against GAD₆₅, but not against GAD₆₇ (see fig. 3.25, B, page 64). No response against GAD₆₅ or GAD₆₇ was observed for control IgG.

To attribute a potentially pathological effect specifically to Anti-GAD AAbs, it would have been necessary to purify Anti-GAD AAbs from the SPS-IgG fraction. However, as it is not known if the Anti-GAD AAbs are the only potentially pathogenic AAbs in SPS patients or if other yet undiscovered AAbs might contribute to the disease progress, the whole SPS-IgG fraction was used to test in a first step whether SPS might have an autoimmune origin.

4.3.3 Effects of SPS-IgG on IOSs

To investigate the effect of SPS-IgG on neuronal network activity, IOSs were recorded during the application of SPS-IgG of patient 2. Unfortunately, during IgG application small particles were observed in the recording chamber, which impaired IOS recording by covering the signal. The amount of particles increased during the course of experiments and correlated with the applied IgG concentration. As this phenomenon was not observed during sham-drug or SMC application, these particles were most likely aggregations of Abs with cell waste. Such aggregations, however, imply that the concentration of free IgG diminished during the course of experiments. These fluctuating particles could be removed by inserting a filter in the perfusion system (see page 23).

This filter caught only the circulating particles, but was permeable to unbound IgG as proven in pilot experiments (data not shown). A change from recirculation to an open ACSF superfusion, which would have provided a higher amount of free IgG, unfortunately was not possible as the available quantity of SPS-IgG was limited. Therefore, it cannot fully be excluded that the amount of free IgG was insufficient to affect neuronal network activity.

In contrast to the GAD inhibitor SMC, application of SPS-IgG of patient 2 did not increase the signal intensity and the signal area of IOSs (see fig. 3.27, page 66). Similar to sham-drug application, a run-down of both parameters was observed during IgG application. Furthermore, no significant difference between IOSs during SPS-IgG and control IgG application was found (see fig. 3.26, page 65). Both SPS-IgG and control IgG, however, significantly decelerated the run-down observed during sham-drug application for up to 2 h (see fig. 3.27, page 66), thus indicating that, even though IgG presumably aggregated with cell waste, the remaining concentration of free IgG was still sufficient to influence IOSs in some way. IOSs did not recover during wash-out with fresh ACSF. Unfortunately, these results could not be reevaluated with SPS-IgG of patient 1 as not enough material was available from this patient.

The present findings are in line with other studies showing no alterations in excitatory postsynaptic currents (EPSCs) in Purkinje cells after application of diluted CSF derived from an ataxic patient positive for Anti-GAD AAbs on cerebellar brain slices (Ishida *et al.*, 1999). Interestingly, both SPS-IgG and control IgG significantly retarded the run-down of IOSs. It is known that intravenously injected Ig scavenges activated complement fragments and attenuates complement-mediated injury and neuronal cell death in an animal model of stroke (Arumugam *et al.*, 2007). In the present *in vitro* system, however, no complement or other parts of the native immune system were present, thus possibly pointing to another mechanism of preventing neuronal cell injury by IgG.

4.3.4 Effects of SPS-IgG on Synaptic Transmission

As IOS recordings did not reveal effects of SPS-IgG on neuronal network activity similar to SMC, whole-cell patch-clamp recordings of GABA_A Minis and sEPSCs, which might be more sensitive than IOS recordings to detect SPS-IgG effects, were performed on motor cortical layer II/III pyramidal neurons after preincubation with SPS-IgG of patient 1 and 2, IgG-free ACSF, and control IgG.

Preincubation of brain slices with control IgG should help to reveal potentially unspecific effects of human IgG on GABA_A Minis or sEPSCs. Compared to brain slices preincubated with IgG-free ACSF, the frequency and amplitude of GABA_A Minis was unaltered in brain slices preincubated with control IgG (see fig. 3.28, page 68). Similar

to the recordings of GABA_A Minis, sEPSC amplitude was not affected by control IgG, while sEPSC frequency was significantly reduced under these conditions (see fig. 3.31, page 71). Therefore, it is suggested that control IgG did influence neither postsynaptic receptors nor vesicle content, but decreased excitatory transmitter release.

In humans, an increase in extracellular hippocampal glutamate levels was observed during spontaneous seizures (During & Spencer, 1993; Wilson *et al.*, 1996). A similar increase in glutamate release was found in epileptic patients when seizures were evoked during surgery (Ronne-Engström *et al.*, 1992). In some studies, a beneficial effect of Ig application in some forms of epilepsy was observed (van Engelen *et al.*, 1994; Villani & Avanzini, 2002). Moreover, in an animal model of epilepsy, convulsions disappeared after Ig treatment and it has been shown that the Ig applied was taken up by neurons and glial cells in the cerebral cortex and deep structures of the CNS (Hirayama *et al.*, 1986). Therefore, IgG is possibly capable of impairing glutamate release and, hence, reduces seizures by a yet unknown mechanism, which might be linked to the reduced sEPSC frequency observed in the present study.

Regarding the effects of SPS-IgG on GABA_A Minis and sEPSCs, preincubation of brain slices with SPS-IgG caused a significant decrease in GABA_A Mini amplitude compared to brain slices preincubated with IgG-free ACSF (see fig. 3.30, page 70). This effect, however, was only statistically significant with the SPS-IgG of patient 1 and was not significant if compared to control IgG preincubation (see fig. 3.29, page 69). GABA_A Mini frequency was significantly decreased by the SPS-IgG fractions from both patients if compared to preincubation with both control IgG (see fig. 3.29, page 69) and IgG-free ACSF (see fig. 3.30, page 70).

Overall, the effects caused by SPS-IgG preincubation mimics those caused by SMC preincubation, even though the decrease of GABA_A Mini amplitude after SPS-IgG treatment was not as pronounced as after SMC treatment and, hence, not significant for all settings. The less pronounced reduction in GABA_A Mini amplitude may be explained by a longer period needed for SPS-IgG to penetrate into cells and/or by an insufficient amount of free SPS-IgG due to the observed aggregations with cell waste. Similar to SMC preincubation, GABA_A Mini frequency responded more sensitive and declined significantly for all settings after SPS-IgG preincubation. These results are in line with previous studies, showing a reduced frequency of spontaneous inhibitory postsynaptic currents (sIPSCs) (Ishida *et al.*, 1999, 2008) and reduced stimulus-induced GABA release (Mitoma *et al.*, 2000; Takenoshita *et al.*, 2001; Mitoma *et al.*, 2003) in cerebellar brain slices after application of diluted CSF or IgG of ataxic patients positive for Anti-GAD AAbs.

As the whole IgG fraction of SPS patients was used in experiments performed in the present study, the effects on GABA_A Minis observed after SPS-IgG preincubation cannot

solely be ascribed to the action of Anti-GAD AAbs impairing GAD activity. It cannot be excluded that yet undiscovered AAbs of the IgG fraction are responsible for the alterations in GABA_A Minis. The reduced GABA_A Mini amplitude could possibly also be mediated by AAbs directed against the GABA_A receptor-associated protein (GABARAP) (Raju *et al.*, 2006). These AAbs, which inhibit the surface expression of GABA_A receptors, are found in about 70% of SPS patients. *In vivo*, evidence for central GABA_A receptor dysfunction in SPS patients was also provided by PET studies (Perani *et al.*, 2007). On Western Blots performed in the present study, however, no clear band in the range of 14 kDa, the expected size of GABARAP, was detected, but it cannot be excluded that the observed unspecific binding was due to a weak reaction against GABARAP.

Application of SPS-IgG enhanced sEPSC frequency compared to brain slices preincubated with control IgG (see fig. 3.32, page 73). Compared to brain slices preincubated with IgG-free ACSF, this decrease was, however, not statistically significant (see fig. 3.33, page 74). The amplitude of sEPSCs remained constant under all conditions.

These results show that the observed reduction in GABA_A Mini frequency was indeed a specific effect caused by SPS-IgG and cannot be attributed to unspecific alterations in the functioning of presynaptic terminals as this would also have decreased sEPSC frequency. The principle that AAbs can influence spontaneous neuronal activity was previously proven in another study by the application of IgG derived from a patient suffering from amyotrophic lateral sclerosis (ALS), which also caused an increase in sEPSC frequency whereas control IgG did not (Andjus *et al.*, 1997). Increased spontaneous activity within a network of cultured hippocampal neurons was also found after application of serum from an Anti-GAD AAbs-positive epileptic patient (Vianello *et al.*, 2008). Therefore, SPS-IgG most likely enhances spontaneous excitatory transmitter release by reducing GABAergic neurotransmission.

4.3.5 Hypotheses Regarding the Induction of GAD Autoimmunity and Mechanism of Action

4.3.5.1 Induction of GAD Autoimmunity

Even though several studies, including the present one, provide evidence that SPS-IgG can modulate GABAergic neurotransmission, many questions remain to be answered. First, it is unknown how an autoimmune response against an intracellular enzyme can be triggered in the CNS. Under normal conditions, the cell surface presents fragments of cytosolic proteins via an MHC class I peptide complex to cytotoxic T cells. Cytotoxic T cells are able to distinguish between normal cellular proteins and proteins that are normally not present in cells indicating a viral infection or cancer. If such a "foreign"

peptide is presented on the cell surface, cytotoxic T cells become activated and induce apoptosis of the infected cell. In autoimmune diseases, it is generally accepted that an initial response to a viral peptide, which is similar to a cytosolic peptide, breaks self-tolerance by reasons of molecular mimicry and causes cytotoxic T cells to attack healthy cells. Antigen presenting cells, which include macrophages, dendritic cells, and B cells, express complexes of MHC class II and peptides derived from extracellular proteins on their surface. These MHC class II peptide complexes specifically activate T helper cells, which in turn activate B cells. These activated B cells differentiate to plasma cells and start to produce Abs.

Apart from SPS, AAbs against GAD can also be found in IDDM, in which an autoimmune-mediated destruction of pancreatic β cells occurs. In some IDDM patients, T cell cross-reactivity between coxsackievirus and GAD was observed (Atkinson *et al.*, 1994; Tian *et al.*, 1994). T cells of an SPS patient showed cross-reactivity with a peptide of the human cytomegalovirus (Hiemstra *et al.*, 2001). In one SPS patient, an elevated level of Anti-Epstein-Barr virus-Abs was found while Anti-GAD AAbs were absent (Ohara *et al.*, 2007). In another patient, SPS and elevated Anti-GAD AAbs were diagnosed following acute West Nile virus infection (Hassin-Baer *et al.*, 2004). Those infections may be the initial immune response, which breaks self-tolerance. Moreover, posttranslational palmitoylation of GAD₆₅ possibly enhances autoimmune response as palmitoylated influenza peptides induce a potent T-cell response *in vivo*, whereas their non-palmitoylated counterparts do not (Deres *et al.*, 1989).

Previously, the CNS was regarded as an immunologically privileged organ, which is isolated by the blood-brain barrier and, therefore, protected from the uncontrolled influence of the immune system. This is essential, as cytotoxic immune response would cause the loss of neurons. More recently, it has been shown that the CNS itself has an innate immune system (Xiao & Link, 1998; Carson & Sutcliffe, 1999). Activated astrocytes and microglia are capable of expressing MHC molecules (Wong *et al.*, 1984; Fontana *et al.*, 1986; Kreutzberg, 1996; Shrikant & Benveniste, 1996; Sriram & Rodriguez, 1997; Aloisi *et al.*, 1998; Xiao & Link, 1998; Carson & Sutcliffe, 1999) and even neurons have been shown to express MHC class I molecules (Wong *et al.*, 1984; Neumann *et al.*, 1995, 1997). The role of T cells in SPS is unclear, but in general a significant effector role of T cells in SPS patients is denied (Ellis & Atkinson, 1996; Schloot *et al.*, 1999; Costa *et al.*, 2002; Raju & Hampe, 2008) as only few cases of T cell reactivity have been reported (Hummel *et al.*, 1998; Lohmann *et al.*, 2000, 2003; Holmøy *et al.*, 2009). It is therefore concluded that SPS is mainly caused by a humoral immune response. As astrocytes express MHC class II molecules, presentation of GAD fragments may trigger T helper cell activation and, hence, B cell activation. Up to now, however, it is controversially discussed whether as-

trocytes express GAD or whether GAD expression is exclusively for neurons (Schousboe *et al.*, 1992; Ochi *et al.*, 1993; Benagiano *et al.*, 2000).

4.3.5.2 Possible Mechanisms of Action of Anti-GAD AAbs in the CNS

A synthesis of Anti-GAD AAbs within the CNS has been shown in SPS patients (Dalakas *et al.*, 2001; Skorstad *et al.*, 2008). Such an intrathecal AAbs synthesis is necessary to provide disease-causing AAbs, as the blood-brain barrier restricts the passage of Abs and as there is no evidence for a disrupted blood-brain barrier in SPS patients (Rakocevic *et al.*, 2004). The weak permeability of the blood-brain barrier for serum Abs possibly explains why no passive transfer study was successfully accomplished until now. Manto *et al.* (2007), however, induced SPS-like symptoms in rats by injecting IgG of a SPS patient directly into the rat brain. Sommer *et al.* (2005) induced SPS-like symptoms by administration of Anti-amphiphysin autoantibodies (Anti-amphiphysin AAbs), another AAb found in SPS patients with breast cancer (De Camilli *et al.*, 1993; Folli *et al.*, 1993; Saiz *et al.*, 1999a; Wessig *et al.*, 2003; Nguyen-Huu *et al.*, 2006), in an animal model of autoimmune encephalomyelitis, which is known for its impaired blood-brain barrier.

Even though it seemed unlikely that a big protein like IgG is taken up by neurons, such an uptake was shown in many studies (Borges & Busis, 1985; Fabian & Ritchie, 1986; Ritchie *et al.*, 1986; Fabian & Petroff, 1987; Fishman *et al.*, 1990, 1991; Fratantoni *et al.*, 1996; Weisbart *et al.*, 2000; Reynolds *et al.*, 2005). The internalization of Abs can result from endocytosis after binding to components of the cell surface or from unspecific fluid-phase endocytosis. Indeed, Anti-Amphiphysin AAbs are believed to pass the cell membrane and block intracellular pathways. Amphiphysin mediates vesicle endocytosis via binding to the SH3 region of dynamin (Wigge & McMahon, 1998). In embryonic motoneurons, a lower surface expression of the $\text{Na}^+ - \text{K}^+ - 2\text{Cl}^-$ cotransporter NKCC1 was observed after application of Anti-amphiphysin AAbs, possibly caused by a disturbance of vesicle trafficking (Geis *et al.*, 2009). As the intracellular chloride concentration in embryonic motoneurons is high, which is achieved by NKCC1 (Owens & Kriegstein, 2002), GABA depolarizes the cell and causes calcium influx. After Anti-amphiphysin AAbs application, however, calcium influx is reduced, possibly caused by a lower chloride gradient due to reduced NKCC1 surface expression (Geis *et al.*, 2009). This study suggests that Anti-amphiphysin AAbs contribute to the pathogenesis of SPS due to impaired GABA signaling most likely by disturbing intracellular vesicle trafficking.

GAD₆₅ is associated with GABA vesicles via its N-terminal region (Christgau *et al.*, 1991; Shi *et al.*, 1994) and coupled to VGAT, which is responsible for packing GABA into synaptic vesicles (Jin *et al.*, 2003). A tight functional coupling between GAD and VGAT is supposed as GABA newly synthesized by membrane-associated GAD₆₅ is taken up

preferentially over preexisting GABA in the cytoplasm and as GAD inhibition also decreases VGAT activity. GAD₆₅ knock-out mice show a higher susceptibility to seizures (Asada *et al.*, 1996; Kash *et al.*, 1997). Since these mice do not show tremors, spasticity or other symptoms of movement disorders, it was thought that Anti-GAD AAbs have no pathological role. Electrophysiological experiments in GAD₆₅ knock-out mice showed that the quantal size and frequency of spontaneous GABA release was normal, but the probability of GABA release in response to depolarization was reduced (Tian *et al.*, 1999). However, the expression of VGAT was found to be upregulated, which may at least partially compensate for the lost functional coupling with GAD₆₅ by taking up enough cytosolic GABA produced by GAD₆₇ (Wu *et al.*, 2007). Due to this regain of function, GAD₆₅ knock-out mice were not used in this PhD study.

Anti-GAD AAbs directed against a linear N-terminal epitope and against two conformation-dependent epitopes in the middle and near the C-terminus are prominent in SPS patients (Butler *et al.*, 1993; Kim *et al.*, 1994; Daw *et al.*, 1996; Raju *et al.*, 2005; Burbelo *et al.*, 2008). Anti-GAD AAbs directed against the C-terminus have been shown to be capable of reducing GAD activity (Ohta *et al.*, 1996; Raju *et al.*, 2005). Anti-GAD AAbs binding to the N-terminus possibly inhibit the binding of GAD₆₅ to GABA vesicle membrane and, therefore, impair the functional coupling of GAD₆₅ and VGAT leading to a decreased transport of GABA into synaptic vesicles. Both mechanisms would reduce the content in GABA vesicles and, hence, GABA_A Mini amplitude. As SPS-IgG preincubation reduced GABA_A Mini frequency more pronounced than GABA_A Mini amplitude, it cannot be excluded that SPS-IgG additionally influences GABA vesicle release. Similar to Anti-Amphiphysin AAbs, which impair intracellular vesicle trafficking, GAD AAbs binding to the middle or C-terminal region of GAD could possibly impair vesicle fusion, e.g. by means of sterical hindrance or IgG-mediated agglutination of vesicles.

Even though it was not possible to clarify the detailed mechanism by which SPS-IgG exerted the effects observed, the findings in this PhD thesis show that IgG of SPS patients is capable of altering GABAergic synaptic transmission, thereby further supporting the hypothesis of an autoimmune origin of SPS.

Summary

The electrical activity of the brain is the result of a complex interaction between excitation and inhibition mediated by several types of neurotransmitters. As the majority of neurons in the brain utilize either the inhibitory neurotransmitter GABA or the excitatory neurotransmitter glutamate, the interplay of these two neurotransmitters principally controls brain excitability and, hence, imbalance between these two neurotransmitters may cause severe pathological conditions.

Inhibition of GAD, the rate-limiting enzyme of GABA synthesis, is believed to change neuronal network activity caused by impaired GABAergic inhibition. IOS recordings and whole-cell patch-clamp measurements of GABA_A Minis and sEPSCs, methods capable of displaying neuronal network activity, were performed in the motor cortex in acute brain slices to unveil the effects of GAD inhibitors at the network level.

By recording IOSs, which represent activity-dependent changes in the optical properties of brain tissue, spread and strength of stimulus-evoked neuronal network activity can be investigated. Whole-cell patch-clamp recording from a neuron can be used to monitor postsynaptic currents and, in this way, to measure action potential-dependent and -independent transmitter release from presynaptic neurons. According to the type of postsynaptic current modulation, drug action can be ascribed to pre- or postsynaptic mechanisms. In the present study, recording GABA_A Minis helped to investigate the effects of GAD inhibitors on GABAergic neurotransmission. Alterations in spontaneous excitatory neuronal network activity due to reduced GABAergic inhibition were displayed by sEPSCs.

As the intracellular uptake of drugs inhibiting GAD activity and the depletion of the preexisting GABA pool was expected to be slow, the first project of this PhD thesis was to test the IOS technique for its capability of monitoring neuronal network activity over several hours. Concurrently, a new software for the analysis of IOS data was developed, which facilitates and significantly accelerates data analysis. The results of long-term measurements with sham-drug application in the present study show that IOS recordings can be performed up to 7 h in the motor cortex in brain slices.

The present study next proved the ability of IOS recording to detect changes in GABAergic inhibition by application of the GABA_A receptor antagonist BIM at a concentration

of 5 μ M. Under these conditions, a significant increase in signal area but not signal intensity of IOSs was observed. Another series of experiments examined whether the IOS technique is capable of displaying changes in neuronal network activity after impairing GAD activity with the well-known GAD inhibitor SMC. If compared to the values of sham-drug application, a stable and reversible increase in both signal intensity and signal area was observed after 2 h of 2 mM SMC application. Due to these effects, IOS recordings are regarded as an appropriate technique to monitor changes in GABAergic inhibition, even if such changes develop slowly.

To find an utmost sensitive assay for detecting changes in neuronal network activity due to GAD inhibition, two mouse strains (Bl/6 and Balb/c) reported to differ in their GAD activity were investigated regarding their sensitivity to display SMC effects on IOSs. Compared to Bl/6 mice, SMC-induced effects on IOSs in Balb/c mice need a markedly longer application time to establish. This difference can be explained by the ability of Balb/c mice to more effectively compensate GAD inhibition due to their higher GAD activity. Therefore, Balb/c mice appear less appropriate to investigate changes in GABAergic inhibition mediated by substances inhibiting GAD.

Consistent with the present findings of IOS recordings, patch-clamp measurements of GABA_A Minis revealed an SMC-induced reduction in the strength of GABAergic inhibition. The results are in line with the assumption that SMC impairs GABA synthesis by blocking GAD activity and, hence, causes a reduced GABA content in vesicles. Consequently, less GABA is released in the synaptic cleft leading to a weaker activation of postsynaptic GABA_A receptors and, therefore, to a diminished GABA_A Mini amplitude. SMC application, however, did not alter spontaneous excitatory neuronal network activity.

The SMC-mediated effects observed were not only of interest with regard to method validation, but also with regard to public health as SMC is found in several food products and causes several pathological symptoms in animals, for instance movement abnormalities. Therefore, a further goal was to assess whether SMC at a concentration lower than 2 mM is also capable of modulating neuronal network activity and, thus, potentially harmful to human health. To do so, IOS recordings were performed during application of 0.5 mM SMC. This SMC concentration, however, was not able to alter IOSs. Nevertheless, possible harmful actions of SMC in humans should further be investigated and the concentration of SMC in food products be kept as low as possible as humans react more sensitive to SMC as rodents and as SMC might accumulate in the brain.

The final aim of this study was to investigate potential effects of Anti-GAD AAbs-containing IgG derived from SPS patients on motor cortical neuronal network activity.

This was done because it is not assured whether these Anti-GAD AAbs contribute to the development and/or appearance of SPS symptoms or are merely a marker for disease. IOS recordings do not reveal changes in neuronal network activity during SPS-IgG application compared to control IgG application. Compared to sham-drug application, however, both SPS-IgG and control IgG decelerated run-down of IOSs. These findings corroborate the hypothesis that Ig may prevent neuronal cell death. Therefore, potentially neuroprotective effects of intravenous Ig treatment in humans should be further investigated.

As both SPS-IgG and control IgG decelerated run-down of IOSs, GABA_A Mini and sEPSC recordings after control-IgG preincubation should further reveal potentially unspecific effects of human IgG on presynaptic transmitter release. Compared to brain slices preincubated with IgG-free ACSF, control IgG did not affect GABA_A Mini amplitude and frequency as well as sEPSC amplitude. The sEPSC frequency, however, was significantly reduced under these conditions. This decreased excitatory transmitter release might explain the beneficial effect of Ig treatment in some forms of epilepsy.

The observed effects on GABA_A Minis caused by SPS-IgG preincubation mimicked those caused by SMC preincubation, even though the decrease of GABA_A Mini amplitude after SPS-IgG treatment was not as pronounced as after SMC treatment. Similar to SMC preincubation, GABA_A Mini frequency responded more sensitive and declined statistically significantly after SPS-IgG preincubation. Application of SPS-IgG enhanced sEPSC frequency indicating that the observed reduction in GABA_A Mini frequency is indeed a specific effect caused by SPS-IgG and cannot be attributed to alterations in the functioning of presynaptic terminals. As in the present study the whole IgG fraction of SPS patients was used for experiments, the effects after SPS-IgG preincubation cannot solely be ascribed to the action of Anti-GAD AAbs impairing GAD activity. It cannot be excluded that other yet undiscovered AAbs of the IgG fraction are responsible for the observed effects. Nevertheless, this PhD thesis shows that IgG of SPS patients is indeed capable of altering GABAergic synaptic transmission, thus further supporting the hypothesis of an autoimmune origin of SPS. Therefore, the present work may help to improve the therapy of this severe neurological disease.

List of Figures

2.1	Labeled picture with the major components of the IOS setup	23
3.1	Labeled transmission image of a coronal mouse brain slice	32
3.2	Temporal changes in light intensity after stimulation	33
3.3	Reduction of noise after binning and filtering	35
3.4	Time course of the IOS	36
3.5	Relative changes in light intensity after $\Delta F/F$ calculation	37
3.6	Comparing $F - F_0$ and $\Delta F/F$ calculation after changes in baseline light intensity	38
3.7	Noise extraction	40
3.8	Different approaches for defining a threshold	42
3.9	Morphological opening	44
3.10	Automatic ROI detection	45
3.11	Time course of signal intensity and signal area	46
3.12	Changes in time course of signal intensity	47
3.13	Abnormalities in signal decay	48
3.14	Reproducibility of IOSs	50
3.15	Correlation of IOSs with stimulation strength	51
3.16	Changes in signal intensity and signal area during long-term measurements	52
3.17	Run-down during long-term measurements	53
3.18	Changes in rise and decay time of signal intensity during long-term measurements	53
3.19	Changes in signal intensity and signal area during BIM application	55
3.20	Comparison of IOSs during sham-drug application and during 0.5 mM SMC application in Bl/6 mouse brain slices	56
3.21	Comparison of IOSs during sham-drug application and during application of 2 mM SMC in Bl/6 mouse brain slices	57
3.22	Comparison of IOSs during sham-drug application and during application of 2 mM SMC in Balb/c mouse brain slices	58
3.23	Effects of SMC preincubation of brain slices on amplitude and frequency of GABA _A Minis	60
3.24	Effects of SMC preincubation of brain slices on amplitude and frequency of sEPSCs	62
3.25	Detection of Anti-GAD AAbs in purified IgG of SPS patients	64
3.26	Comparison of IOSs during application of 40 mg/l control IgG and 40 mg/l SPS-IgG of patient 2 in Bl/6 mouse brain slices	65
3.27	Comparison of IOSs during sham-drug application, during application of 40 mg/l control IgG and during application of 40 mg/l SPS-IgG	66

List of Figures

3.28	Effects of control IgG preincubation of brain slices on amplitude and frequency of GABA _A Minis	68
3.29	Effects of SPS-IgG preincubation of brain slices on amplitude and frequency of GABA _A Minis compared to control IgG	69
3.30	Effects of SPS-IgG preincubation of brain slices on amplitude and frequency of GABA _A Minis compared to brain slices preincubated in IgG-free ACSF	70
3.31	Effects of control IgG preincubation of brain slices on amplitude and frequency of sEPSCs	71
3.32	Effects of SPS-IgG preincubation of brain slices on amplitude and frequency of sEPSCs compared to control IgG	73
3.33	Effects of SPS-IgG preincubation of brain slices on amplitude and frequency of sEPSCs compared to brain slices preincubated in IgG-free ACSF	74

List of Tables

3.1	Comparing $F - F_0$ and $\Delta F/F$ calculation	37
3.2	Susceptibility of $\Delta F/F$ calculation to noise of baseline light intensity	38
3.3	RMS noise of one brain slice	41
3.4	Comparison of stimulation protocols	49

Bibliography

- Abe, M. & Matsuda, M. (1979). Effect of antivitamin B6 on regional GABA metabolism in mouse brain and its relation to convulsions. *J. Nutr. Sci. Vitaminol.* **25**, 459–468.
- Abele, M., Weller, M., Mescheriakov, S., Burk, K., Dichgans, J., & Klockgether, T. (1999). Cerebellar ataxia with glutamic acid decarboxylase autoantibodies. *Neurology*, **52** (4), 857–859. Case Reports.
- Abramsson-Zetterberg, L. & Svensson, K. (2005). Semicarbazide is not genotoxic in the flow cytometry-based micronucleus assay in vivo. *Toxicol. Lett.* **155**, 211–217.
- Aitken, P., Fayuk, D., Somjen, G., & Turner, D. (1999). Use of intrinsic optical signals to monitor physiological changes in brain tissue slices. *Methods*, **18**, 91–103.
- Aloisi, F., Ria, F., Penna, G., & Adorini, L. (1998). Microglia are more efficient than astrocytes in antigen processing and in Th1 but not Th2 cell activation. *J. Immunol.* **160**, 4671–4680.
- Andjus, P. R., Stevic-Marinkovic, Z., & Cherubini, E. (1997). Immunoglobulins from motoneuron disease patients enhance glutamate release from rat hippocampal neurones in culture. *J. Physiol. (Lond.)*, **504** (Pt 1), 103–112.
- Andrew, R., Jarvis, C., & Obeidat, A. (1999). Potential sources of intrinsic optical signals imaged in live brain slices. *Methods*, **18**, 185–196.
- Andrew, R. & MacVicar, B. (1994). Imaging cell volume changes and neuronal excitation in the hippocampal slice. *Neuroscience*, **62**, 371–383.
- Aroniadou, V. & Keller, A. (1995). Mechanisms of LTP induction in rat motor cortex in vitro. *Cereb. Cortex*, **5**, 353–362.
- Arumugam, T. V., Tang, S. C., Lathia, J. D., Cheng, A., Mughal, M. R., Chigurupati, S., Magnus, T., Chan, S. L., Jo, D. G., Ouyang, X., Fairlie, D. P., Granger, D. N., Vortmeyer, A., Basta, M., & Mattson, M. P. (2007). Intravenous immunoglobulin (IVIG) protects the brain against experimental stroke by preventing complement-mediated neuronal cell death. *Proc. Natl. Acad. Sci. U.S.A.* **104**, 14104–14109.
- Asada, H., Kawamura, Y., Maruyama, K., Kume, H., Ding, R., Ji, F. Y., Kanbara, N., Kuzume, H., Sanbo, M., Yagi, T., & Obata, K. (1996). Mice lacking the 65 kDa isoform of glutamic acid decarboxylase (GAD65) maintain normal levels of GAD67 and GABA in their brains but are susceptible to seizures. *Biochem Biophys Res Commun*, **229** (3), 891–895.
- Asada, H., Kawamura, Y., Maruyama, K., Kume, H., Ding, R. G., Kanbara, N., Kuzume, H., Sanbo, M., Yagi, T., & Obata, K. (1997). Cleft palate and decreased brain gamma-aminobutyric acid in mice lacking the 67-kDa isoform of glutamic acid decarboxylase. *Proc Natl Acad Sci U S A*, **94** (12), 6496–6499.
- Atkinson, M. A., Bowman, M. A., Campbell, L., Darrow, B. L., Kaufman, D. L., & Maclaren, N. K. (1994). Cellular immunity to a determinant common to glutamate decarboxylase and coxsackie virus in insulin-dependent diabetes. *J Clin Invest*, **94** (5), 2125–2129.
- Atkinson, M. A., Kaufman, D. L., Newman, D., Tobin, A. J., & Maclaren, N. K. (1993).

- Islet cell cytoplasmic autoantibody reactivity to glutamate decarboxylase in insulin-dependent diabetes. *J Clin Invest*, **91** (1), 350–356.
- Awapara, J., Landua, A. J., Fuerst, R., & Seale, B. (1950). Free gamma-aminobutyric acid in brain. *J. Biol. Chem.* **187**, 35–39.
- Baekkeskov, S., Aanstoot, H. J., Christgau, S., Reetz, A., Solimena, M., Cascalho, M., Folli, F., Richter-Olesen, H., & De Camilli, P. (1990). Identification of the 64K autoantigen in insulin-dependent diabetes as the GABA-synthesizing enzyme glutamic acid decarboxylase. *Nature*, **347** (6289), 151–156.
- Balázs, R., Dahl, D., & Harwood, J. R. (1966). Subcellular distribution of enzymes of glutamate metabolism in rat brain. *J. Neurochem.* **13**, 897–905.
- Banna, N. (1973). Antagonistic effects of semicarbazide and pyridoxine on cuneate presynaptic inhibition. *Brain Res.* **56**, 249–258.
- Bazemore, A., Elliott, K. A., & Florey, E. (1956). Factor I and gamma-aminobutyric acid. *Nature*, **178**, 1052–1053.
- Becker, K., Eder, M., Zieglgansberger, W., & Dodt, H.-U. (2005). WIN 55,212-2 decreases the spatial spread of neocortical excitation in vitro. *Neuroreport*, **16** (9), 993–996. Comparative Study.
- Bell, J. & Anderson, E. (1972). The influence of semicarbazide-induced depletion of aminobutyric acid on presynaptic inhibition. *Brain Res.* **43**, 161–169.
- Ben-Ari, Y., Khazipov, R., Leinekugel, X., Cailard, O., & Gaiarsa, J. (1997). GABAA, NMDA and AMPA receptors: a developmentally regulated 'ménage à trois'. *Trends Neurosci.* **20**, 523–529.
- Benagiano, V., Virgintino, D., Rizzi, A., Flace, P., Troccoli, V., Bormann, J., Monaghan, P., Robertson, D., Roncali, L., & Ambrosi, G. (2000). Glutamic acid decarboxylase-positive neuronal cell bodies and terminals in the human cerebellar cortex. *Histochem. J.* **32**, 557–564.
- Bicknell, R. J., Luckman, S. M., Inenaga, K., Mason, W. T., & Hatton, G. I. (1989). Beta-adrenergic and opioid receptors on pituitary cells cultured from adult rat neurohypophysis: regulation of cell morphology. *Brain Res. Bull.* **22**, 379–388.
- Björk, E., Velloso, L., Kämpe, O., & Karlsson, F. (1994). GAD autoantibodies in IDDM, stiff-man syndrome, and autoimmune polyendocrine syndrome type I recognize different epitopes. *Diabetes*, **43**, 161–165.
- Borelli, K. G., Ferreira-Netto, C., Coimbra, N. C., & Brandao, M. L. (2005). Fos-like immunoreactivity in the brain associated with freezing or escape induced by inhibition of either glutamic acid decarboxylase or GABAA receptors in the dorsal periaqueductal gray. *Brain Res.* **1051** (1-2), 100–111. Comparative Study.
- Borges, L. F. & Busis, N. A. (1985). Intraneuronal accumulation of myeloma proteins. *Arch. Neurol.* **42**, 690–694.
- Bouloukos, A., Lekakis, J., Michael, J., & Kalofoutis, A. (1980). Immunoglobulins in cerebrospinal fluid in various neurologic disorders. *Clin. Chem.* **26**, 115–116.
- Boyton, R. J., Lohmann, T., Londei, M., Kalbacher, H., Halder, T., Frater, A. J., Douek, D. C., Leslie, D. G., Flavell, R. A., & Altmann, D. M. (1998). Glutamic acid decarboxylase T lymphocyte responses associated with susceptibility or resistance to type I diabetes: analysis in disease discordant human twins, non-obese diabetic mice and HLA-DQ transgenic mice. *Int Immunol.* **10** (12), 1765–1776.
- Brandao, M. L., Borelli, K. G., Nobre, M. J., Santos, J. M., Albrechet-Souza, L., Oliveira, A. R., & Martinez, R. C. (2005). Gabaergic regulation of the neural organization of fear in the midbrain tectum. *Neurosci Biobehav Rev.* **29** (8), 1299–1311.

- Brooks, P. A., Glaum, S. R., Miller, R. J., & Spyer, K. M. (1992). The actions of baclofen on neurones and synaptic transmission in the nucleus tractus solitarii of the rat in vitro. *J. Physiol. (Lond.)*, **457**, 115–129.
- Bu, D. F., Erlander, M. G., Hitz, B. C., Tillakaratne, N. J., Kaufman, D. L., Wagner-McPherson, C. B., Evans, G. A., & Tobin, A. J. (1992). Two human glutamate decarboxylases, 65-kDa GAD and 67-kDa GAD, are each encoded by a single gene. *Proc. Natl. Acad. Sci. U.S.A.* **89**, 2115–2119.
- Burbelo, P., Groot, S., Dalakas, M., & Iadarola, M. (2008). High definition profiling of autoantibodies to glutamic acid decarboxylases GAD65/GAD67 in stiff-person syndrome. *Biochem. Biophys. Res. Commun.* **366**, 1–7.
- Burns, T. M., Jones, H. R., Phillips, L. H. n., Bugawan, T. L., Erlich, H. A., & Lennon, V. A. (2003). Clinically disparate stiff-person syndrome with GAD65 autoantibody in a father and daughter. *Neurology*, **61** (9), 1291–1293. Case Reports.
- Burns, T. M., Phillips, L. H. n., & Jones, H. R. (2005). Stiff person syndrome does not always occur with maternal passive transfer of GAD65 antibodies. *Neurology*, **64** (2), 399–400. Comment.
- Butler, M. H., Solimena, M., Dirks, R. J., Hayday, A., & De Camilli, P. (1993). Identification of a dominant epitope of glutamic acid decarboxylase (GAD-65) recognized by autoantibodies in stiff-man syndrome. *J Exp Med*, **178** (6), 2097–2106.
- Carson, M. & Sutcliffe, J. (1999). Balancing function vs. self defense: the CNS as an active regulator of immune responses. *J. Neurosci. Res.* **55**, 1–8.
- Cerne, R. & Haglund, M. (2002). Electrophysiological correlates to the intrinsic optical signal in the rat neocortical slice. *Neurosci. Lett.* **317**, 147–150.
- Chattopadhyay, S., Ito, M., Cooper, J., Brooks, A., Curran, T., Powers, J., & Pearce, D. (2002a). An autoantibody inhibitory to glutamic acid decarboxylase in the neurodegenerative disorder batten disease. *Hum. Mol. Genet.* **11**, 1421–1431.
- Chattopadhyay, S., Kriscenski-Perry, E., Wenger, D., & Pearce, D. (2002b). An autoantibody to GAD65 in sera of patients with juvenile neuronal ceroid lipofuscinoses. *Neurology*, **59**, 1816–1817.
- Chen, C. H., Battaglioli, G., Martin, D. L., Hobar, S. A., & Colon, W. (2003). Distinctive interactions in the holoenzyme formation for two isoforms of glutamate decarboxylase. *Biochim Biophys Acta*, **1645** (1), 63–71. Comparative Study.
- Christgau, S., Schierbeck, H., Aanstoot, H. J., Aagaard, L., Begley, K., Kofod, H., Hejnaes, K., & Baekkeskov, S. (1991). Pancreatic beta cells express two autoantigenic forms of glutamic acid decarboxylase, a 65-kDa hydrophilic form and a 64-kDa amphiphilic form which can be both membrane-bound and soluble. *J Biol Chem*, **266** (31), 21257–21264.
- Christie, M. R., Brown, T. J., & Cassidy, D. (1992). Binding of antibodies in sera from Type 1 (insulin-dependent) diabetic patients to glutamate decarboxylase from rat tissues. Evidence for antigenic and non-antigenic forms of the enzyme. *Diabetologia*, **35**, 380–384.
- Clausen, R. P., Madsen, K., Larsson, O. M., Frølund, B., Krogsgaard-Larsen, P., & Schousboe, A. (2006). Structure-activity relationship and pharmacology of gamma-aminobutyric acid (GABA) transport inhibitors. *Adv. Pharmacol.* **54**, 265–284.
- Clayton, P. T. (2006). B6-responsive disorders: a model of vitamin dependency. *J. Inher. Metab. Dis.* **29**, 317–326.
- Cooper, K., McCracken, R., & Kennedy, D. (2005a). Nitrofurazone accumulates in avian

- eyes—a replacement for semicarbazide as a marker of abuse. *Analyst*, **130**, 824–827.
- Cooper, K., Mulder, P., van Rhijn, J., Kovacsics, L., McCracken, R., Young, P., & Kennedy, D. (2005b). Depletion of four nitrofurantoin antibiotics and their tissue-bound metabolites in porcine tissues and determination using LC-MS/MS and HPLC-UV. *Food Addit Contam*, **22**, 406–414.
- Costa, M., Saiz, A., Casamitjana, R., Castaner, M. F., Sanmarti, A., Graus, F., & Jaraquemada, D. (2002). T-cell reactivity to glutamic acid decarboxylase in stiff-man syndrome and cerebellar ataxia associated with polyendocrine autoimmunity. *Clin Exp Immunol*, **129** (3), 471–478. Case Reports.
- Culav-Sumić, J., Bosnjak, I., Pastar, Z., & Jukić, V. (2008). Anxious depression and the stiff-person plus syndrome. *Cogn Behav Neurol*, **21**, 242–245.
- Dakshinamurti, K., Paulose, C. S., Viswanathan, M., Siow, Y. L., Sharma, S. K., & Bolster, B. (1990). Neurobiology of pyridoxine. *Ann. N. Y. Acad. Sci.* **585**, 128–144.
- Dalakas, M. C. (2006). Role of IVIg in autoimmune, neuroinflammatory and neurodegenerative disorders of the central nervous system: present and future prospects. *J Neurol*, **253 Suppl 5**, v25–v32.
- Dalakas, M. C. (2009). Stiff person syndrome: advances in pathogenesis and therapeutic interventions. *Curr Treat Options Neurol*, **11**, 102–110.
- Dalakas, M. C., Fujii, M., Li, M., Lutfi, B., Kyhos, J., & McElroy, B. (2001). High-dose intravenous immune globulin for stiff-person syndrome. *N Engl J Med*, **345** (26), 1870–1876. Clinical Trial.
- Dalakas, M. C., Fujii, M., Li, M., & McElroy, B. (2000). The clinical spectrum of anti-GAD antibody-positive patients with stiff-person syndrome. *Neurology*, **55** (10), 1531–1535.
- Dalakas, M. C., Li, M., Fujii, M., & Jacobowitz, D. M. (2001). Stiff person syndrome: quantification, specificity, and intrathecal synthesis of GAD65 antibodies. *Neurology*, **57** (5), 780–784.
- D’Arcangelo, G., Dodt, H. U., & Zieglgansberger, W. (1997). Reduction of excitation by interleukin-1 beta in rat neocortical slices visualized using infrared-darkfield videomicroscopy. *Neuroreport*, **8** (8), 2079–2083.
- Das, A. & Gilbert, C. D. (1995). Long-range horizontal connections and their role in cortical reorganization revealed by optical recording of cat primary visual cortex. *Nature*, **375**, 780–784.
- Daw, K. & Powers, A. (1995). Two distinct glutamic acid decarboxylase auto-antibody specificities in IDDM target different epitopes. *Diabetes*, **44**, 216–220.
- Daw, K., Ujihara, N., Atkinson, M., & Powers, A. C. (1996). Glutamic acid decarboxylase autoantibodies in stiff-man syndrome and insulin-dependent diabetes mellitus exhibit similarities and differences in epitope recognition. *J Immunol*, **156** (2), 818–825. Comparative Study.
- Dawson, D. A., Rinaldi, A. C., & Pösch, G. (2002). Biochemical and toxicological evaluation of agent-cofactor reactivity as a mechanism of action for osteolathyrism. *Toxicology*, **177**, 267–284.
- De Aizpurua, H. J., Wilson, Y. M., & Harrison, L. C. (1992). Glutamic acid decarboxylase autoantibodies in preclinical insulin-dependent diabetes. *Proc Natl Acad Sci U S A*, **89** (20), 9841–9845.
- De Camilli, P., Thomas, A., Cofield, R., Folli, F., Lichte, B., Piccolo, G., Meinck, H. M., Austoni, M., Fassetta, G., & Bottazzo, G. (1993). The synaptic vesicle-associated protein amphiphysin is the 128-kD autoantigen of Stiff-Man syndrome with breast cancer. *J Exp Med*, **178** (6), 2219–2223.

- de Jong, P. J., Lakke, J. P., & Teelken, A. W. (1984). CSF GABA levels in Parkinson's disease. *Adv Neurol*, **40**, 427–430.
- de la Calle, M. & Anklam, E. (2005). Semicarbazide: occurrence in food products and state-of-the-art in analytical methods used for its determination. *Anal Bioanal Chem*, **382**, 968–977.
- de la Fuente & del Rey, M. (1986). Teratogenic effect of semicarbazide in Wistar rats. *Biol. Neonate*, **49**, 150–157.
- Deres, K., Schild, H., Wiesmüller, K. H., Jung, G., & Rammensee, H. G. (1989). In vivo priming of virus-specific cytotoxic T lymphocytes with synthetic lipopeptide vaccine. *Nature*, **342**, 561–564.
- Di Scala, G. & Sandner, G. (1989). Conditioned place aversion produced by microinjections of semicarbazide into the periaqueductal gray of the rat. *Brain Res.* **483**, 91–97.
- Dietzel, I., Heinemann, U., Hofmeier, G., & Lux, H. D. (1980). Transient changes in the size of the extracellular space in the sensorimotor cortex of cats in relation to stimulus-induced changes in potassium concentration. *Exp Brain Res*, **40**, 432–439.
- Dietzel, I., Heinemann, U., Hofmeier, G., & Lux, H. D. (1982). Stimulus-induced changes in extracellular Na⁺ and Cl⁻ concentration in relation to changes in the size of the extracellular space. *Exp Brain Res*, **46**, 73–84.
- Dinkel, K., Meinck, H. M., Jury, K. M., Karges, W., & Richter, W. (1998). Inhibition of gamma-aminobutyric acid synthesis by glutamic acid decarboxylase autoantibodies in stiff-man syndrome. *Ann Neurol*, **44** (2), 194–201. In Vitro.
- Dinnerstein, E., Collins, D., & Berman, S. A. (2007). A patient with post-traumatic stress disorder developing stiff person syndrome: is there a correlation? *Cogn Behav Neurol*, **20** (2), 136–137. Case Reports.
- Dobersen, M. J. & Chase, H. P. (1983). Immunologic aspects of type I diabetes. *Pediatrician*, **12**, 173–178.
- Dodt, H., D'Arcangelo, G., Pestel, E., & Zieglgänsberger, W. (1996). The spread of excitation in neocortical columns visualized with infrared-darkfield videomicroscopy. *Neuroreport*, **7** (10), 1553–1558.
- Dodt, H. & Zieglgänsberger, W. (1994). Infrared videomicroscopy: a new look at neuronal structure and function. *Trends Neurosci.* **17**, 453–458.
- Dodt, H. & Zieglgänsberger, W. (1998). Visualization of neuronal form and function in brain slices by infrared videomicroscopy. *Histochem. J.* **30**, 141–152.
- During, M. J. & Spencer, D. D. (1993). Extracellular hippocampal glutamate and spontaneous seizure in the conscious human brain. *Lancet*, **341**, 1607–1610.
- Ebadi, M., Murrin, L. C., & Pfeiffer, R. F. (1990). Hippocampal zinc thionein and pyridoxal phosphate modulate synaptic functions. *Ann. N. Y. Acad. Sci.* **585**, 189–201.
- Ellis, T. M. & Atkinson, M. A. (1996). The clinical significance of an autoimmune response against glutamic acid decarboxylase. *Nat Med*, **2** (2), 148–153.
- Erlander, M., Tillakaratne, N., Feldblum, S., Patel, N., & Tobin, A. (1991). Two genes encode distinct glutamate decarboxylases. *Neuron*, **7**, 91–100.
- Erlander, M. G. & Tobin, A. J. (1991). The structural and functional heterogeneity of glutamic acid decarboxylase: a review. *Neurochem. Res.* **16**, 215–226.
- Esclapez, M., Tillakaratne, N. J., Kaufman, D. L., Tobin, A. J., & Houser, C. R. (1994). Comparative localization of two forms of glutamic acid decarboxylase and their mRNAs in rat brain supports the concept of functional differences between the forms. *J. Neurosci.* **14**, 1834–1855.

- Fabian, R. & Petroff, G. (1987). Intraneuronal IgG in the central nervous system: uptake by retrograde axonal transport. *Neurology*, **37**, 1780–1784.
- Fabian, R. & Ritchie, T. (1986). Intraneuronal IgG in the central nervous system. *J. Neurol. Sci.* **73**, 257–267.
- Fayuk, D., Aitken, P., Somjen, G., & Turner, D. (2002). Two different mechanisms underlie reversible, intrinsic optical signals in rat hippocampal slices. *J. Neurophysiol.* **87**, 1924–1937.
- Federico, P., Borg, S. G., Salkauskus, A. G., & MacVicar, B. A. (1994). Mapping patterns of neuronal activity and seizure propagation by imaging intrinsic optical signals in the isolated whole brain of the guinea-pig. *Neuroscience*, **58**, 461–480.
- Feldblum, S., Erlander, M. G., & Tobin, A. J. (1993). Different distributions of GAD65 and GAD67 mRNAs suggest that the two glutamate decarboxylases play distinctive functional roles. *J. Neurosci. Res.* **34**, 689–706.
- Fenalti, G., Law, R. H. P., Buckle, A. M., Langendorf, C., Tuck, K., Rosado, C. J., Faux, N. G., Mahmood, K., Hampe, C. S., Banga, J. P., Wilce, M., Schmidberger, J., Rossjohn, J., El-Kabani, O., Pike, R. N., Smith, A. I., Mackay, I. R., Rowley, M. J., & Whisstock, J. C. (2007). GABA production by glutamic acid decarboxylase is regulated by a dynamic catalytic loop. *Nat Struct Mol Biol*, **14** (4), 280–286.
- Fishman, P. S., Farrand, D. A., & Kristt, D. A. (1990). Internalization of plasma proteins by cerebellar Purkinje cells. *J Neurol Sci*, **100** (1-2), 43–49.
- Fishman, P. S., Farrand, D. A., & Kristt, D. A. (1991). Penetration and internalization of plasma proteins in the human spinal cord. *J Neurol Sci*, **104** (2), 166–175.
- Fleischman, D., Madan, G., Zesiewicz, T. A., & Fleischman, M. (2009). Stiff-person syndrome: commonly mistaken for hysterical paralysis. *Clin Neurol Neurosurg*, **111**, 644.
- Florey, E. (1991). GABA: history and perspectives. *Can. J. Physiol. Pharmacol.* **69**, 1049–1056.
- Folli, F., Solimena, M., Cofield, R., Austoni, M., Tallini, G., Fassetta, G., Bates, D., Cartledge, N., Bottazzo, G. F., & Piccolo, G. (1993). Autoantibodies to a 128-kd synaptic protein in three women with the stiff-man syndrome and breast cancer. *N Engl J Med*, **328** (8), 546–551. Case Reports.
- Fontana, A., Erb, P., Pircher, H., Zinkernagel, R., Weber, E., & Fierz, W. (1986). Astrocytes as antigen-presenting cells. Part II: Unlike H-2K-dependent cytotoxic T cells, H-2Ia-restricted T cells are only stimulated in the presence of interferon-gamma. *J. Neuroimmunol.* **12**, 15–28.
- Franklin, I. K. & Wollheim, C. B. (2004). GABA in the endocrine pancreas: its putative role as an islet cell paracrine-signalling molecule. *J Gen Physiol*, **123** (3), 185–190.
- Fratantoni, S. A., Dubrovsky, A. L., & Uchitel, O. D. (1996). Uptake of immunoglobulin G from amyotrophic lateral sclerosis patients by motor nerve terminals in mice. *J Neurol Sci*, **137** (2), 97–102.
- Frostig, R. D., Lieke, E. E., Ts'o, D. Y., & Grinvald, A. (1990). Cortical functional architecture and local coupling between neuronal activity and the microcirculation revealed by in vivo high-resolution optical imaging of intrinsic signals. *Proc. Natl. Acad. Sci. U.S.A.* **87**, 6082–6086.
- Frostig, R. D., Masino, S. A., Kwon, M. C., & Chen, C. H. (1995). Using Light to Probe the Brain: Intrinsic Signal Optical Imaging. *Int J Imaging Syst Technol*, **6**, 216–224.
- Gale, K. & Iadarola, M. J. (1980). Seizure protection and increased nerve-terminal GABA: delayed effects of GABA transaminase inhibition. *Science*, **208**, 288–291.
- Geis, C., Beck, M., Jablonka, S., Weishaupt, A., Toyka, K. V., Sendtner, M., & Sommer, C. (2009). Stiff person syndrome associated

- anti-amphiphysin antibodies reduce GABA associated $[Ca^{2+}]_i$ rise in embryonic motoneurons. *Neurobiol. Dis.* **36**, 191–199.
- Gerich, J. E. (1986). Insulin-dependent diabetes mellitus: pathophysiology. *Mayo Clin. Proc.* **61**, 787–791.
- Giometto, B., Miotto, D., Faresin, F., Argentero, V., Scaravilli, T., & Tavolato, B. (1996). Anti-gabaergic neuron autoantibodies in a patient with stiff-man syndrome and ataxia. *J Neurol Sci.* **143** (1-2), 57–59. Case Reports.
- Golan, H. & Grossman, Y. (1996). Block of glutamate decarboxylase decreases GABAergic inhibition at the crayfish synapses: possible role of presynaptic metabotropic mechanisms. *J. Neurophysiol.* **75**, 2089–2098.
- Gold, B. I. & Roth, R. H. (1979). Glutamate decarboxylase activity in striatal slices: characterization of the increase following depolarization. *J. Neurochem.* **32**, 883–888.
- Gong, B., Trent, M. B., Srivastava, D., & Boor, P. J. (2006). Chemical-induced, nonlethal, developmental model of dissecting aortic aneurysm. *Birth Defects Res. Part A Clin. Mol. Teratol.* **76**, 29–38.
- Gourfinkel-An, I., Parain, K., Hartmann, A., Mangiarini, L., Brice, A., Bates, G., & Hirsch, E. C. (2003). Changes in GAD67 mRNA expression evidenced by in situ hybridization in the brain of R6/2 transgenic mice. *J. Neurochem.* **86**, 1369–1378.
- Grafstein, B. (1963). Convulsant drug action on neuronally isolated cerebral cortex. *Science*, **142**, 973–975.
- Grinvald, A., Frostig, R. D., Siegel, R. M., & Bartfeld, E. (1991). High-resolution optical imaging of functional brain architecture in the awake monkey. *Proc. Natl. Acad. Sci. U.S.A.* **88**, 11559–11563.
- Grinvald, A., Lieke, E., Frostig, R. D., Gilbert, C. D., & Wiesel, T. N. (1986). Functional architecture of cortex revealed by optical imaging of intrinsic signals. *Nature*, **324**, 361–364.
- Guardado Santervas, P. L., Arjona Padillo, A., Serrano Castro, P., Olivares Romero, J., Rubi Callejon, J., Alonso Verdegay, G., & Huete Hurtado, A. (2007). Stiff person syndrome (SPS), a basal ganglia disease? Striatal MRI lesions in a patient with SPS. *J Neurol Neurosurg Psychiatry*, **78** (6), 657–659. Case Reports.
- Guilarte, T. R. (1989). Regional changes in the concentrations of glutamate, glycine, taurine, and GABA in the vitamin B-6 deficient developing rat brain: association with neonatal seizures. *Neurochem. Res.* **14**, 889–897.
- Guilarte, T. R. (1991). Abnormal endogenous amino acid release in brain slices from vitamin B-6 restricted neonatal rats. *Neurosci. Lett.* **121**, 203–206.
- Haglund, M., Ojemann, G., & Hochman, D. (1992a). Optical imaging of epileptiform and functional activity in human cerebral cortex. *Nature*, **358**, 668–671.
- Haglund, M. M., Berger, M. S., Kunkel, D. D., Franck, J. E., Ghatan, S., & Ojemann, G. A. (1992b). Changes in gamma-aminobutyric acid and somatostatin in epileptic cortex associated with low-grade gliomas. *J. Neurosurg.* **77**, 209–216.
- Hagopian, W., Michelsen, B., Karlsen, A., Larsen, F., Moody, A., Grubin, C., Rowe, R., Petersen, J., McEvoy, R., & Lernmark, A. (1993). Autoantibodies in IDDM primarily recognize the 65,000-M(r) rather than the 67,000-M(r) isoform of glutamic acid decarboxylase. *Diabetes*, **42**, 631–636.
- Hassin-Baer, S., Kirson, E. D., Shulman, L., Buchman, A. S., Bin, H., Hindiyeh, M., Markevich, L., & Mendelson, E. (2004). Stiff-person syndrome following West Nile fever. *Arch. Neurol.* **61**, 938–941.
- Hayatsu, H., Takeishi, K. I., & Ukita, T. (1966). The modification of nucleosides and nucleotides. 3. A selective modification of cytidine with semicarbazide. *Biochim. Biophys. Acta*, **123**, 445–457.

- Hayatsu, H. & Ukita, T. (1966). The modification of nucleosides and nucleotides. IV. The reaction of semicarbazide with nucleic acids. *Biochim. Biophys. Acta*, **123**, 458–470.
- Helmstaedter, M., Sakmann, B., & Feldmeyer, D. (2009). Neuronal correlates of local, lateral, and translaminar inhibition with reference to cortical columns. *Cereb. Cortex*, **19**, 926–937.
- Helmstaedter, M., Staiger, J. F., Sakmann, B., & Feldmeyer, D. (2008). Efficient recruitment of layer 2/3 interneurons by layer 4 input in single columns of rat somatosensory cortex. *J. Neurosci.* **28**, 8273–8284.
- Henningsen, P. & Meinck, H. (2003). Specific phobia is a frequent non-motor feature in stiff man syndrome. *J. Neurol. Neurosurg. Psychiatr.* **74**, 462–465.
- Hensch, T. K., Fagiolini, M., Mataga, N., Stryker, M. P., Baekkeskov, S., & Kash, S. F. (1998). Local GABA circuit control of experience-dependent plasticity in developing visual cortex. *Science*, **282** (5393), 1504–1508.
- Hertz, L. (1981). Features of astrocytic function apparently involved in the response of central nervous tissue to ischemia-hypoxia. *J. Cereb. Blood Flow Metab.* **1**, 143–153.
- Hiemstra, H. S., Schloot, N. C., van Veelen, P. A., Willemsen, S. J., Franken, K. L., van Rood, J. J., de Vries, R. R., Chaudhuri, A., Behan, P. O., Drijfhout, J. W., & Roep, B. O. (2001). Cytomegalovirus in autoimmunity: T cell crossreactivity to viral antigen and autoantigen glutamic acid decarboxylase. *Proc. Natl. Acad. Sci. U.S.A.* **98**, 3988–3991.
- Hill, D. K. & Keynes, R. D. (1949). Opacity changes in stimulated nerve. *J. Physiol. (Lond.)*, **108**, 278–281.
- Hirayama, H., Kurimoto, T., Wada, S., Machida, N., Shikuma, H., Shoji, S., & Horibe, M. (1986). Antiepileptic effects of globulin-n, an intact human immunoglobulin and its tissue-distribution in kindled cats. *Int J Clin Pharmacol Ther Toxicol*, **24**, 109–122.
- Hoenicke, K., Gatermann, R., Hartig, L., Mandix, M., & Otte, S. (2004). Formation of semicarbazide (SEM) in food by hypochlorite treatment: is SEM a specific marker for nitrofurazone abuse? *Food Addit Contam.* **21**, 526–537.
- Holmøy, T., Skorstad, G., Røste, L. S., Scheie, D., & Alvik, K. (2009). Stiff person syndrome associated with lower motor neuron disease and infiltration of cytotoxic T cells in the spinal cord. *Clin Neurol Neurosurg*, **111**, 708–712.
- Holthoff, K., Dodt, H. U., & Witte, O. W. (1994). Changes in intrinsic optical signal of rat neocortical slices following afferent stimulation. *Neurosci Lett*, **180** (2), 227–230.
- Holthoff, K., Sagnak, E., & Witte, O. (2007). Functional mapping of cortical areas with optical imaging. *Neuroimage*, **37**, 440–448.
- Holthoff, K. & Witte, O. (1998). Intrinsic optical signals in vitro: a tool to measure alterations in extracellular space with two-dimensional resolution. *Brain Res. Bull.* **47**, 649–655.
- Holthoff, K. & Witte, O. W. (1996). Intrinsic optical signals in rat neocortical slices measured with near-infrared dark-field microscopy reveal changes in extracellular space. *J Neurosci*, **16** (8), 2740–2749.
- Holthoff, K. & Witte, O. W. (1997). Recording of neuronal network properties with near-infrared dark-field microscopy and microelectrodes. *Electrochimica Acta*, **42**, 3241–3246.
- Honorat, J., Saiz, A., Giometto, B., Vincent, A., Brieva, L., de Andres, C., Maestre, J., Fabien, N., Vighetto, A., Casamitjana, R., Thivolet, C., Tavalato, B., Antoine, J., Trouillas, P., & Graus, F. (2001). Cerebellar ataxia with anti-glutamic acid decarboxylase antibodies: study of 14 patients. *Arch Neurol*, **58** (2), 225–230. Clinical Trial.
- Hoshino, M., Asakura, T., & Matsuda, M. (1979). Release of gamma-aminobutyric acid from isolated brain synaptosomes during

- semicarbazide-induced convulsions. *J. Nutr. Sci. Vitaminol.* **25**, 367–374.
- Howard, F. M. (1963). A new and effective drug in the treatment of the stiff-man syndrome: preliminary report. *Proc Staff Meet Mayo Clin*, **38**, 203–212.
- Hsu, C. C., Davis, K. M., Jin, H., Foos, T., Floor, E., Chen, W., Tyburski, J. B., Yang, C. Y., Schloss, J. V., & Wu, J. Y. (2000). Association of L-glutamic acid decarboxylase to the 70-kDa heat shock protein as a potential anchoring mechanism to synaptic vesicles. *J Biol Chem*, **275** (27), 20822–20828.
- Hummel, M., Durinovic-Bello, I., Bonifacio, E., Lampasona, V., Endl, J., Fessele, S., Then Bergh, F., Trenkwalder, C., Standl, E., & Ziegler, A. G. (1998). Humoral and cellular immune parameters before and during immunosuppressive therapy of a patient with stiff-man syndrome and insulin dependent diabetes mellitus. *J. Neurol. Neurosurg. Psychiatr.* **65**, 204–208.
- Ishida, K., Mitoma, H., & Mizusawa, H. (2008). Reversibility of cerebellar GABAergic synapse impairment induced by anti-glutamic acid decarboxylase autoantibodies. *J. Neurol. Sci.* **271**, 186–190.
- Ishida, K., Mitoma, H., Song, S. Y., Uchihara, T., Inaba, A., Eguchi, S., Kobayashi, T., & Mizusawa, H. (1999). Selective suppression of cerebellar GABAergic transmission by an autoantibody to glutamic acid decarboxylase. *Ann Neurol*, **46** (2), 263–267. Case Reports.
- Ishida, K., Mitoma, H., Wada, Y., Oka, T., Shibahara, J., Saito, Y., Murayama, S., & Mizusawa, H. (2007). Selective loss of Purkinje cells in a patient with anti-glutamic acid decarboxylase antibody-associated cerebellar ataxia. *J Neurol Neurosurg Psychiatry*, **78** (2), 190–192. Case Reports.
- Ishizawa, K., Komori, T., Okayama, K., Qin, X., Kaneko, K., Sasaki, S., & Iwata, M. (1999). Large motor neuron involvement in Stiff-man syndrome: a qualitative and quantitative study. *Acta Neuropathol (Berl)*, **97** (1), 63–70. Case Reports.
- Jarvis, C., Lilge, L., Vipond, G., & Andrew, R. (1999). Interpretation of intrinsic optical signals and calcein fluorescence during acute excitotoxic insult in the hippocampal slice. *Neuroimage*, **10**, 357–372.
- Jöbsis, F. F. (1977). Noninvasive, infrared monitoring of cerebral and myocardial oxygen sufficiency and circulatory parameters. *Science*, **198**, 1264–1267.
- Jenney, E. & Pfeiffer, C. (1958). The convulsant effect of hydrazides and the antidotal effect of anticonvulsants and metabolites. *J. Pharmacol. Exp. Ther.* **122**, 110–123.
- Jin, H., Wu, H., Osterhaus, G., Wei, J., Davis, K., Sha, D., Floor, E., Hsu, C.-C., Kopke, R. D., & Wu, J.-Y. (2003). Demonstration of functional coupling between gamma -aminobutyric acid (GABA) synthesis and vesicular GABA transport into synaptic vesicles. *Proc Natl Acad Sci U S A*, **100** (7), 4293–4298.
- Kanaani, J., Diacovo, M. J., El-Husseini, A. e. I. D., Brecht, D. S., & Baekkeskov, S. (2004). Palmitoylation controls trafficking of GAD65 from Golgi membranes to axon-specific endosomes and a Rab5a-dependent pathway to presynaptic clusters. *J. Cell. Sci.* **117**, 2001–2013.
- Kanaani, J., Patterson, G., Schaufele, F., Lippincott-Schwartz, J., & Baekkeskov, S. (2008). A palmitoylation cycle dynamically regulates partitioning of the GABA-synthesizing enzyme GAD65 between ER-Golgi and post-Golgi membranes. *J. Cell. Sci.* **121**, 437–449.
- Kash, S. F., Johnson, R. S., Tecott, L. H., Noebels, J. L., Mayfield, R. D., Hanahan, D., & Baekkeskov, S. (1997). Epilepsy in mice deficient in the 65-kDa isoform of glutamic acid decarboxylase. *Proc Natl Acad Sci U S A*, **94** (25), 14060–14065.

- Kaufman, D., Erlander, M., Clare-Salzler, M., Atkinson, M., Maclaren, N., & Tobin, A. (1992). Autoimmunity to two forms of glutamate decarboxylase in insulin-dependent diabetes mellitus. *J. Clin. Invest.* **89**, 283–292.
- Kaufman, D., Houser, C., & Tobin, A. (1991). Two forms of the gamma-aminobutyric acid synthetic enzyme glutamate decarboxylase have distinct intraneuronal distributions and cofactor interactions. *J. Neurochem.* **56**, 720–723.
- Kaufman, D. L., Clare-Salzler, M., Tian, J., Forsthuber, T., Ting, G. S., Robinson, P., Atkinson, M. A., Sercarz, E. E., Tobin, A. J., & Lehmann, P. V. (1993). Spontaneous loss of T-cell tolerance to glutamic acid decarboxylase in murine insulin-dependent diabetes. *Nature*, **366** (6450), 69–72.
- Keller, A., Miyashita, E., & Asanuma, H. (1991). Minimal stimulus parameters and the effects of hyperpolarization on the induction of long-term potentiation in the cat motor cortex. *Exp Brain Res*, **87**, 295–302.
- Kennedy, C., Des Rosiers, M. H., Jehle, J. W., Reivich, M., Sharpe, F., & Sokoloff, L. (1975). Mapping of functional neural pathways by autoradiographic survey of local metabolic rate with (14C)deoxyglucose. *Science*, **187**, 850–853.
- Killam, K. & Bain, J. (1957). Convulsant hydrazides. I. in vitro and in vivo inhibition of vitamin B6 enzymes by convulsant hydrazides. *J. Pharmacol. Exp. Ther.* **119**, 255–262.
- Kilman, V., van Rossum, M. C., & Turrigiano, G. G. (2002). Activity deprivation reduces miniature IPSC amplitude by decreasing the number of postsynaptic GABA(A) receptors clustered at neocortical synapses. *J. Neurosci.* **22**, 1328–1337.
- Kim, J., Namchuk, M., Bugawan, T., Fu, Q., Jaffe, M., Shi, Y., Aanstoot, H. J., Turck, C. W., Erlich, H., Lennon, V., & Baekkeskov, S. (1994). Higher autoantibody levels and recognition of a linear NH2-terminal epitope in the autoantigen GAD65, distinguish stiff-man syndrome from insulin-dependent diabetes mellitus. *J Exp Med*, **180** (2), 595–606.
- Kim, J., Richter, W., Aanstoot, H. J., Shi, Y., Fu, Q., Rajotte, R., Warnock, G., & Baekkeskov, S. (1993). Differential expression of GAD65 and GAD67 in human, rat, and mouse pancreatic islets. *Diabetes*, **42**, 1799–1808.
- Kimelberg, H. K. & Frangakis, M. V. (1985). Furosemide- and bumetanide-sensitive ion transport and volume control in primary astrocyte cultures from rat brain. *Brain Res.* **361**, 125–134.
- Kissel, J. T. & Elble, R. J. (1998). Stiff-person syndrome: stiff opposition to a simple explanation. *Neurology*, **51**, 11–14.
- Koerner, C., Wieland, B., Richter, W., & Meinck, H.-M. (2004). Stiff-person syndromes: motor cortex hyperexcitability correlates with anti-GAD autoimmunity. *Neurology*, **62** (8), 1357–1362. Clinical Trial.
- Kohn, A., Metz, C., Quibrera, M., Tommerdahl, M., & Whitsel, B. (2000). Functional neocortical microcircuitry demonstrated with intrinsic signal optical imaging in vitro. *Neuroscience*, **95**, 51–62.
- Kohn, A., Pinheiro, A., Tommerdahl, M. A., & Whitsel, B. L. (1997). Optical imaging in vitro provides evidence for the minicolumnar nature of cortical response. *Neuroreport*, **8**, 3513–3518.
- Kosel, M., Rudolph, U., Wielepp, P., Luginbühl, M., Schmitt, W., Fisch, H. U., & Schlaepfer, T. E. (2004). Diminished GABA(A) receptor-binding capacity and a DNA base substitution in a patient with treatment-resistant depression and anxiety. *Neuropsychopharmacology*, **29**, 347–350.
- Kossut, M. & Hand, P. (1984a). The development of the vibrissal cortical column: a 2-deoxyglucose study in the rat. *Neurosci. Lett.* **46**, 1–6.

- Kossut, M. & Hand, P. (1984b). Early development of changes in cortical representation of C3 vibrissa following neonatal denervation of surrounding vibrissa receptors: a 2-deoxyglucose study in the rat. *Neurosci. Lett.* **46**, 7–12.
- Kreutzberg, G. W. (1996). Microglia: a sensor for pathological events in the CNS. *Trends Neurosci.* **19**, 312–318.
- Kroeger-Koepke, M. B., Koepke, S. R., McClusky, G. A., Magee, P. N., & Michejda, C. J. (1981). alpha-Hydroxylation pathway in the in vitro metabolism of carcinogenic nitrosamines: N-nitrosodimethylamine and N-nitroso-N-methylaniline. *Proc. Natl. Acad. Sci. U.S.A.* **78**, 6489–6493.
- Krogsgaard-Larsen, P. (1980). Inhibitors of the GABA uptake systems. *Mol. Cell. Biochem.* **31**, 105–121.
- Krogsgaard-Larsen, P. & Falch, E. (1981). GABA agonists. Development and interactions with the GABA receptor complex. *Mol. Cell. Biochem.* **38 Spec No**, 129–146.
- Kukreja, A. & Maclaren, N. K. (1999). Autoimmunity and diabetes. *J. Clin. Endocrinol. Metab.* **84**, 4371–4378.
- Kurtz, D. J., Levy, H., & Kanfer, J. N. (1972). Cerebral lipids and amino acids in the vitamin B6-deficient suckling rat. *J. Nutr.* **102**, 291–298.
- Lamigeon, C., Bellier, J. P., Sacchettoni, S., Rujano, M., & Jacquemont, B. (2001). Enhanced neuronal protection from oxidative stress by coculture with glutamic acid decarboxylase-expressing astrocytes. *J. Neurochem.* **77**, 598–606.
- Langford, S. D., Trent, M. B., Balakumaran, A., & Boor, P. J. (1999). Developmental vasculotoxicity associated with inhibition of semicarbazide-sensitive amine oxidase. *Toxicol. Appl. Pharmacol.* **155**, 237–244.
- Lübke, J. & Feldmeyer, D. (2007). Excitatory signal flow and connectivity in a cortical column: focus on barrel cortex. *Brain Struct. Funct.* **212**, 3–17.
- Leinekugel, X., Khalilov, I., McLean, H., Cailard, O., Gaiarsa, J., Ben-Ari, Y., & Khazipov, R. (1999). GABA is the principal fast-acting excitatory transmitter in the neonatal brain. *Adv Neurol.* **79**, 189–201.
- Lernmark, A. (1996). Glutamic acid decarboxylase—gene to antigen to disease. *J. Intern. Med.* **240**, 259–277.
- Levy, L. M., Dalakas, M. C., & Floeter, M. K. (1999). The stiff-person syndrome: an autoimmune disorder affecting neurotransmission of gamma-aminobutyric acid. *Ann Intern Med.* **131** (7), 522–530.
- Levy, L. M., Levy-Reis, I., Fujii, M., & Dalakas, M. C. (2005). Brain gamma-aminobutyric acid changes in stiff-person syndrome. *Arch Neurol.* **62** (6), 970–974. Comparative Study.
- Lin, C., Lu, S., & Schmechel, D. (1985). Glutamic acid decarboxylase immunoreactivity in layer IV of barrel cortex of rat and mouse. *J. Neurosci.* **5**, 1934–1939.
- Lipton, P. (1973). Effects of membrane depolarization on light scattering by cerebral cortical slices. *J. Physiol. (Lond.)*, **231**, 365–383.
- Lockman, J. & Burns, T. M. (2007). Stiff-person syndrome. *Curr Treat Options Neurol.* **9** (3), 234–240.
- Lohmann, T., Hawa, M., Leslie, R. D., Lane, R., Picard, J., & Londei, M. (2000). Immune reactivity to glutamic acid decarboxylase 65 in stiffman syndrome and type 1 diabetes mellitus. *Lancet*, **356** (9223), 31–35. Clinical Trial.
- Lohmann, T., Londei, M., Hawa, M., & Leslie, R. D. (2003). Humoral and cellular autoimmune responses in stiff person syndrome. *Ann. N. Y. Acad. Sci.* **998**, 215–222.
- Lorish, T. R., Thorsteinsson, G., & Howard, F. M. (1989). Stiff-man syndrome updated. *Mayo Clin. Proc.* **64**, 629–636.

- Lowry, O. H., Rosebrough, N. J., Farr, A. L., & Randall, R. J. (1951). Protein measurement with the Folin phenol reagent. *J. Biol. Chem.* **193**, 265–275.
- Löscher, W., Hönack, D., & Taylor, C. P. (1991). Gabapentin increases aminooxyacetic acid-induced GABA accumulation in several regions of rat brain. *Neurosci. Lett.* **128**, 150–154.
- MacVicar, B. A. (1984). Infrared video microscopy to visualize neurons in the in vitro brain slice preparation. *J. Neurosci. Methods*, **12**, 133–139.
- MacVicar, B. A. & Hochman, D. (1991). Imaging of synaptically evoked intrinsic optical signals in hippocampal slices. *J Neurosci*, **11** (5), 1458–1469. In Vitro.
- Manto, M.-U., Laute, M.-A., Aguera, M., Rogemond, V., Pandolfo, M., & Honnorat, J. (2007). Effects of anti-glutamic acid decarboxylase antibodies associated with neurological diseases. *Ann Neurol*, **61** (6), 544–551.
- Maranghi, F., Tassinari, R., Lagatta, V., Moracci, G., Macrì, C., Eusepi, A., Di Virgilio, A., Scattoni, M. L., & Calamandrei, G. (2009). Effects of the food contaminant semicarbazide following oral administration in juvenile Sprague-Dawley rats. *Food Chem. Toxicol.* **47**, 472–479.
- Maranghi, F., Tassinari, R., Marcoccia, D., Altieri, I., Catone, T., De Angelis, G., Testai, E., Mastrangelo, S., Evandri, M. G., Bolle, P., & Lorenzetti, S. (2010). The food contaminant semicarbazide acts as an endocrine disrupter: Evidence from an integrated in vivo/in vitro approach. *Chem. Biol. Interact.* **183**, 40–48.
- Marco, P., Sola, R. G., Pulido, P., Alijarde, M. T., Sánchez, A., Ramón y Cajal, S., & DeFelipe, J. (1996). Inhibitory neurons in the human epileptogenic temporal neocortex. An immunocytochemical study. *Brain*, **119** (Pt 4), 1327–1347.
- Martin, D. (1987). Regulatory properties of brain glutamate decarboxylase. *Cell. Mol. Neurobiol.* **7**, 237–253.
- Martin, D. L. & Martin, S. B. (1982). Effect of nucleotides and other inhibitors on the inactivation of glutamate decarboxylase. *J. Neurochem.* **39**, 1001–1008.
- Martin, D. L., Martin, S. B., Wu, S. J., & Espina, N. (1991). Regulatory properties of brain glutamate decarboxylase (GAD): the apoenzyme of GAD is present principally as the smaller of two molecular forms of GAD in brain. *J Neurosci*, **11** (9), 2725–2731.
- Martin, D. L. & Rimvall, K. (1993). Regulation of gamma-aminobutyric acid synthesis in the brain. *J. Neurochem.* **60**, 395–407.
- Martin, S. B. & Martin, D. L. (1979). Stimulation by phosphate on the activation of glutamate apodecarboxylase by pyridoxyl-5'-phosphate and its implications for the control of GABA synthesis. *J. Neurochem.* **33**, 1275–1283.
- Martin, D.L., T. A. (2000a). Mechanisms controlling GABA synthesis and degradation in the brain. In: Martin DL, Olsen RW, editors. GABA in the nervous system: the view at fifty years. Philadelphia: Lippincott Williams and Wilkins. , 357–68.
- Martin, T. F. (2000b). Racing lipid rafts for synaptic-vesicle formation. *Nat. Cell Biol.* **2**, 9–11.
- Matsushima, S., Hori, S., & Matsuda, M. (1986). Conversion of 4-aminobutyraldehyde to gamma-aminobutyric acid in striatum treated with semicarbazide and kainic acid. *Neurochem. Res.* **11**, 1313–1319.
- Maynert, E. & Kaji, H. (1962). On the relationship of brain gamma-aminobutyric acid to convulsions. *J. Pharmacol. Exp. Ther.* **137**, 114–121.
- McKnight, K., Jiang, Y., Hart, Y., Cavey, A., Wroe, S., Blank, M., Shoenfeld, Y., Vincent,

- A., Palace, J., & Lang, B. (2005). Serum antibodies in epilepsy and seizure-associated disorders. *Neurology*, **65**, 1730–1736.
- McLaughlin, B. J., Wood, J. G., Saito, K., Roberts, E., & Wu, J. Y. (1975). The fine structural localization of glutamate decarboxylase in developing axonal processes and presynaptic terminals of rodent cerebellum. *Brain Res.* **85**, 355–371.
- Meeley, M. P. & Martin, D. L. (1983). Inactivation of brain glutamate decarboxylase and the effects of adenosine 5'-triphosphate and inorganic phosphate. *Cell. Mol. Neurobiol.* **3**, 39–54.
- Meinck, H. (2001). Stiff man syndrome. *CNS Drugs*, **15**, 515–526.
- Meinck, H. M., Faber, L., Morgenthaler, N., Seissler, J., Maile, S., Butler, M., Solimena, M., DeCamilli, P., & Scherbaum, W. A. (2001). Antibodies against glutamic acid decarboxylase: prevalence in neurological diseases. *J Neurol Neurosurg Psychiatry*, **71** (1), 100–103.
- Meinck, H. M., Ricker, K., Hulser, P. J., Schmid, E., Peiffer, J., & Solimena, M. (1994). Stiff man syndrome: clinical and laboratory findings in eight patients. *J Neurol*, **241** (3), 157–166.
- Meinck, H.-M. & Thompson, P. D. (2002). Stiff man syndrome and related conditions. *Mov Disord*, **17** (5), 853–866.
- Mercier, N., El Hadri, K., Osborne-Pellegrin, M., Nehme, J., Perret, C., Labat, C., Regnault, V., Lamazière, J. M., Challande, P., Lacolley, P., & Fève, B. (2007). Modifications of arterial phenotype in response to amine oxidase inhibition by semicarbazide. *Hypertension*, **50**, 234–241.
- Miller, L. P. & Walters, J. R. (1979). Effects of depolarization on cofactor regulation of glutamic acid decarboxylase in substantia nigra synaptosomes. *J. Neurochem.* **33**, 533–539.
- Mitoma, H., Ishida, K., Shizuka-Ikeda, M., & Mizusawa, H. (2003). Dual impairment of GABAA- and GABAB-receptor-mediated synaptic responses by autoantibodies to glutamic acid decarboxylase. *J Neurol Sci*, **208** (1-2), 51–56. Comparative Study.
- Mitoma, H., Song, S. Y., Ishida, K., Yamakuni, T., Kobayashi, T., & Mizusawa, H. (2000). Presynaptic impairment of cerebellar inhibitory synapses by an autoantibody to glutamate decarboxylase. *J Neurol Sci*, **175** (1), 40–44.
- Mitsumoto, H., Schwartzman, M., Estes, M., Chou, S., La Franchise, E., De Camilli, P., & Solimena, M. (1991). Sudden death and paroxysmal autonomic dysfunction in stiff-man syndrome. *J. Neurol.* **238**, 91–96.
- Moersch, F. P. & Woltman, H. W. (1956). Progressive fluctuating muscular rigidity and spasm ("stiff-man" syndrome); report of a case and some observations in 13 other cases. *Proc Staff Meet Mayo Clin*, **31**, 421–427.
- Molloy, F. M., Dalakas, M. C., & Floeter, M. K. (2002). Increased brainstem excitability in stiff-person syndrome. *Neurology*, **59** (3), 449–451. Comparative Study.
- Mori, K., Yasuno, A., & Matsumoto, K. (1960). Induction of pulmonary tumors in mice with isonicotinic acid hydrazid. *Gann*, **51**, 83–90.
- Murinson, B. B. (2004). Stiff-person syndrome. *Neurologist*, **10** (3), 131–137.
- Murinson, B. B., Butler, M., Marfurt, K., Gleason, S., De Camilli, P., & Solimena, M. (2004). Markedly elevated GAD antibodies in SPS: effects of age and illness duration. *Neurology*, **63** (11), 2146–2148.
- Nestmann, E., Lynch, B., Musa-Veloso, K., Goodfellow, G., Cheng, E., Haighton, L., & Lee-Brotherton, V. (2005). Safety assessment and risk-benefit analysis of the use of azodicarbonamide in baby food jar closure technology: putting trace levels of semicarbazide exposure into perspective—a review. *Food Addit Contam*, **22**, 875–891.

- Neumann, H., Cavalié, A., Jenne, D. E., & Wekerle, H. (1995). Induction of MHC class I genes in neurons. *Science*, **269**, 549–552.
- Neumann, H., Schmidt, H., Cavalié, A., Jenne, D., & Wekerle, H. (1997). Major histocompatibility complex (MHC) class I gene expression in single neurons of the central nervous system: differential regulation by interferon (IFN)-gamma and tumor necrosis factor (TNF)-alpha. *J. Exp. Med.* **185**, 305–316.
- Nguyen-Huu, B. K., Urban, P. P., Schreckenberger, M., Dieterich, M., & Werhahn, K. J. (2006). Antiampiphysin-positive stiff-person syndrome associated with small cell lung cancer. *Mov Disord*, **21** (8), 1285–1287. Case Reports.
- Nobre, M. J., Sandner, G., & Brandao, M. L. (2003). Enhancement of acoustic evoked potentials and impairment of startle reflex induced by reduction of GABAergic control of the neural substrates of aversion in the inferior colliculus. *Hear Res*, **184** (1-2), 82–90.
- Noonan, G., Begley, T., & Diachenko, G. (2008). semicarbazide formation in flour and bread. *J. Agric. Food Chem.* **56**, 2064–2067.
- Noonan, G., Warner, C., Hsu, W., Begley, T., Perfetti, G., & Diachenko, G. (2005). The determination of semicarbazide (N-aminourea) in commercial bread products by liquid chromatography-mass spectrometry. *J. Agric. Food Chem.* **53**, 4680–4685.
- Nusser, Z., Cull-Candy, S., & Farrant, M. (1997). Differences in synaptic GABA(A) receptor number underlie variation in gaba mini amplitude. *Neuron*, **19**, 697–709.
- Obaid, A. L., Flores, R., & Salzberg, B. M. (1989). Calcium channels that are required for secretion from intact nerve terminals of vertebrates are sensitive to omega-conotoxin and relatively insensitive to dihydropyridines. Optical studies with and without voltage-sensitive dyes. *J. Gen. Physiol.* **93**, 715–729.
- Ochi, S., Lim, J. Y., Rand, M. N., During, M. J., Sakatani, K., & Kocsis, J. D. (1993). Transient presence of GABA in astrocytes of the developing optic nerve. *Glia*, **9**, 188–198.
- Ohara, K., Osawa, M., Takeuchi, M., Suzuki, M., Uchiyama, S., & Iwata, M. (2007). Stiff-person syndrome with elevated anti-Epstein-Barr virus antibody. *Rinsho Shinkeigaku*, **47**, 434–436.
- Ohta, M., Obayashi, H., Ichimura, T., Nishimura, M., Itoh, N., & Ohta, K. (1996). Immunological characterization of antibodies against synthetic peptides of glutamic acid decarboxylase. *Clin. Chim. Acta*, **251**, 81–89.
- Owens, D. F. & Kriegstein, A. R. (2002). Is there more to GABA than synaptic inhibition? *Nat. Rev. Neurosci.* **3**, 715–727.
- Parodi, S., Taningher, M., Russo, P., Pala, M., Tamaro, M., & Monti-Bragadin, C. (1981). DNA-damaging activity in vivo and bacterial mutagenicity of sixteen aromatic amines and azo-derivatives, as related quantitatively to their carcinogenicity. *Carcinogenesis*, **2**, 1317–1326.
- Patel, A. B., de Graaf, R. A., Martin, D. L., Battaglioli, G., & Behar, K. L. (2006). Evidence that GAD65 mediates increased GABA synthesis during intense neuronal activity in vivo. *J. Neurochem.* **97**, 385–396.
- Paxinos, G. & Franklin, K. (2001). *The Mouse Brain in Stereotaxic Coordinates* (second edition). *Academic Press*, .
- Perani, D., Garibotto, V., Moresco, R. M., Ortelli, P., Corbo, M., Fazio, F., & Folli, F. (2007). PET evidence of central GABAergic changes in stiff-person syndrome. *Mov Disord*, **22** (7), 1030–1033. Case Reports.
- Pereira, A., Donato, J., & De Nucci, G. (2004). Implications of the use of semicarbazide as a metabolic target of nitrofurazone contamination in coated products. *Food Addit Contam*, **21**, 63–69.

- Petroff, O. A. (2002). GABA and glutamate in the human brain. *Neuroscientist*, **8**, 562–573.
- Petroff, O. A., Behar, K. L., & Rothman, D. L. (1999). New NMR measurements in epilepsy. Measuring brain GABA in patients with complex partial seizures. *Adv Neurol*, **79**, 939–945.
- Petroff, O. A., Rothman, D. L., Behar, K. L., & Mattson, R. H. (1996). Low brain GABA level is associated with poor seizure control. *Ann. Neurol.* **40**, 908–911.
- Pinal, C. S. & Tobin, A. J. (1998). Uniqueness and redundancy in GABA production. *Perspect Dev Neurobiol*, **5**, 109–118.
- Pinder, R. M., Brogden, R. N., Speight, T. M., & Avery, G. S. (1977). Sodium valproate: a review of its pharmacological properties and therapeutic efficacy in epilepsy. *Drugs*, **13**, 81–123.
- Porter, T. G. & Martin, D. L. (1984). Evidence for feedback regulation of glutamate decarboxylase by gamma-aminobutyric acid. *J. Neurochem.* **43**, 1464–1467.
- Porter, T. G. & Martin, D. L. (1987). Rapid inactivation of brain glutamate decarboxylase by aspartate. *J. Neurochem.* **48**, 67–72.
- Pouratian, N., Sheth, S. A., Martin, N. A., & Toga, A. W. (2003). Shedding light on brain mapping: advances in human optical imaging. *Trends Neurosci.* **26**, 277–282.
- Powers, A. C. & Eisenbarth, G. S. (1985). Autoimmunity to islet cells in diabetes mellitus. *Annu. Rev. Med.* **36**, 533–544.
- Raju, R., Foote, J., Banga, J. P., Hall, T. R., Padoa, C. J., Dalakas, M. C., Ortqvist, E., & Hampe, C. S. (2005). Analysis of GAD65 autoantibodies in Stiff-Person syndrome patients. *J Immunol*, **175** (11), 7755–7762. Comparative Study.
- Raju, R. & Hampe, C. S. (2008). Immunobiology of stiff-person syndrome. *Int. Rev. Immunol.* **27**, 79–92.
- Raju, R., Rakocevic, G., Chen, Z., Hoehn, G., Semino-Mora, C., Shi, W., Olsen, R., & Dalakas, M. C. (2006). Autoimmunity to GABAA-receptor-associated protein in stiff-person syndrome. *Brain*, **129** (Pt 12), 3270–3276.
- Rakic, P. (2008). Confusing cortical columns. *Proc. Natl. Acad. Sci. U.S.A.* **105**, 12099–12100.
- Rakocevic, G., Raju, R., & Dalakas, M. C. (2004). Anti-glutamic acid decarboxylase antibodies in the serum and cerebrospinal fluid of patients with stiff-person syndrome: correlation with clinical severity. *Arch Neurol*, **61** (6), 902–904.
- Ramamurti, P. & Taylor, H. E. (1959). Skeletal lesions produced by semicarbazide and experimental analysis of the action of lathyrogenic compounds. *J Bone Joint Surg Br*, **41-B**, 590–599.
- Ramirez-Montealegre, D., Chattopadhyay, S., Curran, T., Wasserfall, C., Pritchard, L., Schatz, D., Petitto, J., Hopkins, D., She, J., Rothberg, P., Atkinson, M., & Pearce, D. (2005). Autoimmunity to glutamic acid decarboxylase in the neurodegenerative disorder batten disease. *Neurology*, **64**, 743–745.
- Ransom, B. R., Yamate, C. L., & Connors, B. W. (1985). Activity-dependent shrinkage of extracellular space in rat optic nerve: a developmental study. *J. Neurosci.* **5**, 532–535.
- Reetz, A., Solimena, M., Matteoli, M., Folli, F., Takei, K., & De Camilli, P. (1991). GABA and pancreatic beta-cells: colocalization of glutamic acid decarboxylase (GAD) and GABA with synaptic-like microvesicles suggests their role in GABA storage and secretion. *EMBO J*, **10** (5), 1275–1284.
- Reynolds, A. J., Kaasinen, S. K., & Hendry, I. A. (2005). Retrograde axonal transport of dopamine beta hydroxylase antibodies by neurons in the trigeminal ganglion. *Neurochem Res*, **30** (6-7), 703–712.
- Rharbaoui, F., Granier, C., Kellou, M., Mani, J. C., van Endert, P., Madec, A. M., Boitard,

- C., Pau, B., & Bouanani, M. (1998). Peptide specificity of high-titer anti-glutamic acid decarboxylase (GAD)65 autoantibodies. *Immunol Lett*, **62** (3), 123–130.
- Ribak, C. & Yan, X.-X. (2000). GABA neurons in the neocortex. In: Martin DL, Olsen RW, editors. *GABA in the nervous system: the view at fifty years*. Philadelphia: Lippincott Williams and Wilkins. , 357–68.
- Ritchie, T. C., Fabian, R. H., Choate, J. V., & Coulter, J. D. (1986). Axonal transport of monoclonal antibodies. *J Neurosci*, **6** (4), 1177–1184.
- Roberts, E. & Frankel, S. (1950). gamma-Aminobutyric acid in brain: its formation from glutamic acid. *J. Biol. Chem.* **187**, 55–63.
- Roberts, E. & Frankel, S. (1951a). Glutamic acid decarboxylase in brain. *J. Biol. Chem.* **188**, 789–795.
- Roberts, E. & Frankel, S. (1951b). Further studies of glutamic acid decarboxylase in brain. *J. Biol. Chem.* **190**, 505–512.
- Rockel, A. J., Hiorns, R. W., & Powell, T. P. (1980). The basic uniformity in structure of the neocortex. *Brain*, **103**, 221–244.
- Ronne-Engström, E., Hillered, L., Flink, R., Spännare, B., Ungerstedt, U., & Carlson, H. (1992). Intracerebral microdialysis of extracellular amino acids in the human epileptic focus. *J. Cereb. Blood Flow Metab.* **12**, 873–876.
- Rorsman, P., Berggren, P. O., Bokvist, K., Ericson, H., Möhler, H., Ostenson, C. G., & Smith, P. A. (1989). Glucose-inhibition of glucagon secretion involves activation of GABAA-receptor chloride channels. *Nature*, **341**, 233–236.
- Rossi, S., Ulivelli, M., Malentacchi, M., Greco, G., Bartalini, S., Borgogni, P., & Giannini, F. (2009). Effects of immunotherapy on motor cortex excitability in Stiff Person Syndrome. *J. Neurol.* .
- Saari, L. & Peltonen, K. (2004). Novel source of semicarbazide: levels of semicarbazide in cooked crayfish samples determined by LC/MS/MS. *Food Addit Contam*, **21**, 825–832.
- Saiz, A., Dalmau, J., Butler, M., Chen, Q., Delattre, J., De Camilli, P., & Graus, F. (1999a). Anti-amphiphysin I antibodies in patients with paraneoplastic neurological disorders associated with small cell lung carcinoma. *J. Neurol. Neurosurg. Psychiatr.* **66**, 214–217.
- Saiz, A., Minguez, A., Graus, F., Marin, C., Tolosa, E., & Cruz-Sanchez, F. (1999b). Stiff-man syndrome with vacuolar degeneration of anterior horn motor neurons. *J Neurol*, **246** (9), 858–860. Case Reports.
- Sakurai, T., Abe, M., Hori, S., & Matsuda, M. (1981). The effects of administration of semicarbazide and aminooxyacetic acid on B6 vitamers levels in subcellular fractions of mouse brain. *J. Nutr. Sci. Vitaminol.* **27**, 529–538.
- Salaün, C., James, D. J., & Chamberlain, L. H. (2004). Lipid rafts and the regulation of exocytosis. *Traffic*, **5**, 255–264.
- Salzberg, B. M., Obaid, A. L., & Gainer, H. (1985). Large and rapid changes in light scattering accompany secretion by nerve terminals in the mammalian neurohypophysis. *J. Gen. Physiol.* **86**, 395–411.
- Sandbrink, F., Syed, N. A., Fujii, M. D., Dalakas, M. C., & Floeter, M. K. (2000). Motor cortex excitability in stiff-person syndrome. *Brain*, **123 (Pt 11)**, 2231–2239.
- Schanker, L. S. (1961). Mechanisms of Drug Absorption and Distribution. *Ann. Rev. Pharmacol*, **1**, 29–45.
- Schloot, N. C., Batstra, M. C., Duinkerken, G., De Vries, R. R., Dyrberg, T., Chaudhuri, A., Behan, P. O., & Roep, B. O. (1999). GAD65-Reactive T cells in a non-diabetic stiff-man syndrome patient. *J Autoimmun*, **12** (4), 289–296. Case Reports.

- Schousboe, A., Westergaard, N., Sonnewald, U., Petersen, S. B., Yu, A. C., & Hertz, L. (1992). Regulatory role of astrocytes for neuronal biosynthesis and homeostasis of glutamate and GABA. *Prog. Brain Res.* **94**, 199–211.
- Seissler, J., Amann, J., Mauch, L., Haubruck, H., Wolfahrt, S., Bieg, S., Richter, W., Holl, R., Heinze, E., & Northemann, W. (1993). Prevalence of autoantibodies to the 65- and 67-kD isoforms of glutamate decarboxylase in insulin-dependent diabetes mellitus. *J Clin Invest*, **92** (3), 1394–1399.
- Shi, Y., Veit, B., & Baekkeskov, S. (1994). Amino acid residues 24–31 but not palmitoylation of cysteines 30 and 45 are required for membrane anchoring of glutamic acid decarboxylase, GAD65. *J Cell Biol*, **124** (6), 927–934.
- Shrikant, P. & Benveniste, E. N. (1996). The central nervous system as an immunocompetent organ: role of glial cells in antigen presentation. *J. Immunol.* **157**, 1819–1822.
- Skorstad, G., Hestvik, A. L., Torjesen, P., Alvik, K., Vartdal, F., Vandvik, B., & Holmøy, T. (2008). GAD65 IgG autoantibodies in stiff person syndrome: clonality, avidity and persistence. *Eur. J. Neurol.* **15**, 973–980.
- Soghomonian, J. J. & Martin, D. L. (1998). Two isoforms of glutamate decarboxylase: why? *Trends Pharmacol Sci*, **19** (12), 500–505.
- Sokoloff, L. (1981). The deoxyglucose method: theory and practice. *Eur. Neurol.* **20**, 137–145.
- Solberg, Y., White, E., & Keller, A. (1988). Types and distribution of glutamic acid decarboxylase (GAD)-immunoreactive neurons in mouse motor cortex. *Brain Res.* **459**, 168–172.
- Solimena, M., Aggujaro, D., Muntzel, C., Dirkx, R., Butler, M., De Camilli, P., & Hayday, A. (1993). Association of GAD-65, but not of GAD-67, with the Golgi complex of transfected Chinese hamster ovary cells mediated by the N-terminal region. *Proc Natl Acad Sci U S A*, **90** (7), 3073–3077.
- Solimena, M., Butler, M. H., & De Camilli, P. (1994). GAD, diabetes, and Stiff-Man syndrome: some progress and more questions. *J Endocrinol Invest*, **17** (7), 509–520.
- Solimena, M. & De Camilli, P. (1991). Autoimmunity to glutamic acid decarboxylase (GAD) in Stiff-Man syndrome and insulin-dependent diabetes mellitus. *Trends Neurosci*, **14** (10), 452–457.
- Solimena, M., Dirkx, R. J., Radzynski, M., Mundigl, O., & De Camilli, P. (1994). A signal located within amino acids 1–27 of GAD65 is required for its targeting to the Golgi complex region. *J Cell Biol*, **126** (2), 331–341.
- Solimena, M., Folli, F., Aparisi, R., Pozza, G., & De Camilli, P. (1990). Autoantibodies to GABA-ergic neurons and pancreatic beta cells in stiff-man syndrome. *N. Engl. J. Med.* **322**, 1555–1560.
- Solimena, M., Folli, F., Denis-Donini, S., Comi, G. C., Pozza, G., De Camilli, P., & Vicari, A. M. (1988). Autoantibodies to glutamic acid decarboxylase in a patient with stiff-man syndrome, epilepsy, and type I diabetes mellitus. *N. Engl. J. Med.* **318**, 1012–1020.
- Sommer, C., Weishaupt, A., Brinkhoff, J., Biko, L., Wessig, C., Gold, R., & Toyka, K. V. (2005). Paraneoplastic stiff-person syndrome: passive transfer to rats by means of IgG antibodies to amphiphysin. *Lancet*, **365** (9468), 1406–1411.
- Sorenson, R. L., Garry, D. G., & Brelje, T. C. (1991). Structural and functional considerations of GABA in islets of Langerhans. Beta-cells and nerves. *Diabetes*, **40**, 1365–1374.
- Spokes, E. G., Garrett, N. J., Rossor, M. N., & Iversen, L. L. (1980). Distribution of GABA in post-mortem brain tissue from control, psychotic and Huntington's chorea subjects. *J. Neurol. Sci.* **48**, 303–313.
- Spreafico, R., Battaglia, G., Arcelli, P., Andermann, F., Dubeau, F., Palmieri, A., Olivier, A., Villemure, J. G., Tampieri, D., Avanzini,

- G., & Avoli, M. (1998). Cortical dysplasia: an immunocytochemical study of three patients. *Neurology*, **50**, 27–36.
- Sriram, S. & Rodriguez, M. (1997). Indictment of the microglia as the villain in multiple sclerosis. *Neurology*, **48**, 464–470.
- Stadler, R., Mottier, P., Guy, P., Gremaud, E., Varga, N., Lalljie, S., Whitaker, R., Kintscher, J., Dudler, V., Read, W., & Castle, L. (2004). Semicarbazide is a minor thermal decomposition product of azodicarbonamide used in the gaskets of certain food jars. *Analyst*, **129**, 276–281.
- Østby, I., Øyehaug, L., Einevoll, G. T., Nagelhus, E. A., Plahte, E., Zeuthen, T., Lloyd, C. M., Ottersen, O. P., & Omholt, S. W. (2009). Astrocytic mechanisms explaining neural-activity-induced shrinkage of extraneuronal space. *PLoS Comput. Biol.* **5**, e1000272.
- Steffek, A. J., Verrusio, A. C., & Watkins, C. A. (1972). Cleft palate in rodents after maternal treatment with various lathyrogenic agents. *Teratology*, **5**, 33–38.
- Stepnoski, R., LaPorta, A., Raccuia-Behling, F., Blonder, G., Slusher, R., & Kleinfeld, D. (1991). Noninvasive detection of changes in membrane potential in cultured neurons by light scattering. *Proc. Natl. Acad. Sci. U.S.A.* **88**, 9382–9386.
- Svaasand, L. O. & Ellingsen, R. (1983). Optical properties of human brain. *Photochem. Photobiol.* **38**, 293–299.
- Takahashi, M., Yoshida, M., Inoue, K., Morikawa, T., & Nishikawa, A. (2009). A ninety-day toxicity study of semicarbazide hydrochloride in Wistar Hannover GALAS rats. *Food Chem. Toxicol.* **47**, 2490–2498.
- Takashima, I., Kajiwara, R., & Iijima, T. (2001). Voltage-sensitive dye versus intrinsic signal optical imaging: comparison of optically determined functional maps from rat barrel cortex. *Neuroreport*, **12**, 2889–2894.
- Takenoshita, H., Shizuka-Ikeda, M., Mitoma, H., Song, S., Harigaya, Y., Igeta, Y., Yaguchi, M., Ishida, K., Shoji, M., Tanaka, M., Mizusawa, H., & Okamoto, K. (2001). Presynaptic inhibition of cerebellar GABAergic transmission by glutamate decarboxylase autoantibodies in progressive cerebellar ataxia. *J Neurol Neurosurg Psychiatry*, **70** (3), 386–389. Case Reports.
- Tang, F. I. & Wei, I. L. (2004). Vitamin B-6 deficiency prolongs the time course of evoked dopamine release from rat striatum. *J. Nutr.* **134**, 3350–3354.
- Tian, J., Lehmann, P. V., & Kaufman, D. L. (1994). T cell cross-reactivity between coxsackievirus and glutamate decarboxylase is associated with a murine diabetes susceptibility allele. *J Exp Med*, **180** (5), 1979–1984.
- Tian, N., Petersen, C., Kash, S., Baekkeskov, S., Copenhagen, D., & Nicoll, R. (1999). The role of the synthetic enzyme GAD65 in the control of neuronal gamma-aminobutyric acid release. *Proc. Natl. Acad. Sci. U.S.A.* **96**, 12911–12916.
- Tisch, R., Yang, X. D., Singer, S. M., Liblau, R. S., Fugger, L., & McDevitt, H. O. (1993). Immune response to glutamic acid decarboxylase correlates with insulinitis in non-obese diabetic mice. *Nature*, **366** (6450), 72–75.
- Toga, A. W., Cannestra, A. F., & Black, K. L. (1995). The temporal/spatial evolution of optical signals in human cortex. *Cereb. Cortex*, **5**, 561–565.
- Toth, B., Shumizu, H., & Erickson, J. (1975). Carbamylhydrazine hydrochloride as a lung and blood vessel tumour inducer in swiss mice. *Eur J Cancer*, **11**, 17–22.
- Toth, L. J., Rao, S. C., Kim, D. S., Somers, D., & Sur, M. (1996). Subthreshold facilitation and suppression in primary visual cortex revealed by intrinsic signal imaging. *Proc. Natl. Acad. Sci. U.S.A.* **93**, 9869–9874.

- Tunnickliff, G., Wimer, C., & Wimer, R. (1973). Relationships between neurotransmitter metabolism and behaviour in seven inbred strains of mice. *Brain Res.* **61**, 428–434.
- Tuomi, T., Björnses, P., Falorni, A., Partanen, J., Perheentupa, J., Lernmark, A., & Miettinen, A. (1996). Antibodies to glutamic acid decarboxylase and insulin-dependent diabetes in patients with autoimmune polyendocrine syndrome type I. *J. Clin. Endocrinol. Metab.* **81**, 1488–1494.
- Tuomi, T., Rowley, M. J., Knowles, W. J., Chen, Q. Y., McAnally, T., Zimmet, P. Z., & Mackay, I. R. (1994). Autoantigenic properties of native and denatured glutamic acid decarboxylase: evidence for a conformational epitope. *Clin Immunol Immunopathol*, **71** (1), 53–59.
- Ujihara, N., Daw, K., Gianani, R., Boel, E., Yu, L., & Powers, A. (1994). Identification of glutamic acid decarboxylase autoantibody heterogeneity and epitope regions in type I diabetes. *Diabetes*, **43**, 968–975.
- van Engelen, B. G., Renier, W. O., Weemaes, C. M., Gabreels, F. J., & Meinardi, H. (1994). Immunoglobulin treatment in epilepsy, a review of the literature. *Epilepsy Res.* **19**, 181–190.
- Vasconcelos, O. & Dalakas, M. (2003). Stiff-person Syndrome. *Curr Treat Options Neurol*, **5**, 79–90.
- Velloso, L. A., Kampe, O., Hallberg, A., Christmanson, L., Betsholtz, C., & Karlsson, F. A. (1993). Demonstration of GAD-65 as the main immunogenic isoform of glutamate decarboxylase in type 1 diabetes and determination of autoantibodies using a radioligand produced by eukaryotic expression. *J Clin Invest*, **91** (5), 2084–2090.
- Vianello, M., Bisson, G., Dal Maschio, M., Vassanelli, S., Girardi, S., Mucignat, C., Fountzoulas, K., & Giometto, B. (2008). Increased spontaneous activity of a network of hippocampal neurons in culture caused by suppression of inhibitory potentials mediated by anti-gad antibodies. *Autoimmunity*, **41**, 66–73.
- Vianello, M., Giometto, B., Vassanelli, S., Canato, M., Betterle, C., & Mucignat, C. (2006). Peculiar labeling of cultured hippocampal neurons by different sera harboring anti-glutamic acid decarboxylase autoantibodies (GAD-ab). *Exp Neurol*, **202** (2), 514–518. Comparative Study.
- Vianello, M., Keir, G., Giometto, B., Betterle, C., Tavolato, B., & Thompson, E. J. (2005). Antigenic differences between neurological and diabetic patients with anti-glutamic acid decarboxylase antibodies. *Eur J Neurol*, **12** (4), 294–299. Comparative Study.
- Vianello, M., Tavolato, B., Armani, M., & Giometto, B. (2003). Cerebellar ataxia associated with anti-glutamic acid decarboxylase autoantibodies. *Cerebellum*, **2** (1), 77–79.
- Villani, F. & Avanzini, G. (2002). The use of immunoglobulins in the treatment of human epilepsy. *Neurol. Sci.* **23 Suppl 1**, S33–37.
- Vlasova, I., Kostiaeva, G., & Luk'ianova, L. (1980). Effect of semicarbazide on the electrical and metabolic activity of cerebellar and visual cortex neurons in tissue culture. *Neirofiziologia*, **12**, 138–145.
- Vlastos, D., Moshou, H., & Epeoglou, K. (2009). Evaluation of genotoxic effects of semicarbazide on cultured human lymphocytes and rat bone marrow. *Food Chem. Toxicol.* .
- Vulliemoz, S., Vanini, G., Truffert, A., Chizzolini, C., & Seeck, M. (2007). Epilepsy and cerebellar ataxia associated with anti-glutamic acid decarboxylase antibodies. *J Neurol Neurosurg Psychiatry*, **78** (2), 187–189. Case Reports.
- Waagepetersen, H. S., Sonnewald, U., & Schousboe, A. (1999). The GABA paradox: multiple roles as metabolite, neurotransmitter, and neurodifferentiative agent. *J. Neurochem.* **73**, 1335–1342.

- Walikonis, J. & Lennon, V. (1998). Radioimmunoassay for glutamic acid decarboxylase (GAD65) autoantibodies as a diagnostic aid for stiff-man syndrome and a correlate of susceptibility to type 1 diabetes mellitus. *Mayo Clin. Proc.* **73**, 1161–1166.
- Warich-Kirches, M., Von Bossanyi, P., Treuheit, T., Kirches, E., Dietzmann, K., Feistner, H., & Wittig, H. (1997). Stiff-man syndrome: possible autoimmune etiology targeted against GABA-ergic cells. *Clin. Neuropathol.* **16**, 214–219.
- Warren, J. D., Scott, G., Blumbergs, P. C., & Thompson, P. D. (2002). Pathological evidence of encephalomyelitis in the stiff man syndrome with anti-GAD antibodies. *J Clin Neurosci*, **9** (3), 328–329. Case Reports.
- Wei, J., Davis, K., Wu, H., & Wu, J. (2004). Protein phosphorylation of human brain glutamic acid decarboxylase (GAD)65 and GAD67 and its physiological implications. *Biochemistry*, **43**, 6182–6189.
- Weisbart, R. H., Baldwin, R., Huh, B., Zack, D. J., & Nishimura, R. (2000). Novel protein transfection of primary rat cortical neurons using an antibody that penetrates living cells. *J Immunol*, **164** (11), 6020–6026.
- Wessig, C., Klein, R., Schneider, M. F., Toyka, K. V., Naumann, M., & Sommer, C. (2003). Neuropathology and binding studies in anti-amphiphysin-associated stiff-person syndrome. *Neurology*, **61** (2), 195–198. Case Reports.
- Wigge, P. & McMahon, H. T. (1998). The amphiphysin family of proteins and their role in endocytosis at the synapse. *Trends Neurosci.* **21**, 339–344.
- Wilson, C. L., Maidment, N. T., Shomer, M. H., Behnke, E. J., Ackerson, L., Fried, I., & Engel, J. (1996). Comparison of seizure related amino acid release in human epileptic hippocampus versus a chronic, kainate rat model of hippocampal epilepsy. *Epilepsy Res.* **26**, 245–254.
- Wilson, R. I. & Nicoll, R. A. (2001). Endogenous cannabinoids mediate retrograde signalling at hippocampal synapses. *Nature*, **410**, 588–592.
- Witte, O., Niermann, H., & Holthoff, K. (2001). Cell swelling and ion redistribution assessed with intrinsic optical signals. *An. Acad. Bras. Cienc.* **73**, 337–350.
- Wong, G. H., Bartlett, P. F., Clark-Lewis, I., Batty, F., & Schrader, J. W. (1984). Inducible expression of H-2 and Ia antigens on brain cells. *Nature*, **310**, 688–691.
- Wood, J. H., Hare, T. A., Glaeser, B. S., Balenger, J. C., & Post, R. M. (1979). Low cerebrospinal fluid gamma-aminobutyric acid content in seizure patients. *Neurology*, **29**, 1203–1208.
- Wu, H., Jin, Y., Buddhala, C., Osterhaus, G., Cohen, E., Jin, H., Wei, J., Davis, K., Obata, K., & Wu, J.-Y. (2007). Role of glutamate decarboxylase (GAD) isoform, GAD(65), in GABA synthesis and transport into synaptic vesicles-evidence from GAD(65)-knockout mice studies. *Brain Res*, **1154**, 80–83.
- Wyborski, R., Bond, R., & Gottlieb, D. (1990). Characterization of a cDNA coding for rat glutamic acid decarboxylase. *Brain Res. Mol. Brain Res.* **8**, 193–198.
- Xiao, B. & Link, H. (1998). Immune regulation within the central nervous system. *J. Neurol. Sci.* **157**, 1–12.
- Yamashita, J. (1976). Convulsive seizure induced by intracerebral injection of semicarbazide (an anti-vitamin B6) in the mouse. *J. Nutr. Sci. Vitaminol.* **22**, 1–6.
- Yamashita, J. & Hirata, Y. (1977). Running fit induced by injection of semicarbazide into the superior colliculus of the mouse. *J. Nutr. Sci. Vitaminol.* **23**, 467–470.
- Yamashita, J. & Hirata, Y. (1979). Running fits and gamma-aminobutyric acid of the superior colliculus of the mouse. *J. Nutr. Sci. Vitaminol.* **25**, 15–22.

Yilmazer-Hanke, D., Roskoden, T., Zilles, K., & Schwegler, H. (2003). Anxiety-related behavior and densities of glutamate, GABAA, acetylcholine and serotonin receptors in the amygdala of seven inbred mouse strains. *Behav. Brain Res.* **145**, 145–159.

Zhou, Q., Petersen, C. C., & Nicoll, R. A. (2000). Effects of reduced vesicular filling on synaptic transmission in rat hippocampal neurones. *J. Physiol. (Lond.)*, **525 Pt 1**, 195–206.

Bibliography

Publication

Published Abstract:

Holfelder C, Eder M, Becker K, Zieglgänsberger W, Buchwald B (2009). Semicarbazide modulates cortical excitation in mouse brain slices. *Pharmacopsychiatry*, 42(5),223

Danksagung

Mein besonderer Dank gilt Frau PD Dr. Brigitte Buchwald, die mich während meiner Promotion durch fachliche Anregung und Diskussion unterstützt hat und mir stets mit Rat und Tat zur Seite stand. Daneben möchte ich Dr. Matthias Eder danken, der mich stets unterstützte und in dessen Arbeitsgruppe ich herzlich aufgenommen wurde, um dort meine Arbeit beenden zu können.

Daneben möchte ich mich bei meinem Doktorvater Prof. Mark Hübener für seine Unterstützung, fachlichen Rat und seine Geduld bedanken.

Max Sperling möchte ich herzlich für die Hilfe bei der Erstellung des Programms zur IOS-Datenanalyse und der Optimierung des IOS-Setups sowie für die Hilfestellung zu sämtlichen Computerproblemen danken. Daneben stand mir noch Dr. Tom Mrsic-Flogel zu Fragen bezüglich der Auswertung optischer Daten beratend zur Seite.

Bei Prof. Hans-Michael Meinck möchte ich mich für die Bereitstellung der Patientenproben bedanken. Prof. Manfred Uhr und Frau Sabine Rickel möchte ich für die Quantifizierung des IgG's danken.

Mein Dank gilt außerdem Barbara Hauger und Christine Hilf für ihre technische Unterstützung sowie Carola Hetzel für die sprachliche Kontrolle meiner Doktorarbeit. Daneben möchte ich mich bei der gesamten Abteilung für ihren Zuspruch und ihre Unterstützung bedanken. Vielen Dank an Simone, Dani, Coco, Charis, Sascha, Rainer, Caro und Gerhard.

Zum Schluss möchte ich mich noch bei meiner Familie, insbesondere bei meinen Eltern, Rita und Josef Holfelder, meinen Bruder, Peter Holfelder, meinen Großeltern, Margareta und Josef Holfelder, und bei Julia Emanuel für ihre Unterstützung bedanken. Mein besonderer Dank gilt meinem Freund Max Sperling, für seine großartige Unterstützung und für seine Geduld während der letzten Jahre.

Curriculum Vitae

PERSONAL DETAILS

Diplom-Biologin Univ.
(*Master of Science in Biology*)
Christina Holfelder
Batzerstrasse 16
81375 Munich
born April 25, 1980; Nabburg

CURRENT POSITION

since Jan/2006 PHD THESIS, MAX PLANCK INSTITUTE OF PSYCHIATRY,
Research Group Neurophysiology/Dynamic neuronal
Networks

STUDIES

Oct/2004 – Nov/2005 DIPLOMA/MASTER THESIS, MAX PLANCK INSTITUTE OF
NEUROBIOLOGY, Department of Cellular and Systems
Neurobiology, Martinsried
Oct/2000 – Nov/2005 STUDY OF BIOLOGY, University of Regensburg, Degree
Diplom-Biologin Univ. (*Master of Science in Biology*)

EDUCATION

Sept/1998 – July/2000 BERUFSOBERSCHULE REGENSBURG
Sept/1996 – July/1998 APPRENTICESHIP IN HOME ECONOMICS, Neumarkt i. d. OPf.
Sept/1992 – July/1996 LOBKOWITZ-REALSCHULE

Munich, April 2010

Erklärung

Hiermit versichere ich, dass ich die vorliegende Arbeit selbständig und ohne unerlaubte Hilfsmittel angefertigt habe. Auch habe ich noch zu keinem früheren Zeitpunkt versucht, eine Dissertation einzureichen oder an einer Doktorprüfung teilzunehmen.

München, April 2010

Christina Holfelder